KIT

Karlsruher Institut für Technologie

Vacuum Structure of Models beyond the Standard Model

Zur Erlangung des akademischen Grades eines

DOKTORS DER NATURWISSENSCHAFTEN

von der KIT-Fakultät für Physik
des Karlsruher Instituts für Technologie (KIT)

genehmigte

DISSERTATION

von

M.Sc. Philipp Basler

aus Rastatt

Referentin: Prof. Dr. M. M. Mühlleitner (KIT, Karlsruhe)

Korreferent: Prof. Dr. U. Nierste (KIT, Karlsruhe)

Tag der mündlichen Prüfung: 06. Dezember 2019

Eidesstattliche Versicherung gemäß § 13 Absatz 2 Ziffer 3 der Promotionsordnung des Karlsruher Instituts für Technologie (KIT) für die KIT-Fakultät für Physik:

1. Bei der eingereichten Dissertation zu dem Thema

   Vacuum Structure of Models beyond the Standard Model

   handelt es sich um meine eigenständig erbrachte Leistung.

2. Ich habe nur die angegebenen Quellen und Hilfsmittel benutzt und mich keiner unzulässigen Hilfe Dritter bedient. Insbesondere habe ich wörtlich oder sinngemäß aus anderen Werken übernommene Inhalte als solche kenntlich gemacht.

3. Die Arbeit oder Teile davon habe ich bislang nicht an einer Hochschule des In- oder Auslands als Bestandteil einer Prüfungs- oder Qualifikationsleistung vorgelegt.

4. Die Richtigkeit der vorstehenden Erklärungen bestätige ich.

5. Die Bedeutung der eidesstattlichen Versicherung und die strafrechtlichen Folgen einer unrichtigen oder unvollständigen eidesstattlichen Versicherung sind mir bekannt.

Ich versichere an Eides statt, dass ich nach bestem Wissen die reine Wahrheit erklärt und nichts verschwiegen habe.

Karlsruhe, den 20. November 2019

. . . .
(Philipp Basler)

"We don't make mistakes, just happy little accidents."

Bob Ross

Abstract

With the measurement of the Higgs boson in 2012 the last particle of the Standard Model of particle physics was found. While its predictions are compatible with the measurements at particle collider experiments, there are many questions which cannot be answered in the Standard Model. Among these open questions is the stability of the vacuum of the Standard Model at high energies as well as the generation of the observed matter-antimatter asymmetry of the universe. To combine these two open questions with the measured constraints from particle collider experiments, theories beyond the Standard Model are investigated.

In this thesis the 2-Higgs-Doublet Model, in its charge-parity-conserving and -violating realisation, and the Next-to-2-Higgs-Doublet Model are investigated as specific realisations to extend the Higgs potential of the Standard Model. For both realisations of the 2-Higgs-Doublet Model the stability of the vacuum at higher energies is calculated. An important ingredient for the matter-antimatter asymmetry of the universe and other effects in the early universe is the electroweak phase transition. During this thesis, the `C++` code `BSMPT` has been developed and published, allowing for the numerical evaluation of the strength of the electroweak phase transition. Through its modular setup `BSMPT` can be adapted for other realisations of physics beyond the Standard Model. This thesis shows the effects of requiring a strong first-order electroweak phase transition on the parameter space of both models. As the charge-parity violating 2-Higgs-Doublet Model provides all necessary ingredients to generate a matter-antimatter asymmetry, it is calculated in this thesis. These calculations are then combined with experimental constraints from particle collider experiments to show the effect on the parameter space of the model.

Zusammenfassung

Mit der Messung des Higgs-Bosons im Jahr 2012 wurde das letzte Elementarteilchen des Standardmodells der Teilchenphysik gefunden. Obwohl dessen Vorhersagen kompatibel mit den Messungen an Teilchenbeschleuniger-Experimenten sind, gibt es noch viele offene Fragen, die vom Standardmodell der Teilchenphysik nicht beantwortet werden können. Zu diesen Fragen gehören unter anderem die Stabilität des Vakuums bei hohen Energien oder die gemessene Asymmetrie zwischen Materie und Antimaterie im Universum. Um diese beiden Fragen mit den Ergebnissen von Teilchenbeschleuniger-Experimenten zu kombinieren, werden verschiedene Theorien mit Physik jenseits des Standardmodells der Teilchenphysik untersucht.

In dieser Arbeit werden hierfür das Zwei-Higgs-Dublett Modell, sowohl in seiner ladungs- und paritätserhaltenden als auch verletzenden Variante, und das Nichtminimale Zwei-Higgs-Dublett Modell als konkrete Modelle für die Erweiterung des Higgs Potentials des Standardmodells untersucht. Für beide Varianten des Zwei-Higgs-Dublett Modells wird die Stabilität des Vakuums bei hohen Energien berechnet. Eine wichtige Komponente für die Asymmetrie zwischen Materie und Antimaterie im Universum und andere Effekte im frühen Universum ist der elektroschwache Phasenübergang. Während dieser Arbeit wurde hierfür der C++ Code `BSMPT` entwickelt und veröffentlicht, welcher die numerische Berechnung der Stärke des elektroschwachen Phasenübergangs ermöglicht. Durch den modularen Aufbau können neue Modelle für Physik jenseits des Standardmodells in `BSMPT` implementiert werden. Diese Arbeit zeigt den Effekt, den die Forderung eines elektroschwachen Phasenübergangs starker erster Ordnung auf den möglichen Parameterraum beider Modelle hat. Da das ladungs- und paritätsverletzende Zwei-Higgs-Dublett Modell alle notwendigen Bausteine für Entstehung einer Asymmetrie zwischen Materie und Antimaterie zur Verfügung stellt, wurde diese während

dieser Arbeit ausgerechnet. Diese Rechnungen werden abschließend mit den Ergebnissen aktueller Teilchenbeschleuniger-Experimente kombiniert und der Effekt auf den möglichen Parameterraum des Modells dargestellt.

List of Publications

This thesis is based on the following publications:

[1] P. Basler, M. Krause, M. Muhlleitner, J. Wittbrodt, and A. Wlotzka. "Strong First Order Electroweak Phase Transition in the CP-Conserving 2HDM Revisited". In: *JHEP* 02 (2016), p. 121. DOI: `10.1007/JHEP02(2017)121`. arXiv: `1612.04086 [hep-ph]`.

[2] Philipp Basler, Pedro M. Ferreira, Margarete Mühlleitner, and Rui Santos. "High scale impact in alignment and decoupling in two-Higgs doublet models". In: *Phys. Rev. D 97, 095024 (2018)* 97.9 (Oct. 28, 2017). DOI: `10.1103/PhysRevD.97.095024`. arXiv: `1710.10410v2 [hep-ph]`.

[3] Philipp Basler, Margarete Mühlleitner, and Jonas Wittbrodt. "The CP-Violating 2HDM in Light of a Strong First Order Electroweak Phase Transition and Implications for Higgs Pair Production". In: *JHEP* 03 (2018), p. 061. DOI: `10.1007/JHEP03(2018)061`. arXiv: `1711.04097 [hep-ph]`.

[4] Philipp Basler and Margarete Mühlleitner. "BSMPT - Beyond the Standard Model Phase Transitions -A Tool for the Electroweak Phase Transition in Extended Higgs Sectors". In: *Comput. Phys. Commun.* 237 (2019), pp. 62–85. DOI: `10.1016/j.cpc.2018.11.006`. arXiv: `1803.02846 [hep-ph]`.

[5] Philipp Basler, Margarete Mühlleitner, and Jonas Müller. "Electroweak Phase Transition in Non-Minimal Higgs Sectors". to be published.

List of Abbreviations

2HDM 2-Higgs-Doublet Model

BAU baryon asymmetry of the universe

BSM beyond the Standard Model

C2HDM CP-violating 2HDM

CB charge breaking

CKM Cabibbo-Kobayashi-Maskawa

DM Dark Matter

EDM electric dipole moment

EWBG electroweak baryogenesis

EWPD electroweak precision data

EWPT electroweak phase transition

FCNC Flavour Changing Neutral Current

HTL hard thermal loop

LO leading-order

N2HDM Next-to-2-Higgs-Doublet Model

NLO next-to-leading-order

ODE ordinary differential equation

QED quantum electrodynamics

QCD quantum chronodynamics

R2HDM CP-conserving 2HDM

RGE renormalization group equation

SFOEWPT strong first-order electroweak phase transition

SM Standard Model

VEV vacuum expectation value

Contents

Introduction

Since the discovery of the Higgs boson in 2012 [6, 7], the mass of the Higgs boson has been measured with very good accuracy [8] and its measured couplings to the Standard Model (SM) particles are very SM-like [9]. Despite the good agreement between the SM and results from collider experiments, there are still many open questions in physics which it cannot answer, eg. the one for the nature of Dark Matter (DM) or the measured baryon asymmetry of the universe (BAU). These questions call for physics beyond the Standard Model (BSM). Many BSM theories have an extended Higgs sector, each with a more complex potential and vacuum than the SM. The structure of the vacuum defines the masses of the Higgs bosons of these extended Higgs sectors and their couplings to other particles. The good understanding of the vacuum structure is therefore crucial when confronting these models with experimental constraints. This thesis deals with two aspects of the vacuum structures of extended Higgs sectors. The first aspect is the stability of the vacuum at high energies. While the vacuum of the SM is only metastable [10], the inclusion of additional Higgs bosons can yield a stable vacuum [2, 11–19]. The other aspect is the generation of the measured BAU. Assuming the universe started in a symmetric phase with an equal amount of matter and antimatter, there must have been a dynamical mechanism to generate the measured BAU. The experimentally measured quantity is given by the ratio of the difference between the number of baryons n_b and antibaryons $n_{\bar{b}}$, given by the dimensionless quantity [20]

$$\eta = \frac{n_b - n_{\bar{b}}}{s} = (6.2 \pm 0.4) \cdot 10^{-10} \,, \tag{1.1}$$

where the difference is normalised to the entropy density s of the universe which is proportional to the number of photons in the universe. The order of magnitude of η shows that there are about six baryons per 10^{10} photons in the universe. For a dynamical generation of the baryon asymmetry, Sakharov postulated three necessary criteria [21], namely the departure from thermal equilibrium, violation of charge conjugation (C) and charge conjugation parity violation (CP-violation) and baryon number violating processes. If these criteria are fulfilled, electroweak baryogenesis (EWBG) [22] provides a mechanism to generate a baryon-antibaryon asymmetry during the electroweak phase transition (EWPT) [23]. While the SM provides a source of CP-violation with the complex phase of the Cabibbo-Kobayashi-Maskawa (CKM)-matrix [20], the measured CP-violation is too suppressed to provide successful EWBG [24].

Additionally, the Higgs mass of the SM is too heavy to provide an EWPT of strong first-order [25–27], necessary for the departure from thermal equilibrium [28].

The goal of this thesis is to investigate different extensions of the SM with respect to vacuum stability at high scales, the possibility of a strong first-order electroweak phase transition (SFOEWPT) and the production of the measured BAU. As the CP-violation in the CKM-matrix is not enough for successful EWBG, the most straightforward extension of the SM including additional sources of CP-violation is the 2-Higgs-Doublet Model (2HDM) [29]. While the 2HDM extends the SM by an additional Higgs doublet, the Next-to-2-Higgs-Doublet Model (N2HDM) extends the 2HDM by an extra Higgs singlet. Both models provide a rich phenomenology, a stable vacuum at high energies and an SFOEWPT. Combining the additional CP-violation with the SFOEWPT, the CP-violating 2HDM (C2HDM) can describe a successful EWBG.

The 2HDM, both the CP-conserving 2HDM (R2HDM) and C2HDM, and the N2HDM are introduced in Chapter 2.
In Chapter 3 the effects of requiring a stable vacuum at high energies in the R2HDM and C2HDM are investigated. While part of the results in the R2HDM was already published in [2], the study has been extended to the C2HDM and new results are presented here.
The calculation of the EWPT requires the extension of the theory to include finite temperature effects. The basics on how to include them and the calculation of the strength of the EWPT are described in Chapter 4. Additionally, this chapter describes the general formalism which is implemented in the `C++` code `Beyond the Standard Model Phase Transitions` (BSMPT) [4].
While previous studies in the R2HDM and C2HDM completed during this thesis have been published in [1, 3], Chapter 5 updates the results in the C2HDM with up-to-date constraints from collider experiments and studies the effects of requiring an SFOEWPT in the C2HDM and N2HDM.
As the C2HDM can provide an SFOEWPT as well as additional sources of CP-violation [29], it is a possible candidate for successful EWBG. In Chapter 6 the calculation of the necessary ingredients to calculate the BAU are presented as well as the comparison of different numerical approaches on how to calculate these ingredients. Although no parameter point fulfilling the current experimental constraints provides a successful EWBG, it is shown that EWBG is possible in the C2HDM without including the experimental constraints.
In Chapter 7 a final conclusion and suggestions on how to extend the provided models to combine up-to-date experimental constraints with EWBG are given.
For the calculations in Chapter 3 the renormalization group equations (RGEs) of the R2HDM and C2HDM are necessary, which are presented in Appendix A. Additionally, during the calculation of the EWPT in Chapter 4 the counterterm potential is introduced to match the input parameters with the parameters of the theory. The necessary formulae for the parameters of the counterterm potential in the C2HDM and N2HDM are given in Appendix B.

Beyond the Standard Model Theories

In this chapter, the SM and all models that are considered in this thesis are introduced. Also, the notation and conventions used in this work are set. For further details on the models, additional references will be given.

In the following, a complex number will be described by its real and imaginary part as

$$x = \Re x + i \Im x \,. \tag{2.1}$$

2.1. The Standard Model of Particle Physics

The SM is a gauge theory with a local $SU(3)_C \times SU(2)_L \times U(1)_Y$ gauge group [30–32]. The $SU(3)_C$ is the gauge group of quantum chronodynamics (QCD) with massless gluons as the corresponding gauge bosons. The electroweak gauge group $SU(2)_L \times U(1)_Y$ unifies the weak and electromagnetic forces. One of the problems of the SM was given by the masses of the gauge bosons. While the electroweak symmetry required them to be massless, otherwise the gauge invariance would be violated, they were measured to have a finite mass [33–35]. A solution to this problem is the Higgs mechanism [36–40], postulated in the 1960s. The Higgs particle was discovered in 2012 by the ATLAS and CMS collaboration [6, 7] with a mass of [8]

$$m_h = 125.09 \pm 0.21(\text{stat}) \pm 0.11(\text{syst}) \,\text{GeV} \,. \tag{2.2}$$

The SM Higgs potential introducing the Higgs mechanism is given by

$$V = \mu^2 \phi^\dagger \phi + \lambda \left(\phi^\dagger \phi \right)^2 \,, \tag{2.3}$$

which is minimised by

$$\langle \phi^\dagger \phi \rangle = \frac{v^2}{2} = \frac{-\mu^2}{2\lambda} \,. \tag{2.4}$$

This minimum can only be a global minimum if the potential is bounded from below, requiring $\lambda > 0$. The necessary condition Eq. (2.4) requires $\mu^2 < 0$ such that this is a minimum of

the potential. The resulting vacuum expectation value (VEV) v spontaneously breaks the $SU(2)_L \times U(1)_Y$ down to the $U(1)_{em}$ symmetry group of quantum electrodynamics (QED). Because of this, the Higgs doublet can be written as

$$\phi = \frac{1}{\sqrt{2}} \begin{pmatrix} \theta_1 + i\theta_2 \\ v + h + i\theta_3 \end{pmatrix} \tag{2.5}$$

after electroweak symmetry breaking, where the three degrees of freedom $\theta_{1,2,3}$ can be rotated away by a $SU(2)_L$ gauge transformation. In the unitarity gauge they will correspond to the longitudinal modes of the massive gauge bosons. The Higgs mechanism induces the masses of the gauge bosons through the mixing term in the kinetic part of the Lagrangian. It reads

$$\mathcal{L}_{H,kin} = (D_\mu \phi)^\dagger (D^\mu \phi) \tag{2.6}$$

with the covariant derivative given by

$$D_\mu = \partial_\mu - i\frac{g_2}{2} W_\mu^a \sigma^a - i\frac{g_1}{2} B_\mu \,. \tag{2.7}$$

Here B_μ describes the $U(1)_Y$ gauge field and W_μ^a, with $a = 1, 2, 3$, the $SU(2)_L$ gauge fields. σ^a are the Pauli matrices and generators of the $SU(2)_L$ gauge group with the corresponding gauge couplings g_1 and g_2. Inserting Eq. (2.5) into Eq. (2.6) yields bilinear terms in B_μ and W_μ^a. After rotating B_μ and W_μ^a in the mass basis, with the W and Z boson and the photon γ as the physical gauge bosons, the bilinear terms yields the masses of the W and Z boson as

$$m_W^2 = \frac{g_2^2 v^2}{4} \,, \qquad m_Z^2 = \frac{(g_1^2 + g_2^2) v^2}{4} \,. \tag{2.8}$$

As the $U(1)_{em}$ is not broken, the photon remains massless. Additionally, the resulting interaction term between two gauge bosons and one Higgs boson solves another problem which occurred before the introduction of the Higgs mechanism in the SM. Through the new contributions of the Higgs boson, the scattering amplitude for longitudinal W bosons into a pair of longitudinal W bosons becomes finite for high energies [41] and therefore perturbative unitarity is restored, if the coupling between the Higgs boson and two gauge bosons is proportional to the mass of the gauge boson squared.

Similar to the W and Z Boson masses, explicit fermion masses would break the chiral symmetry of the theory. Through the Higgs mechanism, they can be generated through the Yukawa interaction Lagrangian

$$-\mathcal{L}_{yuk} = \overline{Q}'_L Y_d \phi D'_R - \overline{Q}'_{L,a} Y_u \epsilon^{ab} \phi_b^\dagger U_R + \overline{L}_L Y_e \phi E_R + h.c. \tag{2.9}$$

with $\epsilon^{12} = -1 = -\epsilon^{21}$ and $\epsilon^{11} = \epsilon^{22} = 0$. Here Q'_L denotes the $SU(2)$ left-handed quark doublet, U_R and D'_R the right-handed up-type and down-type quarks. L_L and E_R denote the left-handed $SU(2)_L$ lepton doublet and the right-handed leptons. They relate to the quarks and leptons through the left- and right-handed chiral projectors $P_{L,R} = \frac{1 \mp \gamma_5}{2}$. The quarks and leptons are given through

$$Q' = \begin{pmatrix} U \\ D' \end{pmatrix} = \begin{pmatrix} U \\ VD \end{pmatrix} \tag{2.10}$$

$$L = \begin{pmatrix} v \\ E \end{pmatrix} \,. \tag{2.11}$$

Here $'$ denotes the flavour basis in the cases where the flavour basis is not equal to the mass basis. The CKM Matrix, which diagonalises the down-type quarks, is denoted by V [42, 43][1]. The neutrinos are denoted by ν. The multipletts are given by

$$
D = \begin{pmatrix} d \\ s \\ b \end{pmatrix}, \qquad U = \begin{pmatrix} u \\ c \\ t \end{pmatrix}, \tag{2.12}
$$

$$
E = \begin{pmatrix} e \\ \mu \\ \tau \end{pmatrix}, \qquad \nu = \begin{pmatrix} \nu_e \\ \nu_\mu \\ \nu_\tau \end{pmatrix}. \tag{2.13}
$$

2.2. The 2-Higgs-Doublet Model

2.2.1. The Higgs Potential

The 2HDM [46–48] is an extension of the SM by an additional $SU(2)_L$ Higgs doublet. The Higgs Lagrangian is given by

$$
\mathcal{L} = \sum_{i=1}^{2} \left(D_\mu \Phi_i\right)^\dagger \left(D^\mu \Phi_i\right) - V_{\text{2HDM}}. \tag{2.14}
$$

As in the SM, the covariant derivative is given by

$$
D_\mu = \partial_\mu - \mathrm{i}\left(\frac{g_1}{2} Y B_\mu + \frac{g_2}{2}\vec{\sigma}\vec{W}_\mu\right). \tag{2.15}
$$

To avoid Flavour Changing Neutral Currents (FCNCs) at tree level, a discrete $\mathbb{Z}_2$ symmetry of the form $\Phi_1 \to \Phi_1, \Phi_2 \to -\Phi_2$ is imposed. The Higgs potential which softly breaks this $\mathbb{Z}_2$ symmetry is given by

$$
V_{\text{2HDM}} = m_{11}^2 \Phi_1^\dagger \Phi_1 + m_{22}^2 \Phi_2^\dagger \Phi_2 + \frac{\lambda_1}{2}\left(\Phi_1^\dagger \Phi_1\right)^2 + \frac{\lambda_2}{2}\left(\Phi_2^\dagger \Phi_2\right)^2 + \lambda_3 \left(\Phi_1^\dagger \Phi_1\right)\left(\Phi_2^\dagger \Phi_2\right)
$$
$$
+ \lambda_4 \left(\Phi_1^\dagger \Phi_2\right)\left(\Phi_2^\dagger \Phi_1\right) + \left[\frac{\lambda_5}{2}\left(\Phi_1^\dagger \Phi_2\right)^2 - m_{12}^2\left(\Phi_1^\dagger \Phi_2\right) + h.c.\right], \tag{2.16}
$$

where m_{ij}^2 are mass parameters and λ_i are quartic couplings. Due to the hermicity of the potential m_{11}^2, m_{22}^2 and λ_1 to λ_4 have to be real while m_{12}^2 and λ_5 can be complex. Although the $\mathbb{Z}_2$-symmetry is imposed the term m_{12}^2 is included which violates this symmetry. As this term has mass dimension 2 this symmetry is only softly broken. The broken $\mathbb{Z}_2$-symmetry induces FCNCs, which are heavily constrained [49] and can be avoided at tree level, as described in Sec. 2.2.6.2. As shown later in Sec. 2.2.2 the complex phase of the $\mathbb{Z}_2$ breaking parameter m_{12}^2 introduces CP-violation [29].

After the electroweak symmetry breaking the doublets are given by

$$
\Phi_1 = \frac{1}{\sqrt{2}}\begin{pmatrix} \rho_1 + \mathrm{i}\eta_1 \\ \zeta_1 + \omega_1 + \mathrm{i}\psi_1 \end{pmatrix} \qquad \Phi_2 = \frac{1}{\sqrt{2}}\begin{pmatrix} \rho_2 + \omega_{\text{CB}} + \mathrm{i}\eta_2 \\ \zeta_2 + \omega_2 + \mathrm{i}\left(\psi_2 + \omega_{CP}\right) \end{pmatrix}. \tag{2.17}
$$

---

[1]While the CP-violation in the CKM Matrix is too suppressed in the SM to provide a successful EWBG [44], there are other approaches varying the Yukawa coupling simultaneously to achieve EWBG [45].

Here $\rho_{1,2}, \eta_{1,2}$ describe the real fields of the charged components, $\zeta_{1,2}$ are the CP-even components of the neutral fields and $\psi_{1,2}$ are the CP-odd components. The doublet Φ_1 has the same structure as in the SM while the second doublet has an additional CP-odd VEV ω_{CP} and a charge breaking (CB) VEV ω_{CB}[2]. These allow for the global minimum of the potential to be either CB or CP-violating. It was shown in [50–54] that two different kinds of minima in the 2HDM cannot co-exist. As the current vacuum has a CP-even structure, the charge breaking and CP-odd VEV have to be saddle points of the potential at tree level. Mathematically two CP-even minima can coexist. To avoid the so-called Panic vacuum [55, 56] solution, describing the scenario that our minimum is not the global one and therefore not stable, the allowed parameter space of the theory will be constrained such that our minimum is the global one. Furthermore, the CB minimum yields non-vanishing photon masses and is therefore unphysical. In general, it is always possible to absorb the CP-odd VEV in the parameters λ_5 and m_{12}^2 through rewriting the second doublet as

$$\Phi_2 = \frac{1}{\sqrt{2}} \begin{pmatrix} \rho_2' + \omega_{CB} \exp(-\mathrm{i}\phi_\omega) + \mathrm{i}\eta_2' \\ \zeta_2' + \tilde{\omega}_2 + \mathrm{i}\psi_2' \end{pmatrix} \exp(\mathrm{i}\phi_\omega) = \tilde{\Phi}_2 \exp(\mathrm{i}\phi_\omega) \qquad (2.18)$$

with

$$\tilde{\omega}_2 \exp(\mathrm{i}\phi_\omega) = \omega_2 + \mathrm{i}\omega_{\mathrm{CP}}\,. \qquad (2.19)$$

By rewriting λ_5 and m_{12}^2 in terms of their absolute values and phases the last term of the potential can be rewritten as

$$\frac{\lambda_5}{2}\left(\Phi_1^\dagger \Phi_2\right)^2 - m_{12}^2 \Phi_1^\dagger \Phi_2 = \frac{|\lambda_5|}{2}\left(\Phi_1^\dagger \tilde{\Phi}_2\right)^2 \exp\left(\mathrm{i}\left(\phi_{\lambda_5} + 2\phi_\omega\right)\right)$$
$$- |m_{12}^2|\Phi_1^\dagger \tilde{\Phi}_2 \exp\left(\mathrm{i}\left(\phi_{m_{12}^2} + \phi_\omega\right)\right) \qquad (2.20)$$
$$= \frac{\tilde{\lambda}_5}{2}\left(\Phi_1^\dagger \tilde{\Phi}_2\right)^2 - \tilde{m}_{12}^2 \Phi_1^\dagger \tilde{\Phi}_2\,, \qquad (2.21)$$

with the redefined

$$\tilde{\lambda}_5 \equiv |\lambda_5| \exp(\mathrm{i}\left(\phi_{\lambda_5} + 2\phi_\omega\right) = \lambda_5 \exp(2\mathrm{i}\phi_\omega)\,, \qquad (2.22)$$
$$\tilde{m}_{12}^2 \equiv |m_{12}^2| \exp\left(\mathrm{i}\left(\phi_{m_{12}^2} + \phi_\omega\right)\right) = m_{12}^2 \exp(\mathrm{i}\phi_\omega)\,. \qquad (2.23)$$

It is therefore possible to absorb the phase of the VEV of the neutral component of the second doublet into λ_5 and m_{12}^2 at tree level. As the potential depends only on the redefined phases of those parameters, it is therefore possible to set $\omega_{\mathrm{CP}} = 0$. Nonetheless the CP-violating and CB VEVs are kept in the calculation to check for transitions into different vacua and spontaneous CP-violation induced through higher-order and finite temperature effects. To discuss the possible changes in the VEVs it is useful to fix the VEVs of the present vacuum at vanishing temperature with a different notation, namely

$$(\omega_1)_{\mathrm{input}} = v_1\,, \qquad (2.24)$$
$$(\omega_2)_{\mathrm{input}} = v_2\,. \qquad (2.25)$$

In order to obtain the W and Z Boson masses of the SM, the VEVs are subject to the constraint

$$v_1^2 + v_2^2 = v^2\,, \qquad (2.26)$$

---

[2]While technically Φ_1 can have VEVs in these components, they can be rotated away into Φ_2 and are neglected here.

where v is the VEV of the SM with $v \approx 246.22\,\text{GeV}$ [57]. Introducing the mixing angle β defined as

$$\tan \beta = \frac{v_2}{v_1} \tag{2.27}$$

yields the following relations for v_1 and v_2

$$v_1 = v \sin \beta \qquad v_2 = v \cos \beta \,. \tag{2.28}$$

Overall the Higgs potential, cf. Eq. (2.16), is defined by the following ten Lagrange parameters

$$\{m_{11}^2, m_{22}^2, \lambda_1, \lambda_2, \lambda_3, \lambda_4, \Re\lambda_5, \Im\lambda_5, \Re m_{12}^2, \Im m_{12}^2\} \,.$$

As noted before, the non-vanishing imaginary parts of λ_5 and m_{12}^2 yield CP-violation, while the model is CP-conserving if they vanish. This will be discussed in detail in Sec. 2.2.3.

2.2.2. The Electroweak Minimum

In order to ensure the minimum of the potential today, meaning at vanishing temperature[3] to be at

$$\langle \Phi_1 \rangle = \frac{1}{\sqrt{2}} \begin{pmatrix} 0 \\ v_1 \end{pmatrix} \,, \qquad \langle \Phi_2 \rangle = \frac{1}{\sqrt{2}} \begin{pmatrix} 0 \\ v_2 \end{pmatrix} \tag{2.29}$$

it is necessary that Eq. (2.29) solves the necessary minimum condition

$$\left. \frac{\partial V}{\partial \Phi_a^\dagger} \right|_{\Phi_1 = \langle \Phi_1 \rangle, \Phi_2 = \langle \Phi_2 \rangle} \overset{!}{=} 0 \qquad a \in \{1, 2\} \,. \tag{2.30}$$

This yields the tadpole relations

$$\Re m_{12}^2 v_2 - m_{11}^2 v_1 = \frac{v_1}{2} \left(\lambda_1 v_1^2 + (\lambda_3 + \lambda_4 + \Re\lambda_5) v_2^2 \right) \,, \tag{2.31a}$$

$$\Re m_{12}^2 v_1 - m_{22}^2 v_2 = \frac{v_2}{2} \left(\lambda_2 v_2^2 + (\lambda_3 + \lambda_4 + \Re\lambda_5) v_1^2 \right) \,, \tag{2.31b}$$

$$\Im m_{12}^2 v_2 = \frac{1}{2} v_1 v_2^2 \Im\lambda_5 \,. \tag{2.31c}$$

Assuming that $v_1, v_2 \neq 0$ it is possible to use Eqs. (2.31a) and (2.31b) to exchange m_{11}^2 and m_{22}^2 for v_1 and v_2 as input parameters. Eq. (2.31c) can be used the eliminate $\Im m_{12}^2$ as a free parameter and reduce the number of free parameters by one. The replacement rules are given by

$$m_{11}^2 = \Re m_{12}^2 \frac{v_2}{v_1} - \frac{\lambda_1}{2} v_1^2 - \frac{\lambda_3 + \lambda_4 + \Re\lambda_5}{2} v_2^2 \,, \tag{2.32a}$$

$$m_{22}^2 = \Re m_{12}^2 \frac{v_1}{v_2} - \frac{\lambda_2}{2} v_2^2 - \frac{\lambda_3 + \lambda_4 + \Re\lambda_5}{2} v_1^2 \,, \tag{2.32b}$$

$$\Im m_{12}^2 = \Im\lambda_5 \frac{v_1 v_2}{2} \,. \tag{2.32c}$$

Applying these, the model is left with nine independent parameters

$$\{\lambda_1, \lambda_2, \lambda_3, \lambda_4, \Re\lambda_5, \Im\lambda_5, \Re m_{12}^2, \tan \beta, v\} \,, \tag{2.33}$$

with only one free complex phase $\phi_{\lambda_5} = \arg(\lambda_5)$.

---

[3]While the background temperature of the universe strictly speaking is given by $T = 2.7\,\text{K} \approx 10^{-13}\,\text{GeV}$ the numerical influence can be neglected.

2.2.3. CP-Violation

One of the great merits of the 2HDM compared to the SM is the possibility to have CP-violation already at tree level in the potential. For this it is neccesary that at least one of the four CP invariants I_1 to I_4 or one of the three CP invariants J_1 to J_3, given in [48], do not vanish. In the 2HDM the CP invariants I_1 to I_4, that check for explicit CP-violation in the potential, are given by [48][4]

$$I_1 = 2\mathrm{i}\left[\left(\left(\Im m_{12}^2\right)^2 - \left(\Re m_{12}^2\right)^2\right)\Im\lambda_5 + 2\Im m_{12}^2\,\Re\lambda_5\,\Re m_{12}^2\right](\lambda_1 - \lambda_2)\,, \qquad (2.34\text{a})$$

$$I_2 = 0\,, \qquad (2.34\text{b})$$

$$I_3 = 0\,, \qquad (2.34\text{c})$$

$$I_4 = \left(m_{22}^2 - m_{11}^2\right)\left[(\lambda_1 - \lambda_3 - \lambda_4)(\lambda_2 - \lambda_3 - \lambda_4) - \left(\Re\lambda_5^2 + \Im\lambda_5^2\right)\right]$$
$$\times\left[\left(\left(\Re m_{12}^2\right)^2 - \left(\Im m_{12}^2\right)^2\right)\Im\lambda_5 - 2\Im m_{12}^2\,\Re\lambda_5\,\Re m_{12}^2\right]\,. \qquad (2.34\text{d})$$

The CP invariants J_1 to J_3, checking for spontaneous CP-violation in the vacuum, read as

$$J_1 = \frac{1}{16}\Im m_{12}^2\,(\lambda_1 - \lambda_2)\,v_1 v_2\,, \qquad (2.35\text{a})$$

$$J_2 = \frac{m_{11}^2 - m_{22}^2}{32}\left((\lambda_1 + \lambda_2 - 2\lambda_3 - 2\lambda_4 + 2\Re\lambda_5)\Im m_{12}^2 - 2\Re m_{12}^2\,\Im\lambda_5\right)v_1 v_2$$
$$+ \frac{1}{16}\left(v_1^2 - v_2^2\right)\left(\left(\Im m_{12}^2 - \Re m_{12}^2\right)\Im\lambda_5 + 2\Re m_{12}^2\,\Im m_{12}^2\,\Re\lambda_5\right)\,, \qquad (2.35\text{b})$$

$$J_3 = 0\,. \qquad (2.35\text{c})$$

There are two non-trivial cases[5] in which the invariants I_1 to I_4 and J_1 to J_3 vanish. The first case is given by $\Im\lambda_5 = 0$ which leads to $\Im m_{12}^2 = 0$ through Eq. (2.31c). This is expected as a potential with only real parameters does not have mixed couplings between CP-even and CP-odd fields. The other case is given by setting $\lambda_1 = \lambda_2$ and $m_{11}^2 = m_{22}^2$ which implies $v_1 = v_2$ through the tadpole equations Eqs. (2.31a) and (2.31b), yielding $\tan\beta = 1$. While this parameter choice yields vanishing CP invariants, the model is still CP-violating through the couplings of the Higgs bosons with the fermions [58], as the symmetry implying $\lambda_1 = \lambda_2$ and $\tan\beta = 1$ also needs to be imposed on the fermion sector.

For the remainder of this work, the case $\Im\lambda_5 = 0$ will be referred to as the R2HDM, while C2HDM describes the case $\Im\lambda_5 \neq 0$, and 2HDM if the discussion is independent of the choice of $\Im\lambda_5$.

2.2.4. The Higgs Spectrum of the 2HDM

The Higgs spectrum of the 2HDM is given by a charged Higgs-pair $H^\pm$ and three neutral Higgs bosons $h_{1,2,3}$. In the R2HDM two of them are CP-even and one is CP-odd while in the C2HDM all three neutral Higgs states mix and are CP-violating. The charged scalar sector is rotated to the mass eigenbasis by

$$\begin{pmatrix} G^+ \\ H^+ \end{pmatrix} = \begin{pmatrix} \cos\beta & \sin\beta \\ -\sin\beta & \cos\beta \end{pmatrix}\begin{pmatrix} \frac{1}{\sqrt{2}}\left(\rho_1 + \mathrm{i}\eta_1\right) \\ \frac{1}{\sqrt{2}}\left(\rho_2 + \mathrm{i}\eta_2\right) \end{pmatrix}\,, \qquad (2.36)$$

---

[4]While the parameters m_{11}^2, m_{22}^2 and $\Im m_{12}^2$ can be expressed through Eq. (2.32) the following expressions are expressed in a more compact form if they are not exchanged.

[5]These two cases are not the only solution of $I_1 = I_4 = J_1 = J_2 = 0$ but they are the simplest cases in which the invariants vanish.

with G^+ describing the charged and massless Goldstone boson. At tree level β coincides with $\tan\beta = v_2/v_1$. The mass of the charged Higgs boson is given by

$$m_{H^\pm}^2 = \Re m_{12}^2 \frac{v^2}{v_1 v_2} - \frac{v^2}{2}\left(\lambda_4 + \Re\lambda_5\right). \tag{2.37}$$

The same rotation matrix rotates the neutral CP-odd scalar sector into the neutral and massless Goldstone boson G^0 and the CP-odd field ζ_3, given by

$$\begin{pmatrix} G^0 \\ \zeta_3 \end{pmatrix} = \begin{pmatrix} \cos\beta & \sin\beta \\ -\sin\beta & \cos\beta \end{pmatrix} \begin{pmatrix} \psi_1 \\ \psi_2 \end{pmatrix}. \tag{2.38}$$

While ζ_3 is no mass eigenstate in the C2HDM, in the R2HDM ζ_3 describes the massive and pseudoscalar mass eigenstate A. In order to describe the interaction of the three phyiscal, massive, neutral and CP-mixing particles it is necessary to diagonalise the mass matrix of the C2HDM, given by the Hessian matrix of the potential evaluated in the electroweak minimum. In the basis $\{\zeta_1, \zeta_2, \zeta_3\}$ the mass matrix is given by

$$\mathcal{M}_N^2 = \begin{pmatrix} \lambda_1 v_1^2 + \Re m_{12}^2 \frac{v_2}{v_1} & v_1 v_2 \left(\lambda_3 + \lambda_4 + \Re\lambda_5\right) - \Re m_{12}^2 & -\Im\lambda_5 \frac{v v_2}{2} \\ v_1 v_2 \left(\lambda_3 + \lambda_4 + \Re\lambda_5\right) - \Re m_{12}^2 & \lambda_2 v_2^2 + \Re m_{12}^2 \frac{v_1}{v_2} & -\Im\lambda_5 \frac{v v_1}{2} \\ -\Im\lambda_5 \frac{v v_2}{2} & -\Im\lambda_5 \frac{v v_1}{2} & \Re m_{12}^2 \frac{v^2}{v_1 v_2} - \Re\lambda_5 \end{pmatrix}. \tag{2.39}$$

In the R2HDM Eq. (2.39) simplifies to

$$\mathcal{M}_N^{2,\text{R2HDM}} = \begin{pmatrix} \lambda_1 v_1^2 + \Re m_{12}^2 \frac{v_2}{v_1} & v_1 v_2 \left(\lambda_3 + \lambda_4 + \Re\lambda_5\right) - \Re m_{12}^2 & 0 \\ v_1 v_2 \left(\lambda_3 + \lambda_4 + \Re\lambda_5\right) - \Re m_{12}^2 & \lambda_2 v_2^2 + \Re m_{12}^2 \frac{v_1}{v_2} & 0 \\ 0 & 0 & \Re m_{12}^2 \frac{v^2}{v_1 v_2} - \Re\lambda_5 v^2 \end{pmatrix}, \tag{2.40}$$

with the eigenvalues

$$m_h^2 = \frac{1}{2}\left[\lambda_1 v_1^2 + \lambda_2 v_2^2 + \Re m_{12}^2 \left(\frac{v_2}{v_1} + \frac{v_1}{v_2}\right)\right]$$
$$- \frac{1}{2}\sqrt{\left(\lambda_1 v_1^2 - \lambda_2 v_2^2 + \Re m_{12}^2 \left(\frac{v_2}{v_1} - \frac{v_1}{v_2}\right)\right)^2 + 4\left(v_1 v_2 \left(\lambda_3 + \lambda_4 + \Re\lambda_5\right) - \Re m_{12}^2\right)^2}, \tag{2.41a}$$

$$m_H^2 = \frac{1}{2}\left[\lambda_1 v_1^2 + \lambda_2 v_2^2 + \Re m_{12}^2 \left(\frac{v_2}{v_1} + \frac{v_1}{v_2}\right)\right]$$
$$+ \frac{1}{2}\sqrt{\left(\lambda_1 v_1^2 - \lambda_2 v_2^2 + \Re m_{12}^2 \left(\frac{v_2}{v_1} - \frac{v_1}{v_2}\right)\right)^2 + 4\left(v_1 v_2 \left(\lambda_3 + \lambda_4 + \Re\lambda_5\right) - \Re m_{12}^2\right)^2}, \tag{2.41b}$$

$$m_A^2 = \Re m_{12}^2 \frac{v^2}{v_1 v_2} - \Re\lambda_5 v^2, \tag{2.41c}$$

where A is a CP-odd particle and h and H are CP-even with $m_h^2 \leq m_H^2$.

In the most general case, Eq. (2.39) cannot be diagonalised analytically. The rotation matrix R, in its general form, is given by

$$R = \begin{pmatrix} c_1 c_2 & s_1 c_2 & s_2 \\ -(c_1 s_2 s_3 + s_1 c_3) & c_1 c_3 - s_1 s_2 s_3 & c_2 s_3 \\ -c_1 s_2 c_3 + s_1 s_3 & -(c_1 s_3 + s_1 s_2 c_3) & c_2 c_3 \end{pmatrix}, \tag{2.42}$$

with

$$c_i = \cos \alpha_i, \qquad s_i = \sin \alpha_i, \qquad -\frac{\pi}{2} \leq \alpha_i < \frac{\pi}{2}, \tag{2.43}$$

which diagonalizes Eq. (2.39) such as

$$R \mathcal{M}_N^2 R^T = \text{diag} \left(m_{h_1}^2, m_{h_2}^2, m_{h_3}^2 \right) \tag{2.44}$$

with $m_{h_1}^2 \leq m_{h_2}^2 \leq m_{h_3}^2$. Using this, together with the charged Higgs Mass, cf. Eq. (2.37), the input parameters $\{\lambda_1, \lambda_2, \lambda_3, \lambda_4, \Re\lambda_5, \Im\lambda_5\}$ can be expressed through the masses and mixing angles as [59]

$$\lambda_1 = \frac{1}{v_1^2} \left[m_{h_1}^2 c_1^2 c_2^2 + m_{h_2}^2 (c_3 s_1 + c_1 s_2 s_3)^2 + m_{h_3}^2 (c_1 s_2 c_3 - s_1 s_3)^2 - \Re m_{12}^2 \frac{v_2}{v_1} \right], \tag{2.45a}$$

$$\lambda_2 = \frac{1}{v_2^2} \left[m_{h_1}^2 s_1^2 c_2^2 + m_{h_2}^2 (c_1 c_3 - s_1 s_2 s_3)^2 + m_{h_3}^2 (s_1 s_2 c_3 + c_1 s_3)^2 - \Re m_{12}^2 \frac{v_1}{v_2} \right], \tag{2.45b}$$

$$\lambda_3 = \frac{1}{v_1 v_2} \left[\left(m_{h_1}^2 c_2^2 + m_{h_2}^2 (s_2^2 s_3^2 - c_3^2) + m_{h_3}^2 (s_2^2 c_3^2 - s_3^2) \right) c_1 s_1 + \left(m_{h_3}^2 - m_{h_2}^2 \right) (c_1^2 - s_1^2) s_2 c_3 s_3 \right]$$
$$+ \frac{1}{v^2} \left(2 m_{H^\pm}^2 - \frac{\Re m_{12}^2 v^2}{v_1 v_2} \right), \tag{2.45c}$$

$$\lambda_4 = \frac{1}{v^2} \left[m_{h_1}^2 s_2^2 + \left(m_{h_2}^2 s_3^2 + m_{h_3}^2 c_3^2 \right) c_2^2 + \frac{\Re m_{12}^2 v^2}{v_1 v_2} - 2 m_{H^\pm}^2 \right], \tag{2.45d}$$

$$\Re\lambda_5 = \frac{1}{v^2} \left[-m_{h_1}^2 s_2^2 - \left(m_{h_2}^2 s_3^2 + m_{h_3}^2 c_3^2 \right) c_2^2 + \frac{\Re m_{12}^2 v^2}{v_1 v_2} \right], \tag{2.45e}$$

$$\Im\lambda_5 = \frac{2}{v v_2} c_2 \left[\left(-m_{h_1}^2 + m_{h_2}^2 s_3^2 + m_{h_3}^2 c_3^2 \right) c_1 s_2 + \left(m_{h_2}^2 - m_{h_3}^2 \right) s_1 s_3 c_3 \right]. \tag{2.45f}$$

For the C2HDM a possible set of input parameters can be chosen as

$$\{ m_{h_1}^2, m_{h_2}^2, m_{H^\pm}^2, \alpha_1, \alpha_2, \alpha_3 \tan\beta, v \} \tag{2.46}$$

where the third mass is given by

$$m_{h_3}^2 = \frac{m_{h_1}^2 R_{13} (R_{12} \tan\beta - R_{11}) + m_{h_2}^2 R_{23} (R_{22} \tan\beta - R_{21})}{R_{33} (R_{31} - R_{32} \tan\beta)}. \tag{2.47}$$

Taking the limit

$$\alpha_2, \alpha_3 \to 0, \alpha_1 \to \alpha + \frac{\pi}{2}, h_1 \to h, h_2 \to -H, h_3 \to A \tag{2.48}$$

yields the R2HDM with the input parameters

$$\{ m_h^2, m_H^2, m_A^2, m_{H^\pm}^2, \alpha, \tan\beta, v \}. \tag{2.49}$$

In principle, it is a matter of taste which basis is chosen to describe the parameter points, but choosing the mass basis will be more efficient in the phenomenological investigation of the model as it is possible to set one of the Higgs boson masses to the measured value of 125.09 GeV.

2.2.5. Theoretical Constraints

While in principle the input parameters can be chosen freely not all combinations yield physical valid parameter points. While Eq. (2.31) ensures that Eq. (2.29) is a local minimum it has to be ensured that the potential has a global minimum such that the physics described at the present minimum is stable. As the model is described at fixed-order perturbation theory it is also necessary to ensure that the approximation parameters of the theory are small enough. As the theoretical constraints yield the same inequalities for the C2HDM and the R2HDM, the checks in the following subsection applicable for both cases if not otherwise stated.

2.2.5.1. Boundedness from below and Global Minimum

It was shown that the SM is metastable if there is no new physics until the Planck scale [60–62]. The minimum of the 2HDM, on the other hand, can be chosen stable if it is the global minimum. For this, the potential needs to be bounded from below. This is checked in the strong sense, namely that in all possible field directions the potential has to be strictly positive for the fields approaching infinity. This leads to the necessary and sufficient conditions [63–65]

$$0 < \lambda_1 \,, \tag{2.50a}$$

$$0 < \lambda_2 \,, \tag{2.50b}$$

$$-\sqrt{\lambda_1 \lambda_2} < \lambda_3 + \min(0, \lambda_4 - |\lambda_5|) \,. \tag{2.50c}$$

In principle the general form of the doublets, given in Eq. (2.17), cannot only lead to neutral, CP-conserving extrema with $\omega_{\text{CP}} = \omega_{\text{CB}} = 0$ but also lead to charge or CP-breaking ones. It was shown in [50–56] that if a CP-even solution exists it will always be the minimum of the potential and the CB and CP-violating solutions will be saddle points of the potential. Those papers found that in the C2HDM, while there can be two CP-even minima, the relation

$$\left[\left(\frac{\Re m_{12}^2}{v_1 v_2} - \frac{\Re \lambda_5}{2} \right)^2 - \frac{|\lambda_5|^2}{4} \right] \left[\frac{\Re m_{12}^2}{v_1 v_2} - \frac{\lambda_4 + \Re \lambda_5}{2} + \frac{\sqrt{\lambda_1 \lambda_2} - \lambda_3}{2} \right] \geq 0 \tag{2.51}$$

enforces our minimum to be the global one. In the R2HDM this relation can be expressed as

$$m_{12}^2 \left(m_{11}^2 - \sqrt{\frac{\lambda_1}{\lambda_2}} m_{22}^2 \right) \left(\tan \beta - \sqrt[4]{\frac{\lambda_1}{\lambda_2}} \right) \geq 0 \,. \tag{2.52}$$

2.2.5.2. Unitarity Constraints

The requirement of tree-level perturbative unitarity follows directly from the unitarity of the S-matrix [66]. Usually, this is guaranteed by all eigenvalues of the $2 \to 2$ scattering matrix to

be less than 8π. The eigenvalues of the full $2 \to 2$ scattering matrix have been calculated in [66–68] and are given by

$$a_\pm = \frac{3}{2}\left(\lambda_1 + \lambda_2\right) \pm \sqrt{\frac{9}{4}\left(\lambda_1 - \lambda_2\right)^2 + \left(2\lambda_3 + \lambda_4\right)^2}\,, \tag{2.53a}$$

$$b_\pm = \frac{1}{2}\left(\lambda_1 + \lambda_2\right) \pm \frac{1}{2}\sqrt{\left(\lambda_1 - \lambda_2\right)^2 + 4\lambda_4^2}\,, \tag{2.53b}$$

$$c_\pm = \frac{1}{2}\left(\lambda_1 + \lambda_2\right) \pm \frac{1}{2}\sqrt{\left(\lambda_1 - \lambda_2\right)^2 + 4|\lambda_5|^2}\,, \tag{2.53c}$$

$$e_1 = \lambda_3 + 2\lambda_4 - 3|\lambda_5|\,, \tag{2.53d}$$

$$e_2 = \lambda_3 - |\lambda_5|\,, \tag{2.53e}$$

$$f_+ = \lambda_3 + 2\lambda_4 + 3|\lambda_5|\,, \tag{2.53f}$$

$$f_- = \lambda_3 + |\lambda_5|\,, \tag{2.53g}$$

$$f_1 = \lambda_3 + \lambda_4\,, \tag{2.53h}$$

$$p_1 = \lambda_3 - \lambda_4\,. \tag{2.53i}$$

For the unitarity conditions the following constraints[6] are enforced

$$|a_\pm, b_\pm, c_\pm, e_{1,2}, f_\pm, f_1, p_1| < 8\pi\,. \tag{2.54}$$

2.2.6. Higgs Couplings to the SM Particles

The couplings between the SM particles and the Higgs bosons play an important role in the phenomenological discussion. As the experiments provide their signal strengths normalised to the SM the couplings will be given, whenever possible, normalised to their SM counterparts as well. While the following couplings are given for the C2HDM, the couplings for the R2HDM can be derived by applying the limit given in Eq. (2.48).

2.2.6.1. Higgs Couplings to Gauge Bosons

The couplings between Higgs and gauge bosons are given through the interaction term in the Lagrangian, namely

$$\mathcal{L}_\text{G} = \sum_{i=1}^{2}\left(D_\mu \Phi_i\right)^\dagger \left(D^\mu \Phi_i\right)\,. \tag{2.55}$$

Expressing the neutral fields of the doublets in the mass basis h_i, $i = 1, 2, 3$, the couplings normalized to the SM coupling are given by

$$c(h_i Z_\mu Z_\nu) = c(h_i W_\mu^\pm W_\nu^\mp) = \frac{c^\text{C2HDM}(h_i Z_\mu Z_\nu)}{c^\text{SM}(h Z_\mu Z_\nu)} = \cos\beta R_{i1} + \sin\beta R_{i2}\,, \tag{2.56}$$

with the SM coupling

$$c^\text{SM}(h Z_\mu Z_\nu) = \frac{v}{2}g_{\mu\nu}\left(g_1^2 + g_2^2\right) = g_{\mu\nu}\frac{2m_Z^2}{v} \tag{2.57}$$

and $g_{\mu\nu}$ as the metric tensor. The coupling between two Higgs bosons and one Z boson in the C2HDM is given by

$$c^\text{C2HDM}(Z h_j h_k) = -\frac{g}{2\cos\theta_W}\left[\left(\sin\beta R_{j1} - \cos\beta R_{j2}\right)R_{k3}\right.$$
$$\left. - \left(\sin\beta R_{k1} - \cos\beta R_{k2}\right)R_{j3}\right]\left(p_\mu^j - p_\mu^k\right)\,, \tag{2.58}$$

---

[6]While [69] found that the limit can be lower then 8π once including higher-order effects the phenomenological discussion in this work is based on tree level relations and therefore 8π as an upper limit will be used.

where $p_\mu^{j,k}$ are the incoming momenta of the two Higgs bosons. Taking the limit of the R2HDM, cf. Eq. (2.48), the coupling Eq. (2.58) vanishes unless one Higgs boson is an CP-even one, with $R_{j1}^2 + R_{j2}^2 = 1$ and $R_{j3} = 0$, and the other being the CP-odd one with $R_{k1} = R_{k2} = 0$ and $R_{k3} = 1$. In the R2HDM limit Eq. (2.56) vanishes for the pseudoscalar particle A as $R_{A1} = R_{A2} = 0$. The coupling between a neutral Higgs boson, a charged one and a W boson is given by

$$c(h_i H^\mp W^{\pm,\mu}) = \frac{g_2}{2} \left[\mp \left(\sin\beta R_{j1} - \cos\beta R_{j2} \right) + \mathrm{i} R_{j3} \right] \left(p_\mu^i - p_\mu^\mp \right) , \qquad (2.59)$$

where p_μ^i is the incoming momenta of the neutral Higgs boson and $p_\mu^\mp$ of the charged one.

2.2.6.2. Couplings to Fermions and FCNC

As in the SM, the interaction between Higgs bosons and fermions is given by the Yukawa Lagrangian. Expanding Eq. (2.9) for two Higgs doublets yields

$$-\mathcal{L}_y = \sum_{i=1}^2 \overline{Q'}_L \Gamma_i \Phi_i D'_R - \overline{Q'}_L \Delta_i \epsilon \Phi_i^* U'_R + \overline{L'}_L \Pi_i \Phi_i E'_R + h.c. , \qquad (2.60)$$

where Γ_i, Δ_i and Π_i are generic coupling matrices. The antisymmetric tensor ϵ is given by

$$\epsilon = \begin{pmatrix} 0 & -1 \\ 1 & 0 \end{pmatrix} . \qquad (2.61)$$

Expressing the doublets through their neutral and charged components, Φ_i^0 and Φ^+ respectively, the Yukawa Lagrangian can be cast into the form

$$-\mathcal{L}_y = \sum_{i=1}^2 \overline{U}_L \Gamma_i V D_R \Phi_i^+ + \overline{D}_L V^\dagger \Gamma_i V D_R \Phi_i^0 + \overline{U}_L \Delta_i U_R \Phi_i^{0*} - \overline{D}_L V^\dagger \Delta_i U_R \Phi_i^-$$
$$+ \overline{E}_L \Pi_i E_R \Phi_i^0 + \overline{\nu}_L \Pi_i E_R \Phi_i^+ + h.c. . \qquad (2.62)$$

The doublets expressed in the mass eigenstates of the C2HDM read

$$\Phi_1^\pm = c_\beta G^\pm - s_\beta H^\pm , \qquad \Phi_2^\pm = s_\beta G^\pm + c_\beta H^\pm , \qquad (2.63)$$

$$\Phi_1^0 = \frac{1}{\sqrt{2}} \left(v_1 + \rho_1 + \mathrm{i}\psi_1 \right) = \frac{1}{\sqrt{2}} \left(v_1 + (R_{j1} - \mathrm{i}s_\beta R_{j3}) h_j + \mathrm{i}c_\beta G^0 \right) , \qquad (2.64)$$

$$\Phi_2^0 = \frac{1}{\sqrt{2}} \left(v_2 + (R_{j2} + \mathrm{i}c_\beta R_{j3}) h_j + \mathrm{i}s_\beta G^0 \right) . \qquad (2.65)$$

A concern for a general Yukawa Langrangian are FCNCs. Since these are severly constrained by experimental results [70, 71] additional assumptions on the couplings to fermions are assumed to avoid FCNCs. Common practice is to assume on of the four Types I, II, Flipped (FL) and Lepton-Specific (LS) in which the up and down-type quarks and the leptons only couple to one of the both Higgs doublets. The types are categorized in Tab. 2.1. As only one doublet couples to up-type , down-type quarks and leptons in these types, it is possible to express the coupling matrices as

$$V^\dagger \Gamma_i V = \mathrm{diag}(y_d, y_s, y_b) , \qquad (2.66)$$

$$\Delta_2 = \mathrm{diag}(y_u, y_c, y_t) , \qquad (2.67)$$

$$\Pi_i = \mathrm{diag}(y_e, y_\mu, y_\tau) , \qquad (2.68)$$

Type	up-type quarks couples to	down-type quarks couple to	charged leptons couple to
Type I	Φ_2	Φ_2	Φ_2
Type II	Φ_2	Φ_1	Φ_1
LS	Φ_2	Φ_2	Φ_1
FL	Φ_2	Φ_1	Φ_2

Table 2.1.: Couplings of the fermions to the Higgs doublets

	Type I		Type II		FL		LS	
	c^e	c^o	c^e	c^o	c^e	c^o	c^e	c^o
up-type quarks	$\dfrac{R_{i2}}{\sin\beta}$	$-\dfrac{R_{i3}}{\tan\beta}$	$\dfrac{R_{i2}}{\sin\beta}$	$-\dfrac{R_{i3}}{\tan\beta}$	$\dfrac{R_{i2}}{\sin\beta}$	$-\dfrac{R_{i3}}{\tan\beta}$	$\dfrac{R_{i2}}{\sin\beta}$	$-\dfrac{R_{i3}}{\tan\beta}$
down-type quarks	$\dfrac{R_{i2}}{\sin\beta}$	$\dfrac{R_{i3}}{\tan\beta}$	$\dfrac{R_{i1}}{\cos\beta}$	$-R_{i3}\tan\beta$	$\dfrac{R_{i1}}{\cos\beta}$	$R_{i3}\tan\beta$	$\dfrac{R_{i2}}{\sin\beta}$	$-\dfrac{R_{i3}}{\tan\beta}$
leptons	$\dfrac{R_{i2}}{\sin\beta}$	$\dfrac{R_{i3}}{\tan\beta}$	$\dfrac{R_{i1}}{\cos\beta}$	$-R_{i3}\tan\beta$	$\dfrac{R_{i2}}{\sin\beta}$	$-\dfrac{R_{i3}}{\tan\beta}$	$\dfrac{R_{i1}}{\cos\beta}$	$R_{i3}\tan\beta$

Table 2.2.: The couplings between two fermions and a neutral Higgs boson h_i of the form
$\mathcal{L}_Y \supset -\dfrac{m_f}{v}\overline{f}\left(c^e(h_i f f) + \mathrm{i}\gamma_5 c^o(h_i f f)\right) f h_i$.

where the index i is the index of the Higgs doublet which couples to the corresponding fermion. The other coupling matrices vanish. The couplings between one neutral Higgs boson and two fermions, normalized to the SM, are given in Table 2.2. The masses of the fermions are then given as

$$m_u = y_u \frac{v_2}{\sqrt{2}}\,, \tag{2.69a}$$

$$m_d = y_d \frac{v_d}{\sqrt{2}}\,, \tag{2.69b}$$

$$m_l = y_l \frac{v_l}{\sqrt{2}}\,, \tag{2.69c}$$

where v_d and v_l are the VEVs of the doublets given in Table 2.1.

2.2.6.3. Couplings between three Higgs Bosons

The couplings between three neutral Higgs Bosons in the C2HDM are given by[7]

$$c(h_i h_j h_k) = \partial_{h_i}\partial_{h_j}\partial_{h_k}\mathcal{L} \tag{2.70}$$

$$= -\partial_{h_i}\partial_{h_j}\partial_{h_k}V_{\text{2HDM}}\,. \tag{2.71}$$

---

[7]Depending on the literature this definition varies as symmetry factors are sometimes included or not. For this work they are not included.

As these are rather lengthy expressions they will not be given here explicitly. They can be found on the webpage [72]. The coupling between a neutral and two charged Higgs boson is given by

$$
\begin{aligned}
c(h_i H^+ H^-) = &- \partial_{h_i} \partial_{H^+} \partial_{H^-} V_{2\text{HDM}} && (2.72) \\
= &- v \left[\Im\lambda_5 R_{i3} \cos\beta \sin\beta \right. \\
&+ R_{i1} \cos\beta \left(\lambda_3 \cos^2\beta - (\Re\lambda_5 - \lambda_1 + \lambda_4) \sin^2\beta \right) \\
&\left. + R_{i2} \sin\beta \left(-(\Re\lambda_5 - \lambda_2 + \lambda_4) \cos^2\beta + \lambda_3 \sin\beta \right) \right]. && (2.73)
\end{aligned}
$$

2.3. The Next-to-Two-Higgs-Doublet Model

2.3.1. The Higgs Potential

Based on the R2HDM a possible extension of the SM is given by adding a real, hypercharge zero, $SU(2)_L$ singlet field Φ_S to the R2HDM. This model is refered to as N2HDM [73]. The potential is given by

$$
\begin{aligned}
V_{N2HDM} = &\, m_{11}^2 |\Phi_1|^2 + m_{22}^2 |\Phi_2|^2 - m_{12}^2 \left(\Phi_1^\dagger \Phi_2 + h.c. \right) + \frac{\lambda_1}{2} |\Phi_1|^4 + \frac{\lambda_2}{2} |\Phi_2|^2 \\
&+ \lambda_3 |\Phi_1|^2 |\Phi_2|^2 + \lambda_4 |\Phi_1^\dagger \Phi_2|^2 + \frac{\lambda_5}{2} \left(\left(\Phi_1^\dagger \Phi_2 \right)^2 + h.c. \right) \\
&+ \frac{1}{2} \mu_S^2 \Phi_S^2 + \frac{\lambda_6}{8} \Phi_S^4 + \frac{\lambda_7}{2} |\Phi_1|^2 \Phi_S^2 + \frac{\lambda_8}{2} |\Phi_2|^2 \Phi_S^2,
\end{aligned} \tag{2.74}
$$

where m_{ij}^2 and μ_S^2 are mass parameters and λ_i are quartic couplings. Due to the hermicitiy of the potential all parameters must be real. As in the R2HDM the N2HDM has the $\mathbb{Z}_2$ symmetry $\Phi_1 \rightarrow \Phi_1, \Phi_2 \rightarrow -\Phi_2$ which is softly broken by the m_{12}^2 parameter. The singlet field Φ_s is expanded around its VEV

$$
\Phi_s = \zeta_s + \omega_s. \tag{2.75}
$$

Analogous to the 2HDM it is useful to label the minimum of the singlet field in the present vaccum at vanishing temperature, namely

$$
(\omega_s)_{\text{input}} = v_s. \tag{2.76}
$$

In contrast to the C2HDM, the CP-even components of the two Higgs doublets do not mix with the CP-odd component but with the singlet field. As the singlet field does not couple to gauge bosons or fermions and the massive Higgs bosons are a mixture between components of the doublets and the singlets, the couplings are reduced which influences the production and decay into SM particles. Because of the reduced couplings, it is possible to have a light Higgs boson in the spectrum which couples very weakly to the SM particles. In the limit of a vanishing singlet VEV v_s the field ζ_s is a possible DM candidate [74].

2.3.2. The Electroweak Minimum

Analogous to the R2HDM in Sec. 2.2.2 the electroweak symmetry breaking combined with the minimum of the singlet requires the present potential at vanishing temperature to be minimised at

$$
\langle \Phi_1 \rangle = \frac{1}{\sqrt{2}} \begin{pmatrix} 0 \\ v_1 \end{pmatrix}, \qquad \langle \Phi_2 \rangle = \frac{1}{\sqrt{2}} \begin{pmatrix} 0 \\ v_2 \end{pmatrix}, \qquad \langle \Phi_S \rangle = v_s. \tag{2.77}
$$

Requiring Eq. (2.77) to be a minimum of the potential, the equations

$$\frac{\partial V}{\partial \Phi_a^\dagger}\bigg|_{\Phi_1=\langle\Phi_1\rangle,\Phi_2=\langle\Phi_2\rangle,\Phi_s=\langle\Phi_s\rangle} \overset{!}{=} 0 \qquad a \in \{1,2\}, \tag{2.78}$$

$$\frac{\partial V}{\partial \Phi_s}\bigg|_{\Phi_1=\langle\Phi_1\rangle,\Phi_2=\langle\Phi_2\rangle,\Phi_s=\langle\Phi_s\rangle} \overset{!}{=} 0 \tag{2.79}$$

have to be satisfied. Simplifying these equations yields the following tadpole conditions

$$v_2 m_{12}^2 - m_{11}^2 v_1 = \frac{v_1}{2}\left(\lambda_1 v_1^2 + \lambda_{345} v_2^2 + \lambda_7 v_s^2\right), \tag{2.80a}$$

$$v_1 m_{12}^2 - m_{22}^2 v_2 = \frac{v_2}{2}\left(\lambda_2 v_2^2 + \lambda_{345} v_1^2 + \lambda_8 v_s^2\right), \tag{2.80b}$$

$$-\mu_s^2 v_s = \frac{v_s}{2}\left(\lambda_7 v_1^2 + \lambda_8 v_2^2 + \lambda_6 v_s^2\right), \tag{2.80c}$$

where the notation

$$\lambda_{345} = \lambda_3 + \lambda_4 + \lambda_5 \tag{2.81}$$

was used. In the following Eq. (2.80) is used to express $m_{11}^2, m_{22}^2, \mu_s^2$ through the other parameters in the potential.

2.3.3. The Higgs Spectrum of the N2HDM

The Higgs spectrum of the N2HDM is given by a charged Higgs pair $H^\pm$, a pseudoscalar neutral Higgs boson A and three neutral CP-even Higgs bosons h_1, h_2, h_3. The masses of the charged and pseudoscalar particle are the same as in the R2HDM and are given by

$$m_{H^\pm}^2 = \frac{m_{12}^2 v^2}{v_1 v_2} - v^2\left(\lambda_4 + \lambda_5\right), \qquad m_A^2 = \frac{m_{12}^2 v^2}{v_1 v_2} - \lambda_5 v^2. \tag{2.82}$$

The neutral CP-even mass matrix in the basis $(\zeta_1, \zeta_2, \zeta_s)$ is given by

$$\mathcal{M}_N^{\text{N2HDM}} = \begin{pmatrix} \lambda_1 v_1^2 + m_{12}^2\frac{v_2}{v_1} & v_1 v_2 \lambda_{345} - m_{12}^2 & \lambda_7 v_1 v_s \\ v_1 v_2 \lambda_{345} - m_{12}^2 & \lambda_2 v_2^2 + m_{12}^2\frac{v_1}{v_2} & \lambda_8 v_2 v_s \\ \lambda_7 v_1 v_s & \lambda_8 v_2 v_s & \lambda_6 v_s^2 \end{pmatrix}, \tag{2.83}$$

which is diagonalised by the rotation matrix R that can be parameterised the same way as in Eq. (2.42) for the C2HDM, through

$$R = \begin{pmatrix} c_1 c_2 & s_1 c_2 & s_2 \\ -(c_1 s_2 s_3 + s_1 c_3) & c_1 c_3 - s_1 s_2 s_3 & c_2 s_3 \\ -c_1 s_2 c_3 + s_1 s_3 & -(c_1 s_3 + s_1 s_2 c_3) & c_2 c_3 \end{pmatrix}, \tag{2.84}$$

with

$$c_i = \cos\alpha_i \qquad s_i = \sin\alpha_i \qquad -\frac{\pi}{2} \leq \alpha_i < \frac{\pi}{2}. \tag{2.85}$$

The mass matrix Eq. (2.83) is then diagonalised through

$$R\mathcal{M}_N^{\text{N2HDM}}R^T = \text{diag}\left(m_{h_1}^2, m_{h_2}^2, m_{h_3}^2\right) \tag{2.86}$$

where the masses are sorted such that $m_{h_1} \leq m_{h_2} \leq m_{h_3}$. The eigenstates are defined by

$$\begin{pmatrix} h_1 \\ h_2 \\ h_3 \end{pmatrix} = R \begin{pmatrix} \zeta_1 \\ \zeta_2 \\ \zeta_s \end{pmatrix} . \tag{2.87}$$

Using Eq. (2.80) to express m_{11}^2, m_{22}^2 and μ_S^2 through the other parameters, the potential is defined through the following parameters of the Lagrangian

$$\{v, \tan\beta, v_s, \lambda_1, \lambda_2, \lambda_3, \lambda_4, \lambda_5, \lambda_6, \lambda_7, \lambda_8, m_{12}^2\} \tag{2.88}$$

or through the masses and mixing angles

$$\{v, \tan\beta, v_s, m_{h_1}, m_{h_2}, m_{h_3}, m_A, m_{H^\pm}, \alpha_1, \alpha_2, \alpha_3, m_{12}^2\} . \tag{2.89}$$

In case of vanishing v_s Eq. (2.80c) cannot be used anymore to express μ_s^2 through the other input parameters and μ_s^2 has to be given as an input parameter. In the broken case with $v_s \neq 0$ the parameters of the parameters of the Lagrangian can be expressed through the masses and mixing angles through the following relations [75]

$$\lambda_1 = \frac{1}{v_1^2} \left[-m_{12}^2 \frac{v_2}{v_1} + \sum_{i=1}^{3} m_{h_i}^2 R_{i1}^2 \right] , \tag{2.90a}$$

$$\lambda_2 = \frac{1}{v_2^2} \left[-m_{12}^2 \frac{v_1}{v_2} + \sum_{i=1}^{3} m_{h_i}^2 R_{i2}^2 \right] , \tag{2.90b}$$

$$\lambda_3 = \frac{1}{v_1 v_2} \left[-m_{12}^2 + \sum_{i=1}^{3} m_{h_i}^2 R_{i1} R_{i2} + 2 m_{H^\pm}^2 \right] , \tag{2.90c}$$

$$\lambda_4 = \frac{1}{v^2} \left[m_{12}^2 \frac{v^2}{v_1 v_2} + m_A^2 - 2 m_{H^\pm}^2 \right] , \tag{2.90d}$$

$$\lambda_5 = \frac{1}{v^2} \left[m_{12}^2 \frac{v^2}{v_1 v_2} - m_A^2 \right] , \tag{2.90e}$$

$$\lambda_6 = \frac{1}{v_s^2} \sum_{i=1}^{3} m_{h_i}^2 R_{i3}^2 , \tag{2.90f}$$

$$\lambda_7 = \frac{1}{v_s v_1} \sum_{i=1}^{3} m_{h_i}^2 R_{i1} R_{i3} , \tag{2.90g}$$

$$\lambda_8 = \frac{1}{2 v_2 v_s} \sum_{i=1}^{3} m_{h_i}^2 R_{i2} R_{i3} , \tag{2.90h}$$

where R_{ij} are the elements of the rotation matrix R, cf. Eq. (2.84).

In the special case $v_s = 0$ the singlet is a DM candidate [74]. As DM studies are not in the scope of this work, the case $v_s \neq 0$ will be assumed for the N2HDM.

2.3.4. Theoretical Constraints

As in the 2HDM, cf. Sec. 2.2.5, it has to be ensured that Eq. (2.77) is a global minimum and that the approximation parameters of the perturbative expansion are small enough.

2.3.4.1. Unitarity Constraints

To ensure the approximation parameters being small enough, tree-level perturbative unitarity requires the unitarity of the S-matrix [66]. As in the 2HDM the eigenvalues of the $2 \rightarrow 2$ scattering matrix are required to be less than 8π. They have been calculated in [75] and are given by

$$\left| \frac{1}{2} a_{1,2,3}, b_\pm, c_\pm, e_{1,2}, f_\pm, f_1, p_1, s_1, s_2 \right| < 8\pi \,, \tag{2.91}$$

with

$$b_\pm = \frac{1}{2} (\lambda_1 + \lambda_2) \pm \frac{1}{2} \sqrt{(\lambda_1 - \lambda_2)^2 + 4\lambda_4^2} \,, \tag{2.92a}$$

$$c_\pm = \frac{1}{2} (\lambda_1 + \lambda_2) \pm \frac{1}{2} \sqrt{(\lambda_1 - \lambda_2)^2 + 4\lambda_5^2} \,, \tag{2.92b}$$

$$e_1 = \lambda_3 + 2\lambda_4 - 3\lambda_5 \,, \tag{2.92c}$$

$$e_2 = \lambda_3 - \lambda_5 \,, \tag{2.92d}$$

$$f_+ = \lambda_3 + 2\lambda_4 + 3\lambda_5 \,, \tag{2.92e}$$

$$f_- = \lambda_3 + \lambda_5 \,, \tag{2.92f}$$

$$f_1 = \lambda_3 + \lambda_4 \,, \tag{2.92g}$$

$$p_1 = \lambda_3 - \lambda_4 \,, \tag{2.92h}$$

$$s_1 = \lambda_7 \,, \tag{2.92i}$$

$$s_2 = \lambda_8 \tag{2.92j}$$

and the eigenvalues $a_{1,2,3}$ that are the real roots of the cubic polynomial

$$\begin{aligned} f(x) = & x^3 + x^2 \left[-6 (\lambda_1 + \lambda_2) - 3\lambda_6 \right] \\ & + x \left[36\lambda_1\lambda_2 - 16\lambda_3^2 - 16\lambda_3\lambda_4 - 4\lambda_4^2 + 18\lambda_1\lambda_6 + 18\lambda_2\lambda_6 - 4\lambda_7^2 - 4\lambda_8^2 \right] \\ & + 4 \left(-27\lambda_1\lambda_2\lambda_6 + 12\lambda_3^2\lambda_6 + 12\lambda_3\lambda_4\lambda_6 + 3\lambda_4^2\lambda_6 + 6\lambda_2\lambda_7^2 - 8\lambda_3\lambda_7\lambda_8 \right. \\ & \left. -4\lambda_4\lambda_7\lambda_8 + 6\lambda_1\lambda_8^2 \right) \,. \end{aligned} \tag{2.93}$$

2.3.4.2. Boundedness from Below

For the potential to be bounded from below in the strong case, requiring the potential to be strictly positive for the fields to approaching infinity in all possible directions, the allowed region is specified by two areas in the parameter space [64]. After translating the notation from [64] to Eq. (2.74) the allowed regions are given by

$$\Omega_1 = \left\{ \lambda_1 > 0, \lambda_2 > 0, \lambda_6 > 0, \lambda_7 + \sqrt{\lambda_1\lambda_6} > 0, \lambda_8 + \sqrt{\lambda_2\lambda_6} > 0, \lambda_3 + D + \sqrt{\lambda_1\lambda_2} > 0, \right.$$
$$\left. \lambda_7 + \lambda_8 \sqrt{\frac{\lambda_1}{\lambda_2}} \geq 0 \right\} \,, \tag{2.94a}$$

$$\Omega_2 = \left\{ \lambda_1 > 0, \lambda_2 > 0, \lambda_6 > 0, \sqrt{\lambda_2\lambda_6} \geq \lambda_8 > -\sqrt{\lambda_2\lambda_6}, \sqrt{\lambda_1\lambda_6} > \lambda_7 \geq \lambda_8 \sqrt{\frac{\lambda_1}{\lambda_2}}, \right.$$
$$\left. \lambda_6 (\lambda_3 + D) > \lambda_7\lambda_8 - \sqrt{(\lambda_1\lambda_6 - \lambda_7)^2 (\lambda_2\lambda_6 - \lambda_8)^2} \right\} \,, \tag{2.94b}$$

with

$$D = \min(0, \lambda_4 - |\lambda_5|) \,. \tag{2.95}$$

The allowed region is given by

$$\Omega = \Omega_1 \cup \Omega_2 \,. \tag{2.96}$$

2.3.4.3. Global Minimum

Due to the addition of the singlet VEV v_s it is not possible to derive analytic criteria to decide if our minimum is the global one as it was possible in the 2HDM. Calculating the necessary condition for a minimum of Eq. (2.74) with the general ansatz, including the possibility for a CB or CP-breaking VEV, yields [75]

$$\omega_2 m_{12}^2 - \omega_1 m_{11}^2 = \frac{\omega_1}{2} \left(\lambda_1 \omega_1^2 + \lambda_{345} \omega_2 + \omega_{\mathrm{CB}}^2 \lambda_3 + \omega_{\mathrm{CP}} \lambda_{34-5} + \omega_S^2 \lambda_7 \right) , \tag{2.97a}$$

$$\omega_1 m_{12}^2 - \omega_2 m_{22}^2 = \frac{\omega_2}{2} \left(\omega_1^2 \lambda_{345} + \lambda_2 \left(\omega_2^2 + \omega_{\mathrm{CB}}^2 + \omega_{\mathrm{CP}}^2 \right) + \lambda_8 \omega_S^2 \right) , \tag{2.97b}$$

$$-\omega_{\mathrm{CB}} m_{22}^2 = \frac{\omega_{\mathrm{CB}}}{2} \left(\lambda_3 \omega_1^2 + \lambda_2 \left(\omega_2^2 + \omega_{\mathrm{CB}}^2 + \omega_{\mathrm{CP}}^2 \right) + \lambda_8 \omega_S^2 \right) , \tag{2.97c}$$

$$-\omega_{\mathrm{CP}} m_{22}^2 = \frac{\omega_{\mathrm{CP}}}{2} \left(\lambda_{34-5} \omega_1^2 + \lambda_2 \left(\omega_2^2 + \omega_{\mathrm{CB}}^2 + \omega_{\mathrm{CP}}^2 \right) + \lambda_8 \omega_S^2 \right) , \tag{2.97d}$$

$$-\omega_S \mu_S^2 = \frac{\omega_S}{2} \left(\lambda_7 \omega_1^2 + \lambda_8 \left(\omega_2^2 + \omega_{\mathrm{CB}}^2 + \omega_{\mathrm{CP}}^2 \right) + \lambda_6 \omega_S^2 \right) , \tag{2.97e}$$

with the additional conditions

$$0 = \omega_{\mathrm{CB}} \left(\omega_1 \omega_2 \left(\lambda_4 + \lambda_5 \right) - 2 m_{12}^2 \right) , \tag{2.98a}$$

$$0 = \omega_1 \omega_{\mathrm{CB}} \omega_{\mathrm{CP}} \left(\lambda_4 - \lambda_5 \right) , \tag{2.98b}$$

$$0 = \omega_{\mathrm{CP}} \left(\omega_1 \omega_2 \lambda_5 - m_{12}^2 \right) . \tag{2.98c}$$

To check if Eq. (2.77) is the global minimum all possible solutions of Eq. (2.97) fulfilling Eq. (2.98) need to be calculated and the potential evaluated at Eq. (2.77) has to be compared to the potential of all other stationary points. The necessary formulae for this have been given in Appendix C of [75].

2.3.5. N2HDM Higgs Couplings to SM Particles

As the singlet does not couple to gauge bosons or fermions, the couplings to the Higgs boson are determined by the admixture of the doublet components R_{i1} and R_{i2} to the Higgs mass eigenstate. The interaction Lagrangian between gauge and Higgs bosons is the same as in the 2HDM, given in Eq. (2.55) and Eq. (2.60). This yields for the couplings between one Higgs boson and two gauge bosons normalised to the SM

$$c^{\mathrm{N2HDM}}(h_i Z Z) = c^{\mathrm{N2HDM}}(h_i W^{\pm} W^{\mp}) = \cos\beta R_{i1} + \sin\beta R_{i2} . \tag{2.99}$$

The coupling between a CP-even Higgs boson h_i, the CP-odd Higgs boson A and the Z boson as well as the couplings between a CP-even Higgs boson h_i, a charged Higgs boson and the charged W boson, are given by

$$c^{\mathrm{N2HDM}}(h_i Z A) = -\frac{\sqrt{g_1^2 + g_2^2}}{2} (p_\mu^i - p_\mu^A)(\sin\beta R_{i1} - \cos\beta R_{i2}) , \tag{2.100}$$

$$c^{\mathrm{N2HDM}}(h_i W^{\pm} H^{\mp}) = \pm \frac{g_2}{2} (\sin\beta R_{i1} - \cos\beta R_{i2}) \left(p_\mu^i - p_\mu^{A/H^{\mp}} \right) . \tag{2.101}$$

Since the singlet field Φ_S does not couple to the fermions, it is possible to introduce the same four distinct types as in the 2HDM, described in Tab. 2.1, to avoid FCNCs. The couplings between a CP-even Higgs boson and to fermions in the N2HDM are given in Tab. 2.3. The coupling of the CP-odd Higgs boson A to two fermions is given in Tab. 2.4.

The couplings between three Higgs bosons are derived from

$$c(\phi_i \phi_j \phi_k) = -\partial_{\phi_i} \partial_{\phi_j} \partial_{\phi_k} V_{\mathrm{N2HDM}} \tag{2.102}$$

with the Higgs fields

$$\phi_{i,j,k} \in \{ H^{\pm}, A, h_1, h_2, h_3 \} . \tag{2.103}$$

The explicit formulae are given in Appendix B of [75].

	Type I	Type II	FL	LS
up-type quarks	$\dfrac{R_{j2}}{\sin\beta}$	$\dfrac{R_{j2}}{\sin\beta}$	$\dfrac{R_{j2}}{\sin\beta}$	$\dfrac{R_{j2}}{\sin\beta}$
down-type quarks	$\dfrac{R_{j2}}{\sin\beta}$	$\dfrac{R_{j1}}{\cos\beta}$	$\dfrac{R_{j1}}{\cos\beta}$	$\dfrac{R_{j2}}{\sin\beta}$
Leptons	$\dfrac{R_{j2}}{\sin\beta}$	$\dfrac{R_{j1}}{\cos\beta}$	$\dfrac{R_{j2}}{\sin\beta}$	$\dfrac{R_{j1}}{\cos\beta}$

Table 2.3.: Couplings between two fermions and a neutral CP-even Higgs boson h_j of the form $\mathcal{L}_Y \supset -\dfrac{m_f}{v}\overline{f}c(h_iff)fh_i$.

	Type I	Type II	FL	LS
up-type quarks	$-1/\tan\beta$	$-1/\tan\beta$	$-1/\tan\beta$	$-1/\tan\beta$
down-type quarks	$1/\tan\beta$	$-\tan\beta$	$\tan\beta$	$-1/\tan\beta$
Leptons	$1/\tan\beta$	$-\tan\beta$	$-1/\tan\beta$	$\tan\beta$

Table 2.4.: Couplings between two fermions and a neutral CP-odd Higgs boson A of the form $\mathcal{L}_Y \supset -\mathrm{i}\dfrac{m_f}{v}\overline{f}\gamma_5 c(Aff)fA$.

The 2HDM at High Scales - How to Solve the Metastability Problem

Depending on the exact value of the top and the Higgs mass, the SM might not have a stable vacuum, as seen through the change of the parameters while increasing the renormalisation scale μ [60–62, 76]. The scale μ is introduced as perturbation theory is evaluated at fixed order. The dependence of a physical observable on μ would drop out if it was possible to sum over all orders. The dependence of the $\overline{\text{MS}}$ renormalised couplings on the scale μ is given through the RGEs. These equations can be obtained[8] by extracting the divergent parts of the corresponding loop corrected quantities. New physics beyond the SM is necessary if the SM is not stable up until the Planck scale [10]. Models with extended Higgs sectors provide a possibility for a stable vacuum up until the Planck scale, e.g. in the R2HDM studied by [11–19]. While they either considered an exact $\mathbb{Z}_2$ symmetry or assumed that the lightest CP-even Higgs boson is the SM-like one, we were the first ones to analyze the R2HDM without these limitations in [2] using the RGEs at one-loop order, given in Appendix A. In this chapter, the main results from [2] are represented while additionally investigating the CP-violating phase at higher energies in the C2HDM.

At first in Sec. 3.1 the theoretical and experimental constraints applied for the discussion in this chapter are described. In Sec. 3.2 only the theoretical constraints and the limits in the $m_{H^\pm} - \tan\beta$ plane are applied to the model and the effect of the RGEs is investigated. In Sec. 3.3 the remaining constraints described in Sec. 3.1 are applied to investigate if the findings of Sec. 3.2 are still valid including the constraints from collider phenomenology. The impact of the RGEs for the softly broken $\mathbb{Z}_2$ symmetry with the heavier Higgs boson being the SM-like one is described in Sec. 3.4. While the R2HDM is capable of providing a stable vacuum up until the Planck scale, it is an interesting question to see the impact of the RGEs on the CP-violating phase in the C2HDM. This is described in Sec. 3.5. This chapter concludes with a short remark on the effect of higher-order corrections on the findings of this chapter in Sec. 3.6.

While the results and methods described in Secs. 3.1 to 3.4 and 3.6 were already published in [2] the results of Sec. 3.5 are unpublished so far. My contribution to [2] was the implementation of the RGEs in a `C++` code, the numerical evaluation of them for every parameter point in

---

[8]As the RGEs are only used as a calculational tool in this thesis, the reader is referred to [77] for a general introduction.

input parameter	minimal value	maximal value
$m_{H^\pm}$ (Type I)	$80\,\text{GeV}$	$1\,\text{TeV}$
$m_{H^\pm}$ (Type II)	$580\,\text{GeV}$	$1\,\text{TeV}$
$\tan\beta$	0.8	35
α	$-\dfrac{\pi}{2}$	$\dfrac{\pi}{2}$
m_{12}^2	$0\,\text{GeV}^2$	$10^5\,\text{GeV}^2$
m_A	$30\,\text{GeV}$	$1\,\text{TeV}$
$m_{h/H}$	$30\,\text{GeV}$	$1\,\text{TeV}$

Table 3.1.: The ranges for the input parameters of the R2HDM as used for the scan described in Sec. 3.1. Here $m_{h/H}$ describes the mass of the non-SM-like CP-even Higgs boson. While all ranges are of the form minimal value $\leq$ parameter $\leq$ maximal value α is of the form minimal value $\leq \alpha <$ maximal value. This distinction is made as the case $\alpha = \pi/2$ describes the same parameter point as the case $\alpha = -\pi/2$. The same ranges were used in [2].

the data sample and the production of the plots as well as contributing to the discussion on the interpretation of the plots.

3.1. Allowed Parameter Space and the Calculation of the High Scale Behaviour

To investigate the phenomenological implications of the high scale behaviour in the R2HDM a data sample was generated using `ScannerS` [68, 78]. The R2HDM was implemented and checked for the theoretical constraints, namely boundedness from below, cf. Eq. (2.50), positive discriminant, cf. Eq. (2.52), and unitarity constraints, cf. Eq. (2.54). The LHC Run1 data, LEP and Tevatron Higgs searches were checked using `HiggsBounds` v4.3.1 [79–84][9]. The decay widths and branching ratios were calculated with `HDECAY` [85–87]. The cross sections of the production via gluon fusion and b-quark fusion were obtained from `SusHi` v1.6.0 [88, 89], at next-to-next-to-leading-order QCD. The SM-like Higgs signal rates were required to be within a $2 \times 1\sigma$ bound of the fitted experimental values given in [9]. The most stringent constraints in the $m_{H^\pm} - \tan\beta$ plane are coming through $B \to s\gamma$ measurements [90–94]. In the type II scenario of the R2HDM this translates into an lower limit of $m_{H^\pm} \geq 580\,\text{GeV}$. Furthermore, all points are required to be within a 2σ limit of the electroweak precision data (EWPD) [95]. For the scan, the input parameters were restricted to be in the ranges given in Tab. 3.1.

The necessary one-loop RGEs and the values of all parameters at the scale of the Z boson mass, given in Appendix A, were implemented in a `C++` program. The Runge-Kutta algorithm, provided through the `C++` library `Boost` [96], was used to solve the RGEs stepwise up to the Planck scale ($10^{19}\,\text{GeV}$). The lowest energy scale Λ was stored as the cut-off scale at which either the potential was no longer bounded from below, the discriminant became

---

[9]At the time of the analysis the Run2 Data was not implemented yet in `HiggsBounds`. Nonetheless, it has been verified that the general statement of this chapter is still valid.

negative or perturbative unitarity was not fulfilled anymore or a Landau pole appeared. A Landau pole[10] is defined through the divergence of one of the couplings.

The sample was then divided in two smaller ones, the light Higgs scenario with $130\,\text{GeV} \leq m_H \leq 1\,\text{TeV}$ and the heavy Higgs scenario with $30\,\text{GeV} \leq m_h \leq 120\,\text{GeV}$, while the mass of the SM-like Higgs boson is fixed to 125.09 GeV. Through setting the boundaries to 120 and 130 GeV the additional neutral CP-even Higgs boson is not too close to the SM-like one and an interference between the signals of them does not need to be considered.

3.2. The Light Higgs Scenario at High Scales without Collider Phenomenology

As a first step, the effects of the running of the couplings with the RGEs on the parameter space are investigated while only taking theoretical constraints and $B \to s\gamma$ measurements into account. In the *alignment limit* the SM-like Higgs boson couples exactly like the SM Higgs to SM particles. In this limit the additional CP-even Higgs bosons does not couple to SM particles and, therefore, only contributes to the vacuum stability through its couplings to the SM-like one. This limit can be classified through the coupling between two gauge bosons and a CP-even Higgs boson. The couplings, normalised to the SM, cf. Eq. (2.56), in the R2HDM are given by

$$c_{HVV} = \cos(\beta - \alpha)\,, \tag{3.1}$$
$$c_{hVV} = \sin(\beta - \alpha) \tag{3.2}$$

and therefore

$$|c_{hVV}| = \sqrt{1 - c_{HVV}^2}\,. \tag{3.3}$$

The *alignment limit*, is therefore given by the limit $\cos(\beta - \alpha) = 0$ if the lighter CP-even Higgs boson h is the SM-like one. Applying the alignment limit yields exact SM-like couplings between the SM-like Higgs boson and all SM particles. While the other CP-even Higgs boson does not couple to two gauge bosons in this limit, the couplings to fermions scale with $\tan\beta$ and $1/\tan\beta$ w.r.t. the SM depending on the fermion generation and the type, cf. Tab. 2.2. Therefore, the different types can yield large or small couplings to the fermions. To investigate this limit, and its natural occurrence, the charged Higgs mass is shown in Figs. 3.1 and 3.2 for type I and type II respectively as a function of $\cos(\beta - \alpha)$. In the left figure the grey points show all points surviving all theoretical constraints and $B \to s\gamma$, while all coloured points survive up to a cut-off scale of at least 1 TeV and the colour scale shows the value of m_H. The parameter points in this figure and all following with a colour bar are sorted such, that the colour denotes the maximum value of the parameter described through the colour bar in the corresponding pixel. The left figure in Fig. 3.1 can be divided in two areas, above and below $m_{H\pm} \approx 500\,\text{GeV}$. In the area $m_{H\pm} \lesssim 500\,\text{GeV}$ all possible values of $\cos(\beta - \alpha)$ are allowed, but for $m_{H\pm} \gtrsim 500\,\text{GeV}$ there is only a narrow band around $\cos(\beta - \alpha) \approx 0$ that guarantees validity of the model up to a cut-off scale of at least 1 TeV. The colour bar indicates that heavy masses for the second Higgs boson are close to the mass of the heavy charged Higgs bosons. In the type II model, on the other hand, shown in the left panel of Fig. 3.2, only a small band around $\cos(\beta - \alpha) \approx 0$ provides parameter points valid up to at least 1 TeV. For those points, the mass of the heavy CP-even Higgs boson is similar to the mass of the charged

---

[10]While a Landau pole is technically defined through the divergence of at least one parameter, numerically it was defined if either one of the dimensionless couplings fulfilled $|\lambda_i| \geq 100$ or if the dimension two parameters fulfilled $|m_{ij}^2| \geq 10^{10}\,\text{GeV}^2$. These numbers have been varied to ensure that they exact cut-off does not influence the result.
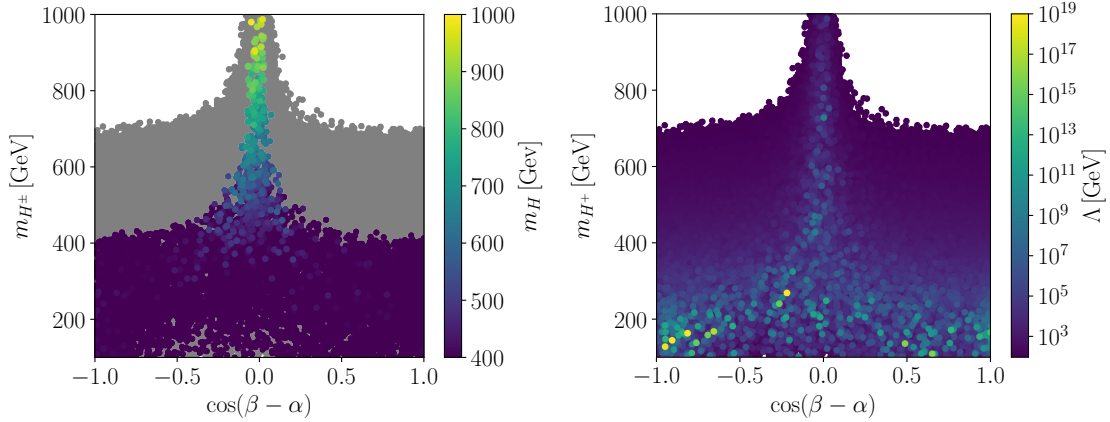
Figure 3.1.: The charged Higgs mass is shown as a function of $\cos(\beta - \alpha)$ in the type I R2HDM. All quantities are the parameters at the m_Z scale. On the left panel the points that passed the theoretical constraints and $B \to s\gamma$ at the scale m_Z are shown in grey. The remaining points have survived the RGE running up to a scale of 1 TeV. The colour bar shows the value of m_H. On the right panel, the same plot is represented but now the colour bar shows the cut-off scale Λ. Figures taken from [2].
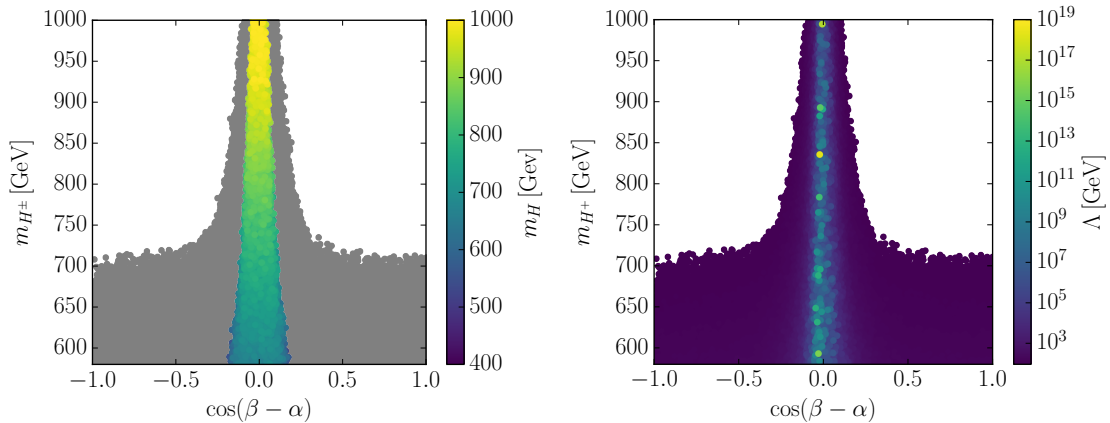
Figure 3.2.: Same as Fig. 3.1, but for type II of the R2HDM. Figures also published in [2].

Higgs boson. The difference to the type I scenario is given by the $B \to s\gamma$ constraints, which force $m_{H^\pm} \geq 580\,\text{GeV}$, and therefore cut off the lower half of the left figure in Fig. 3.1. The limit of $\cos(\beta - \alpha)$ is, therefore, a natural property of the model if the charged Higgs mass is high enough. This is again seen on the right side of both figures. Here the colour scale is determined by the cut-off scale Λ. In type I there are some points with values of $\cos(\beta - \alpha)$ not close to zero with a high cut-off scale in the low $m_{H^\pm}$ region but in the high $m_{H^\pm}$ region, as well as in type II, the brightest points are for almost $\cos(\beta - \alpha) \approx 0$.

A severe constraint on the parameter space is given by the EWPD. The S, T, U parameters depend on the mixing between the neutral Higgs bosons but also on the difference between the mass of the charged and the neutral Higgs bosons. To investigate this at higher scales, it is useful to rewrite the mass of the charged Higgs boson, cf. Eq. (2.37) as

$$M^2 - m_{H^\pm}^2 = -\frac{v^2}{2}(\lambda_4 + \lambda_5) , \tag{3.4}$$

with the over all mass scale

$$M^2 = m_{12}^2 \frac{v^2}{v_1 v_2} \,. \tag{3.5}$$

The mass of the heavier CP-even neutral Higgs boson, cf. Eq. (2.41b), yields in first order approximation $\lambda_i v^2 \ll M^2$

$$m_H^2 = M^2 + f(\lambda_i, v_1, v_2) \,, \tag{3.6}$$

where $f(\lambda_i, v_1, v_2)$ is a linear combination of its arguments. In the limit of $\lambda_i v^2 \ll M^2$ the masses $m_{H,A,H^\pm}^2$ are all approximately given by M^2. This limit is called the *decoupling limit*. In Fig. 3.3 the mass scale $|M|$ and the combination $\lambda_4 + \lambda_5$ are shown as a function of the cut-off scale Λ on the left and right side, respectively, in the type II R2HDM. A steep rise in $|M|$ is visible in the left panel yielding $|M| \gtrsim 423\,\text{GeV}$ for a cut-off Scale Λ above 1 TeV, yielding that the $\mathbb{Z}_2$ symmetric limit is not allowed for a cut-off scale above 1 TeV. These high values of the mass scale are driven by the constraints on the charged Higgs mass, enforcing it to be above 580 GeV. Simultaneously, the right plot shows small values of $\lambda_4 + \lambda_5$ for high cut-off scales. Inserting this in Eq. (3.4) shows that the charged Higgs mass is almost exclusively determined by the high mass scale $|M|$ for parameter points with a high cut-off scale. The limit of vanishing quartic couplings λ_1 to λ_5 can be explained through their RGEs, cf. Eq. (A.11). They show that derivatives of the quartic couplings becoming larger for larger starting values. Running these up to high scales generates large values of the couplings which are then dismissed by the perturbativity and unitarity constraints. The same conclusion can be drawn from Fig. 3.4. Here the difference $m_A - m_{H^\pm}$ is displayed as a function of the difference $m_H - m_{H^\pm}$. All points shown fulfil the applied theoretical constraints and the limits of $B \to s\gamma$ at the scale m_Z. Additionally, on the left the coloured points present those surviving up to a cut-off scale of $\Lambda \geq 1\,\text{TeV}$ while the colour bar indicates the value of $\tan\beta$. Here a clear reduction of the allowed parameter space, down to a maximal difference of 200 GeV between the masses is visible. In combination with Figs. 3.2 and 3.3 this means that for a cut-off scale above 1 TeV all masses are very close together and rather heavy. Combining this with the limit of $m_{H^\pm} \geq 580\,\text{GeV}$ no Higgs boson with a mass below 380 GeV is to be expected if the parameter point should also be stable up to high cut-off scales. Additionally, the colour bar shows that large values of $\tan\beta$ are centred more around the origin of the plot, meaning all three masses are almost degenerate. This increased constraint results from larger coupling to the down-type quarks, forcing the values of λ_i to be lower at the m_Z scale and, therefore, even smaller mass differences. The right panel of Fig. 3.4 shows that for cut-off scales above 1 TeV the parameter points concentrate around almost vanishing mass difference. This corresponds to the decoupling limit.

3.3. The Light Higgs Scenario at High Scales including Collider Phenomenology

As already seen in Sec. 3.2 the type II is driven into the decoupling and alignment limit for high cut-off scales, even without further experimental constraints. While the type I case still allows for points outside those limits in Sec. 3.2, it is necessary to check if this is still true if the experimental constraints, described in Sec. 3.1, are applied. For this, the left panel of Fig. 3.5 shows the charged Higgs mass again as a function of $\cos(\beta - \alpha)$ while the right panel shows the mass difference $m_A - m_{H^\pm}$ as a function of the difference $m_H - m_{H^\pm}$. Both figures have the cut-off scale encoded as the colour bar. Comparing the left figure of Fig. 3.5 with the right figure of Fig. 3.1 shows that the additional collider constraint does not change the conclusions made for the higher cut-off scales. The different density for the parameter points
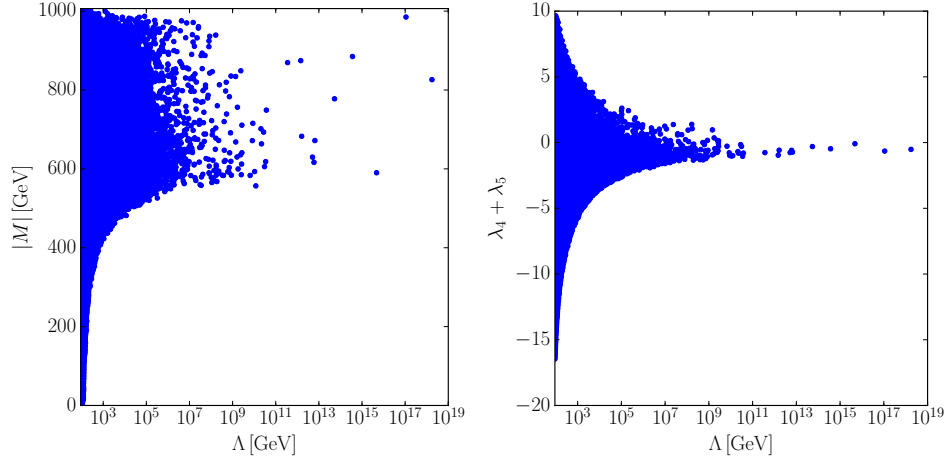
Figure 3.3.: On the left (right) panel $|M|$ $(\lambda_4 + \lambda_5)$ at the scale m_Z is presented as a function of the cut-off scale Λ in the type II R2HDM. The points have passed both the theoretical constraints and $B \to s\gamma$ at the scale m_Z and have also survived the RGE running up to the cut-off scale shown on the x-axis. Figures also published in [2].
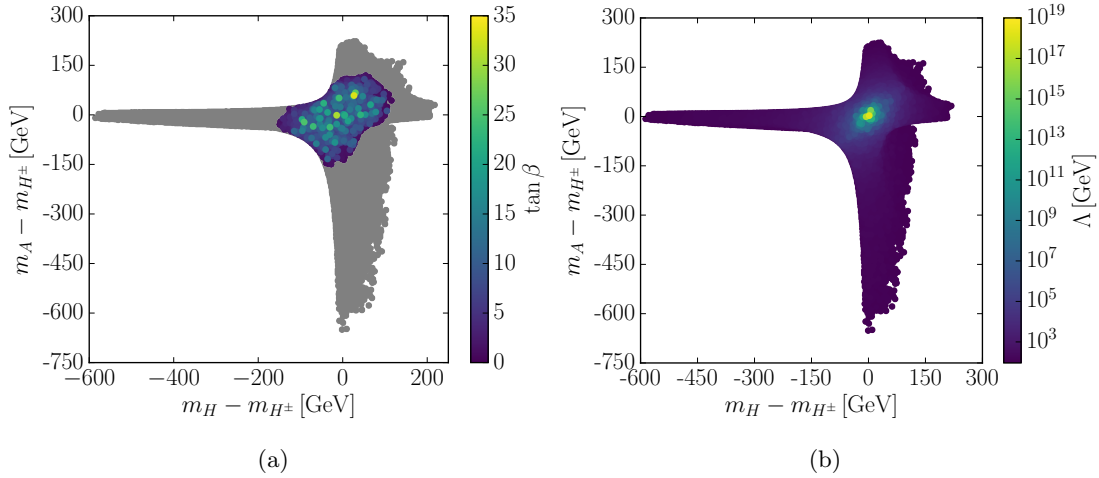
Figure 3.4.: The mass difference $m_A - m_{H^\pm}$ as a function of $m_H - m_{H^\pm}$ at the scale m_Z in the type II R2HDM. On the left, parameter points passing the theoretical constraints and $B \to s\gamma$ at the scale m_Z are presented in grey. The remaining coloured points yield a cut-off scale above $1\,\mathrm{TeV}$ with the colour bar showing the value of $\tan\beta$. On the right panel, the colour bar indicates the cut-off scale Λ. Figures also published in [2].
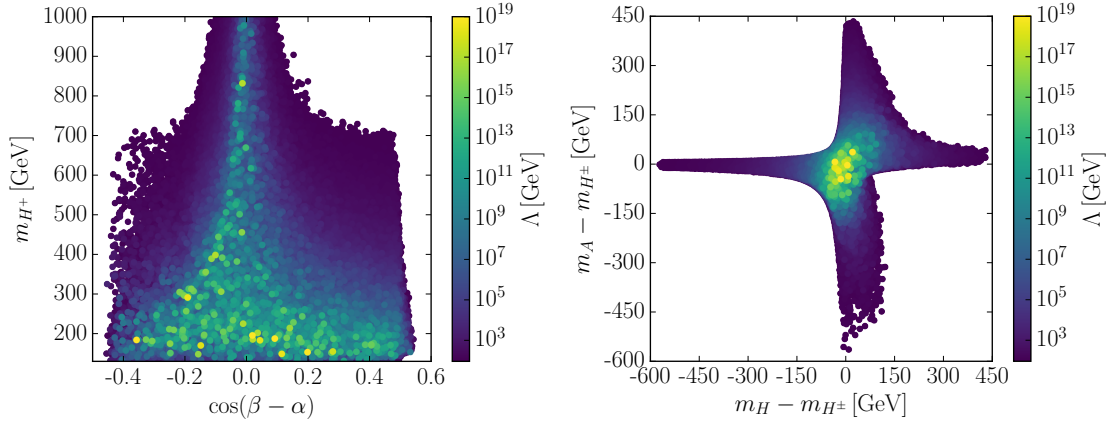
Figure 3.5.: On the left panel the charged Higgs mass is shown as a function of $\cos(\beta - \alpha)$ in the type I R2HDM taking into account the experimental constraints. On the right, the mass difference $m_A - m_{H^\pm}$ is shown as a function of $m_H - m_{H^\pm}$. In both panels, the cut-off scales is shown as the colour code. The parameters shown on the horizontal and vertical axis are the values at the m_Z scale. Figures also published in [2].

up to a certain cut-off scale Λ is an artefact of the scan. As too few points for the scan used in Fig. 3.1 survived the collider constraints, a new sample with the same limits was generated. Through the inclusion of additional constraints the density of allowed parameter points varies as the scan searches as long as it takes to generate a given number of parameter points. As in the type II case, the right figure shows that higher cut-off scales prefer a much smaller mass difference compared to low scales. Although the tendency is not as strictly vanishing as in type II the mass differences are nonetheless reduced to around 150 GeV instead of 600 GeV at low scales.

While the difference between the mass of the neutral and the charged Higgs boson shrinks for higher values of the cut-off scale, the allowed region of the overall mass scale $|M|$ is shown in Fig. 3.6. Here small values of $|M|$ can achieve much higher cut-off scales than in the type II scenario, as seen in Fig. 3.3, even with additional experimental constraints. In type I values of $|M|$ below 100 GeV are only excluded for cut-off scales $\Lambda \gtrsim 10^7$ GeV. This yields that the $\mathbb{Z}_2$, meaning $M = 0$, cannot provider points being stable up until the Planck scale. Due to this the type I R2HDM is not driven into the decoupling limit like the type II model.

3.4. The Heavy Higgs Scenario

The difference in the phenomenology between type I and II increases drastically if the heavy Higgs scenario, defined by $m_h < m_H = 125.09$ GeV, is considered. In this scenario, the masses of the additional Higgs boson cannot be degenerate in type II as the CP-even Higgs bosons are light while the charged Higgs boson is still required to be above 580 GeV. To investigate the implications of the RGE running in this scenario the mass of the charged Higgs boson is shown as a function of the cut-off scale Λ in Fig. 3.7. On the left panel the effects on type I are shown with the colour bar depicting the mass of the pseudoscalar Higgs boson. This figure can be divided into two areas. One area is defined through the mass of the charged Higgs boson is near or below the SM-like boson mass. In this case the necessary degeneracy for the EWPD can be achieved between the light CP-even and the charged Higgs boson, therefore, yielding no strong constraints on the mass of the pseudoscalar Higgs boson. The second region with the mass of the charge Higgs boson being above the CP-even neutral ones which constraints the pseudoscalar Higgs boson to be close to the charged one to fulfil EWPD. Furthermore, Fig. 3.7 shows that for charged Higgs boson masses below 200 GeV it is still
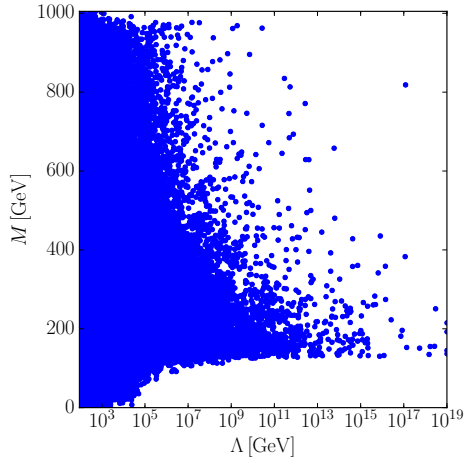
Figure 3.6.: The overall mass scale M at the m_Z scale as a function of the cut-off scale Λ for type I. These points fulfil all experimental and theoretical bounds described in Sec. 3.1. Figure also published in [2].

possible to obtain cut-off scales as high as the Planck scale. This is once more shown on the left panel of Fig. 3.8. For most of the parameter points with a degenerate pseudoscalar and charged Higgs boson their mass is above the CP-even neutral ones. On the other hand, if the charged and the lightest CP-even Higgs boson are degenerate in most cases the pseudoscalar Higgs boson is heavier. There is a small area in which the non-degenerate mass is below the degenerates one and the parameter points on the diagonal in the lower right corner show a degeneracy between the lightest CP-even and the pseudoscalar Higgs boson. For large cut-off scales, the preferred parameter region is given if the pseudoscalar and charged Higgs are not more than 100 GeV apart, which overall yields small quartic couplings. On the right panel of Fig. 3.7 the situation is shown for type II. As the lower limit on the charged Higgs mass through $B \to s\gamma$ results in heavy charged Higgs bosons the charged and either of the two CP-even Higgs bosons cannot be degenerate. Therefore, the charged and the pseudoscalar Higgs bosons have to be degenerate to fulfil the constraints from the EWPD. For all parameter points shown in the right panel of Fig. 3.7 the difference between the two masses is between -15 and 10 GeV, as shown in the right panel of Fig. 3.8. Through the large mass splitting between the light CP-even Higgs boson and the pseudoscalar and charged Higgs boson the quartic couplings of these parameter points are large. Through the large values already at the m_Z scale the parameters grow to larger values through the running of the RGEs and at least one of the constraints fails at a low cut-off scale. This results in all parameter points yielding a cut-off scale below 150 GeV.

3.5. The CP-violating phase of the CP-violating 2HDM at High Scales

While the previous work was done in the limit of the R2HDM it is an interesting question to ask whether the CP-violating phase in the C2HDM correlates with the cut-off scale. For this a parameter scan with the same criteria as in Sec. 3.1 was performed while additionally enforcing the `ACME` [97][11] results on the electric dipole moments (EDMs) for the C2HDM. As the type I model has still a larger allowed parameter space than the type II model the scan was performed in this scenario. As the RGEs of λ_1 to λ_4 and m_{11}^2, m_{22}^2 and the real part of λ_5, cf. Eqs. (A.10), (A.12a) and (A.12b) do not change compared to the R2HDM the

---

[11]The discussion in this section does not change if the improved constraints on the electron EDMs [98] are taken into account.
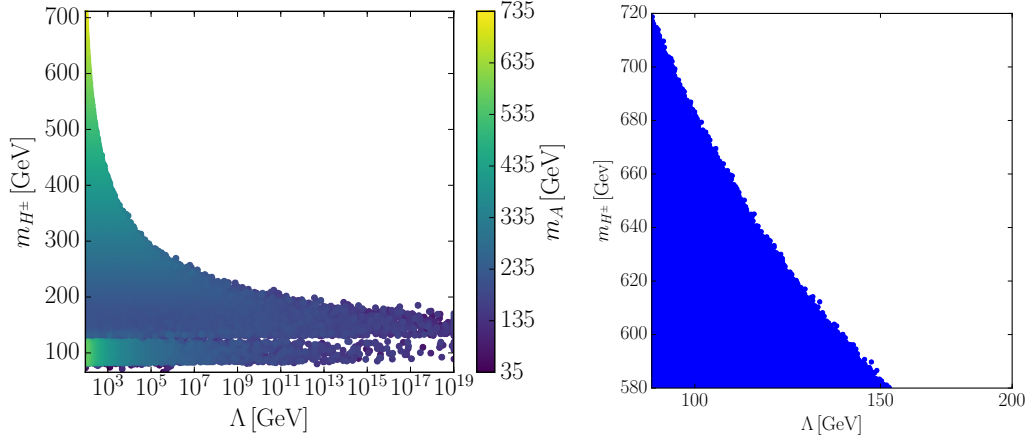
Figure 3.7.: The mass of the charged Higgs $m_{H^\pm}$ at the m_Z scale as a function of the cut-off scale Λ is shown for the heavy Higgs scenario for type I on the left and type II on the right. The colour code on the left shows the value of m_A. Figures also published in [2].
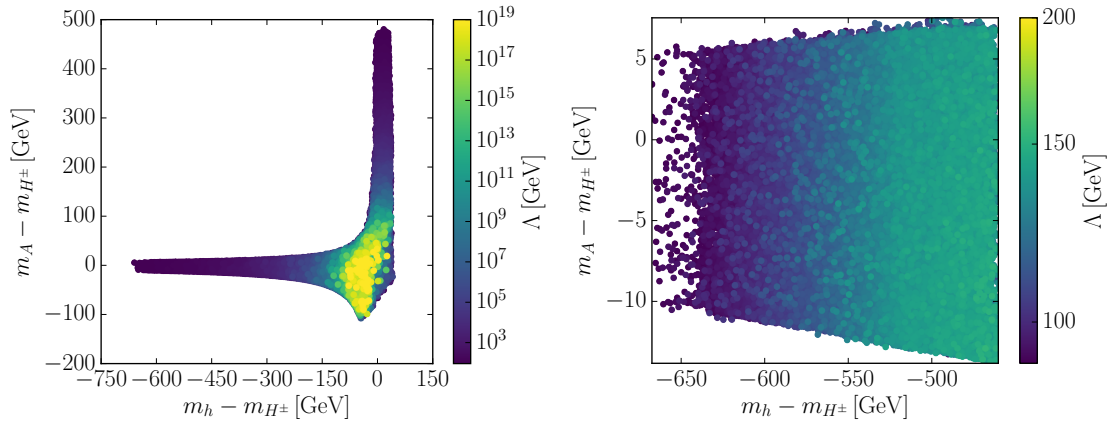
Figure 3.8.: The mass difference $m_A - m_{H^\pm}$ vs. $m_h - m_{H^\pm}$ at the m_Z scale for the heavy Higgs scenario for type I on the left and type II on the right. The colour code shows the cut-off scale Λ. Figures also published in [2].
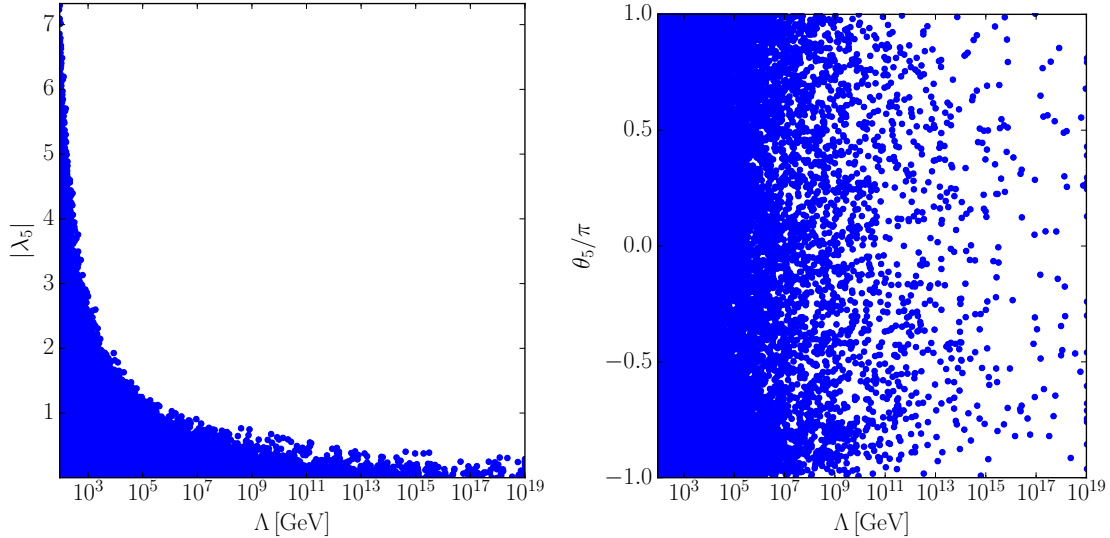
Figure 3.9.: The absolute value (phase) of $\lambda_5 = |\lambda_5| \exp(i\theta_5)$ at the m_Z scale as a function of the cut-off scale Λ on the left (right) in the type I C2HDM with $m_{h_1} = 125.09\,\text{GeV}$.

discussion from the R2HDM can be applied to the corresponding parameters in the C2HDM. The additional degree of freedom, compared to the R2HDM, is given through the phase of λ_5. For this, Fig. 3.9 shows λ_5 as a function of the cut-off scale Λ. The left panel of Fig. 3.9 shows the absolute value of λ_5 which vanishes for high cut-off scales, as only the absolute value of λ_5 enters in the perturbative unitarity and boundedness from below constraints, cf. Eqs. (2.50) and (2.54). Therefore, the results of λ_5 in the R2HDM, cf. Secs. 3.3 and 3.4, can be translated to the absolute value of λ_5 in the C2HDM. The right panel of Fig. 3.9, on the other hand, shows the complex phase of λ_5, where all values are possible up to the Planck scale. While the phases of λ_5 and m_{12}^2 are coupled through the minimum condition, cf. Eq. (2.31c), at the m_Z scale, this relation does not have to be satisfied at higher scales any longer. The left (right) side of Fig. 3.10 shows the absolute value (phase) of m_{12}^2 at the m_Z scale as a function of the cut-off scale. As in the R2HDM, an overall mass scale M can be defined through the charged Higgs boson mass, cf. Eq. (2.37), and vanishing quartic couplings. In the C2HDM the mass scale is therefore defined as

$$M^2 = \Re m_{12}^2 \frac{v^2}{v_1 v_2}\,. \tag{3.7}$$

In the C2HDM this scale M is directly proportional to the real part of m_{12}^2. As the absolute values of the quartic couplings become small for high cut-off scales the masses of the Higgs bosons are, therefore, defined through the real part of m_{12}^2 and, therefore, yielding the same behaviour as shown in previous sections for the R2HDM. As the imaginary part of m_{12}^2 is related through the minimums condition to the imaginary part of λ_5 at the m_Z scale, cf. Eq. (2.31c), all parameter points with a large cut-off scale not only have a vanishing imaginary part of λ_5 but also a vanishing imaginary part of m_{12}^2. Combining these two conditions yields that for parameter points with large cut-off scale the mass scale is given by the absolute value of m_{12}^2 with vanishing phases, as seen in Fig. 3.10. Furthermore, Eqs. (A.10e) and (A.12c) show that the RGEs of $\Im\lambda_5$ and $\Im m_{12}^2$ are made up of parts directly proportional to $\Im\lambda_5$ and $\Im m_{12}^2$. Therefore, the CP-conserving limit of the R2HDM is a fixed point of the RGEs as both parameters do not change w.r.t. the renormalisation scale if they start at zero. This means that the R2HDM cannot evolve into the C2HDM through RGE running.
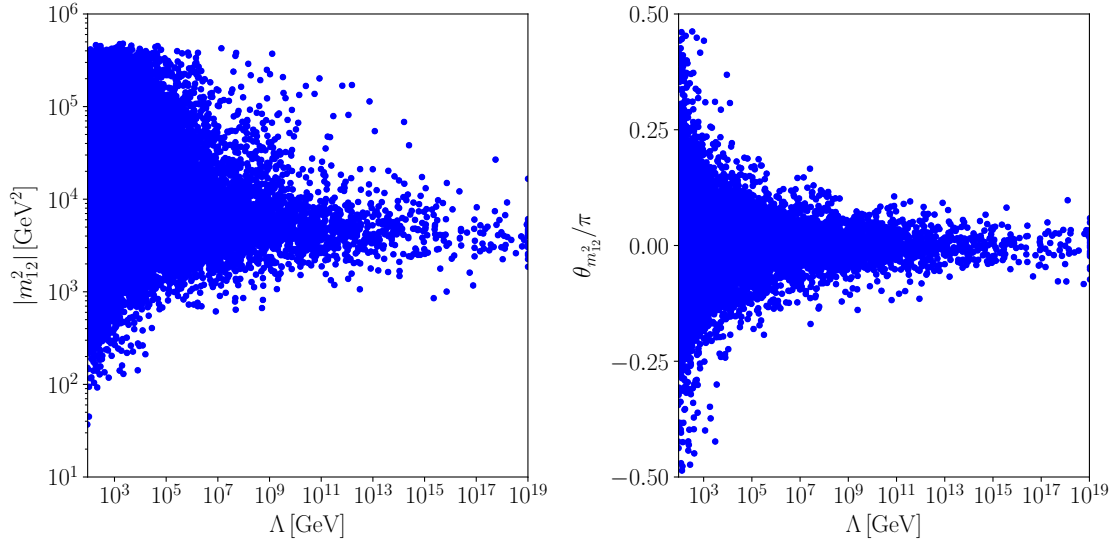
Figure 3.10.: The absolute value (phase) of $m_{12}^2 = |m_{12}^2| \exp(\mathrm{i}\theta_{m_{12}^2})$ at the m_Z scale as a function of the cut-off scale Λ on the left (right) in the type I C2HDM with $m_{h_1} = 125.09\,\mathrm{GeV}$.

3.6. Including Higher-Order Effects

While this chapter discussed the influence of one-loop RGEs on the phenomenology, it has been shown [17, 99, 100] that the two-loop RGEs can have a substantial impact on a single parameter point. To check if the two-loop RGEs change the result of this chapter they have been calculated with SARAH [101–105]. Using the two-loop RGEs requires one-loop matching of the $\overline{\mathrm{MS}}$ parameters on the input parameters. The necessary one-loop expressions for the masses of the quarks and gauge bosons are given in [106, 107] while those for the scalar masses are given in [108]. For the quartic couplings, the matching relations are given in [4]. Additionally, one-loop expressions for the unitarity constraints [17, 109] were taken into account. It has been shown that one-loop corrections to quartic couplings can be large for a single parameter point [110, 111]. As the focus of the work in this chapter was not the evolution of a single parameter point but the tendency of the whole sample, the calculation of the cut-off scale for every parameter point was redone. As an example the right panel of Fig. 3.5 is shown again in Fig. 3.11 using two-loop RGEs, one-loop matching and one-loop unitarity constraints. The comparison of these two figures shows that there are no significant changes and, therefore, the overall picture does not change. This is not surprising as the high cut-off limit already enforced the parameter space to very small quartic couplings which then would usually lead to small corrections in the RGEs.

3.7. Conclusion

The investigation in this chapter has shown that both the R2HDM and C2HDM can provide a stable vacuum up until the Planck scale. Additionally, the requirement of a stable vacuum at a scale higher than 1 TeV already requires the alignment limit in type II. For higher cut-off scales type I and II both require a nearly degenerate mass spectrum, as the quartic couplings are required to be small. Through the small quartic couplings, the degenerate masses are defined through a common mass scale, given by M, which is directly proportional to the softly $\mathbb{Z}_2$ breaking parameter m_{12}^2. Therefore, the $\mathbb{Z}_2$ symmetric model cannot provide a stable vacuum up until the Planck scale. The new insight gained from this study, shown in Sec. 3.4, is that the type I scenario of the R2HDM can provide a stable vacuum up until the Planck scale even if the SM-like Higgs boson is the heavier of the two CP-even Higgs boson.
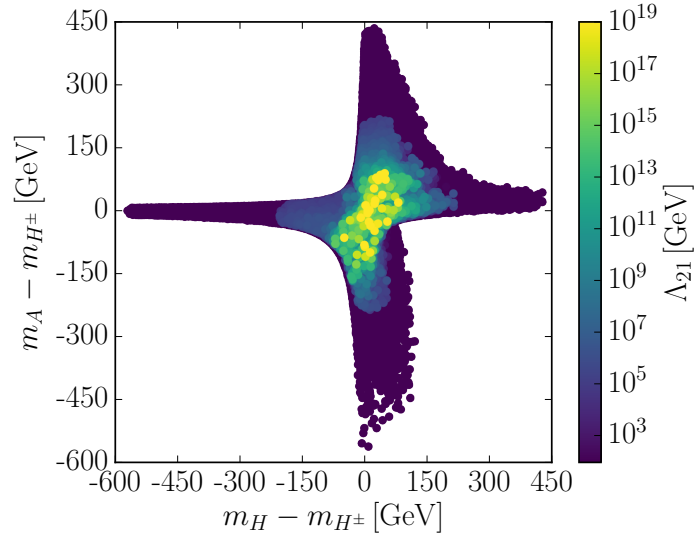
Figure 3.11.: Using two-loop RGEs, one-loop matching and one-loop unitarity constraints to recreate the right panel of Fig. 3.5. Figures also published in [2].

While these results have been published in [2], Sec. 3.5 presents new and unpublished insights on the values of the CP-violating phase of the C2HDM for higher cut-off scales. While the phase of λ_5 is not affected by this, the allowed region of the phase of m_{12}^2 is reduced as the overall mass scale in the C2HDM is dependent on the real part of m_{12}^2. To ensure that the results of [2] are still valid at higher orders, Sec. 3.6 repeats the investigation with two-loop RGEs with no significant difference in the overall result of the work.

The Electroweak Phase Transition

In recent years the EWPT has received increased interest. One of the reasons is the possibility to provide gravitational waves thate are possibly detectable in the next years [112–120]. Another reason is the possibility to explain the BAU through EWBG [23, 45, 120–155] as described in more detail in Chapter 6. This requires a SFOEWPT [154, 155] such that the necessary Sakharov conditions [21] are fulfilled.

The concept of the EWPT is visualised by Fig. 4.1, which shows the Higgs potential as a function of the expectation value v of the Higgs field at fixed temperature[12]. Here the dotted line shows the electroweak potential at very high temperatures ($T \gg T_c$) with the symmetric minimum ($v = 0\,\text{GeV}$) being the only minimum of the potential. Once the universe has cooled down to lower temperatures, yet above the critical temperature, a second, this time local, minimum develops, as shown by the dashed line. When the temperature has cooled down to the *critical temperature* T_c this second minimum becomes degenerate with the symmetric one. The value of the VEV v at this temperature is called the *critical VEV* v_c. Once the temperature falls below T_c the broken minimum ($v \neq 0$) becomes the global one and the vacuum state transitions from the symmetric phase into the broken phase. This procedure is called EWPT. The decide wether or not the EWPT is of strong first-oder the *baryon warshout condition* [28, 156]

$$\xi_c = \frac{v_c}{T_c} \geq 1\,,\tag{4.1}$$

is applied. If Eq. (4.1) is fulfilled the phase transition is an SFOEWPT. While the symmetric and critical phase coexist at the critical temperature, for temperatures slightly below the fields in the symmetric phase transitions into the broken minimum. During this transition, the broken vacuum expands through nucleation of bubbles in spacetime. At the front of the bubbles, EWBG can occur and the collisions of these bubbles produce gravitational waves. It has been shown in [25–27] that the EWPT in the SM is not of strong first-order if the the mass of the Higgs boson is above 70 GeV. Therefore, physics beyond the SM is necessary to achieve an SFOEWPT.

---

[12]While Fig. 4.1 shows the dependence on one Higgs expectation value, the picture can also be applied to theories with an extended Higgs sector.
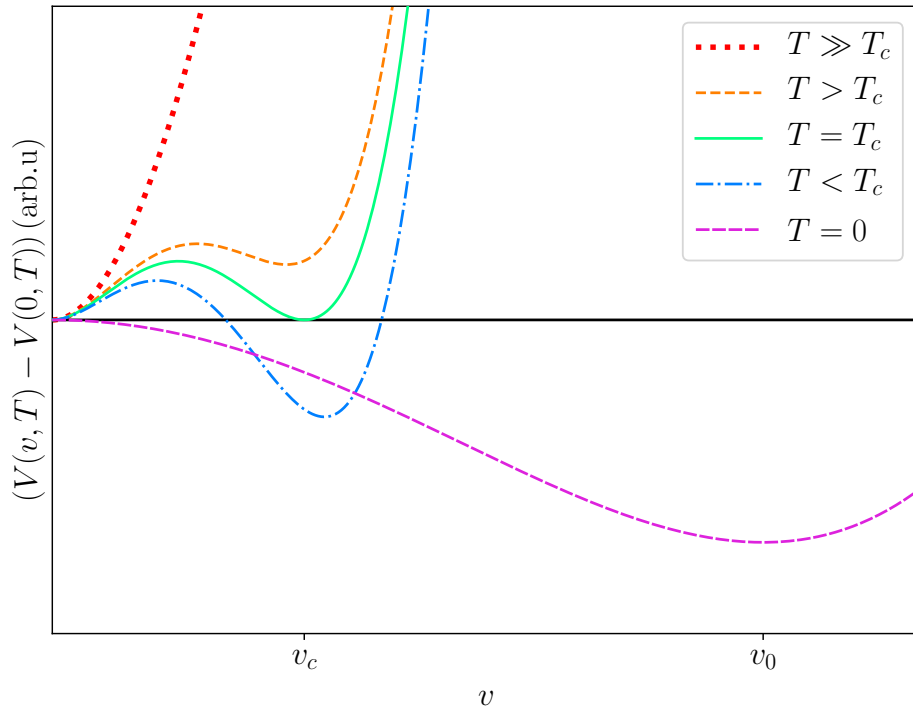
Figure 4.1.: The electroweak potential V at different temperatures as a function of the expectation value v of the Higgs field at fixed temperatures.

In this chapter, the necessary ingredients for the calculation of the EWPT are described. Short introductions in finite temperature field theory and the effective potential approach are given in Secs. 4.1 and 4.2. They are described using the operator approach in [157, 158] with a more detailed introduction into the effective potential can be found in [77]. An alternative approach using the closed time formalism for the finite temperature field theory is given in [159]. While Sec. 4.2 describes the concept of the effective potential at finite temperature, a general framework for models with extended Higgs sectors is given in Sec. 4.3. In Sec. 4.3 the analytically not solvable integral $J_{\pm}$ is defined. Section 4.4 describes a fast and numerically stable interpolation of $J_{\pm}$. In addition to the effective potential at finite temperatures, Sec. 4.5 introduces the a renormalisation scheme through the counterterm potential which can be used to fix the masses and mixing angles of the theory at vanishing temperature at next-to-leading-order (NLO) to the leading-order (LO) inputs. This chapter concludes with a short description of how the `C++` code `BSMPT` [4] calculates the strength of the EWPT in Sec. 4.6 and additional applications of `BSMPT` in Sec. 4.7.

4.1. Finite Temperature Field Theory

In the thermal bath of the early universe annihilation of particles is present and the particle number is not conserved. To describe a system with particle interactions in a thermal bath, the partition function of the grand canonical ensemble is necessary. It is given by

$$\mathcal{Z}(\beta) = \mathrm{Tr}\rho(\beta) = \mathrm{Tr}\exp\left(-\beta(H - \mu)\right), \tag{4.2}$$

where β is the inverse temperature in natural units ($k_B = 1$), μ is the chemical potential, ρ the density matrix, H the Hamiltonian of the system and $\mathrm{Tr}A$ describes the trace of the

matrix A. To describe observable quantities in a statistical ensemble the thermal average of the corresponding operator is needed. The thermal average of an operator $\mathcal{O}$ is given by

$$\langle \mathcal{O} \rangle_\beta = \frac{\text{Tr}[\rho(\beta)\mathcal{O}]}{\mathcal{Z}(\beta)} \, . \tag{4.3}$$

For two operators $\mathcal{O}_1$ and $\mathcal{O}_2$ at times t_1 and t_2 the cyclicity of the trace leads to the Kubo-Martin-Schwinger equation [160, 161]

$$\begin{aligned}
\langle \mathcal{O}_1(t_1)\mathcal{O}_2(t_2) \rangle_\beta &= \frac{1}{Z(\beta)}\text{Tr}[\rho(\beta)\mathcal{O}_1(t_1)\mathcal{O}(t_2)] \\
&= \frac{1}{\mathcal{Z}(\beta)}\text{Tr}[\exp(-\beta H + \beta\mu)\mathcal{O}_1(t_1)\exp(\beta H)\exp(-\beta H)\mathcal{O}(t_2)] \\
&= \frac{1}{\mathcal{Z}(\beta)}\text{Tr}[\mathcal{O}_1(t_1 + \mathrm{i}\beta)\exp(-\beta H + \beta\mu)\mathcal{O}_2(t_2)] \\
&= \frac{1}{\mathcal{Z}(\beta)}\text{Tr}[\mathcal{O}_1(t_1 + \mathrm{i}\beta)\rho(\beta)\mathcal{O}_2(t_2)] \\
&= \langle \mathcal{O}_2(t_2)\mathcal{O}_1(t_1 + \mathrm{i}\beta) \rangle_\beta \, .
\end{aligned} \tag{4.4}$$

From the second to the third line it was used that the chemical potential is not an operator but a scalar and, therefore, can be commutated with the operators. The imaginary time formalism with $t = \mathrm{i}\tau$ provides a method to fulfil Eq. (4.4) and allows to define the partition function for a given thermodynamical system. This is achieved by a Wick rotation, changing from the Minkowski space to Euclidian space. Furthermore, the imaginary time formalism allows for the description through the path integral formalism, cf. [159]. Equation (4.4) requires the time τ to be periodic with the inverse temperature, reducing the Euclidean space $\mathbb{R}^4$ down to the periodic space $\mathbb{R}^3 \times S^1$. For the calculation of the higher-order effects of the underlying theory, it is necessary to describe the n point Greens functions in the thermal bath. In the operator approach they can be written as

$$\mathcal{G}_\beta(x_1, \ldots, x_n) = \langle \mathcal{T}_C \phi(x_1) \ldots \phi(x_n) \rangle \tag{4.5}$$

with the path order operator $\mathcal{T}_C$. Assuming that it is possible to formulate a parametrisation for the path C the Greens function can be rewritten as

$$\mathcal{G}_\beta(x - y) = \mathcal{G}_\beta^+(x - y)\Theta_C(x^0 - y^0) + \mathcal{G}_\beta^-(x - y)\Theta_C(y^0 - x^0) \, , \tag{4.6}$$

where Θ_C is the Heaviside step function along the path for the complex time t. Expressing the fields ϕ through the eigenbasis $H|n\rangle = E_n|n\rangle$ with $\vec{x} = \vec{y} = 0$, the Greens function for the positive modes can be expressed as

$$\begin{aligned}
\mathcal{G}_\beta^+ &= \langle \phi(x^0, 0)\phi(y^0, 0) \rangle_\beta \\
&\propto \sum_{i,j} |\langle j|\phi(0)|i\rangle|^2 \exp\left(-\mathrm{i}E_i\left(x^0 - y^0\right)\right) \exp\left(\mathrm{i}E_j\left(x^0 - y^0 + \mathrm{i}\beta\right)\right) \, .
\end{aligned} \tag{4.7}$$

The requirement of convergence for the Greens function forces

$$\beta + \Im(x^0 - y^0) \geq 0 \, , \tag{4.8}$$

while an analogous calculation for G_β^- yields

$$\beta - \Im(x^0 - y^0) \geq 0 \, . \tag{4.9}$$

Combining both constraints yields

$$-\beta \leq \Im(x^0 - y^0) \leq \beta \,. \tag{4.10}$$

Choosing the Matsubara integration contour [159] $t \to -i\tau$ and using the periodicity of the Greens function yields

$$\mathcal{G}_\beta(\tau) = \pm \mathcal{G}_\beta(\tau + \beta) \,, \tag{4.11}$$

where $+(-)$ corresponds to bosonic (fermionic) fields. The periodicity in τ reduces the Fourier transformation of the Greens function to a discrete sum, given by

$$\mathcal{G}_\beta(\tau) = \frac{1}{\beta} \sum_n \exp(-i\omega_n \tau) \mathcal{G}_\beta(\omega_n) \,, \tag{4.12}$$

$$\mathcal{G}_\beta(\omega_n) = \frac{1}{2} \int_{-\beta}^{\beta} \exp(i\omega_n \tau) \mathcal{G}_\beta(\tau) \, d\tau \,, \tag{4.13}$$

with $\omega_n = \pi n/\beta$. Using Eq. (4.11) the two-point Greens function vanishes for an odd number of bosons and an even number of fermions. Therefore, the frequencies can be split in the so-called *Matsubara* frequencies

$$\omega_n = \begin{cases} \dfrac{2n\pi}{\beta} & \text{bosons} \\ \dfrac{(2n+1)\pi}{\beta} & \text{fermions} \end{cases} \,. \tag{4.14}$$

With this, the Greens function in momentum space is given by

$$\mathcal{G}_\beta(\vec{k}, \omega_n) = \frac{1}{\omega_n^2 + \vec{k}^2 + m^2} \,. \tag{4.15}$$

The periodicity of the Greens functions directly translates into a periodicity of the fields. Combining this with a Wick rotation the field space of the particles reduces from $\mathbb{R}^4$ to $\mathbb{R}^3 \times S^1$. In a real scalar field theory, therefore, the propagators at vanishing temperature have to be replaced by

$$\mathcal{D}(\omega_n, \vec{k}) = \frac{1}{\omega_n^2 + \vec{k}^2 + m^2} \,, \tag{4.16a}$$

$$p_E = (p_0, \vec{p}) \to (\omega_n, \vec{p}) \,, \tag{4.16b}$$

$$\int \frac{d^4 k_E}{(2\pi)^4} \to \frac{1}{\beta} \sum_n \int \frac{d^3 k}{(2\pi)^3} \,, \tag{4.16c}$$

in Euclidean space to describe the potential at finite temperature.

4.2. Effective Potential at Finite Temperature

It was shown in [162] that radiative corrections can have a large influence on the symmetry breaking patterns of the underlying theory and that broken symmetries can be restored through radiative corrections. Therefore, it is important to include such corrections. They are included through the effective potential which describes the theory as a zeroth-order expansion in external momenta of the effective action. As no closed-form exists it is necessary to calculate the corrections order by order. In this work, the corrections are calculated at

one-loop order. For a detailed review on how to derive the following relations the reader is referred to [28, 77, 159]. According to [77], the effective potential at NLO is given by

$$V_{eff}^{(1)} = \frac{1}{2} \int \frac{\mathrm{d}^4 k_E}{(2\pi)^4} \log \mathrm{Det} \left[-\mathcal{D}^{-1}(\omega, \vec{k}) \right] . \tag{4.17}$$

Applying the replacement rules for finite temperature, cf. Eq. (4.16), the effective potential is replaced by

$$V_{eff}^{(1)} \to \frac{1}{2\beta} \sum_n \int \frac{\mathrm{d}^3 k}{(2\pi)^3} \log \mathrm{Det} \left[-\mathcal{D}^{-1}\left(\omega_n, \vec{k} \right) \right] . \tag{4.18}$$

This can be split in a temperature independent and temperature-dependent part as

$$V_{eff}^{(1)} = \int \frac{\mathrm{d}^3 k}{(2\pi)^3} \frac{\omega_k}{2} + \int \frac{\mathrm{d}^3 k}{(2\pi)^3} \frac{\log\left(1 - \exp\left(-\beta\omega_k\right)\right)}{\beta} \tag{4.19}$$

with

$$\omega_k^2 = m^2 + \vec{k}^2 . \tag{4.20}$$

The temperature independent part is known as the Coleman-Weinberg contribution V^{CW}. As it is UV divergent it must be renormalised. In the $\overline{\mathrm{MS}}$ scheme the temperature independent part for a scalar particle is then given by

$$V^{\mathrm{CW}} = \frac{m^4}{64\pi^2} \left(\log\left(\frac{m^2}{\mu^2}\right) - \frac{3}{2} \right) \tag{4.21}$$

where μ is the $\overline{\mathrm{MS}}$ renormalisation scale. The temperature-dependent part can be rewritten as

$$\begin{aligned} V_T &= \int \frac{\mathrm{d}^3 k}{(2\pi)^3} \frac{\log\left(1 - \exp\left(-\beta\omega_k\right)\right)}{\beta} \\ &= \frac{1}{2\pi^2} \frac{1}{\beta^4} J_-\left(m^2\beta^2\right) \end{aligned} \tag{4.22}$$

with

$$J_-(x^2) = \int\limits_0^\infty \mathrm{d}k k^2 \log\left[1 - \exp\left(-\sqrt{k^2 + x^2}\right)\right] . \tag{4.23}$$

To investigate the details of the correction to the potential, the calculation is applied to the ϕ^4 theory with the Lagrangian

$$\mathcal{L} = \frac{1}{2} \left(\partial_\mu \phi\right)^2 - \left(\mu^2 \phi^2 + \lambda \phi^4\right) , \tag{4.24}$$

where the field ϕ fluctuates around its VEV $\langle \phi \rangle = \omega$. The VEV v at vanishing temperature denotes the minimum of the scalar potential in Eq. (4.24). This yields the minimum condition

$$0 = 2v \left(2\lambda v^2 + \mu^2\right) . \tag{4.25}$$

The mass term of the field ϕ is then given by

$$m^2(\omega) = 12\lambda\omega^2 + 2\mu^2 . \tag{4.26}$$

By replacing λ and μ^2 through Eq. (4.25), the mass for a general ω can be rewritten as

$$m^2(\omega) = \frac{1}{2} m^2(\omega = v) \left(\frac{3\omega^2}{v^2} - 1 \right) . \tag{4.27}$$

Applying the high temperature expansion of $J_-(m^2\beta^2)$ [163], defined through $m^2/T^2 \ll 1$, the temperature dependent potential at the VEV ω of ϕ is then given by

$$V^{\mathrm{T}}(\omega) = T^4 \left[-\frac{\pi^2}{90} + \frac{m^2(\omega)}{24T^2} - \frac{m^3(\omega)}{12\pi T^3} + \mathcal{O}\left(m^4/T^4\right) \right] . \tag{4.28}$$

The NLO correction to the temperature-dependent potential is given through m^3 and therefore of order $\lambda^{3/2}$, meaning the corrections of order $\lambda^{3/2}$ have to be taken into account. These so-called *Debye* corrections [164] are needed to cure the divergences emerging from the Matsubara zero modes ($n = 0$) of the bosons. While the zero mode of the fermions is given by

$$\omega_0 = (2 \times 0 + 1)\pi = \pi \tag{4.29}$$

the zero mode of the bosons

$$\omega_0 = 2 \times 0\pi = 0 \tag{4.30}$$

vanishes and therefore the effective potential diverges as

$$V_{\mathrm{eff}} \propto \log(-\mathcal{D}^{-1}) \xrightarrow{\vec{p} \to 0} \infty . \tag{4.31}$$

The Debye corrections can be obtained as next-to-leading-order corrections to the thermal loops which can be expressed as a correction to the self-energies in the infrared limit. For the calculation, the hard thermal loop (HTL) approximation [159], in which loop momenta and masses are assumed to be small compared to the temperature scale, is applied. In [164] it was shown that this limit is a good approximation as for large ratios of m/T the Debye corrections are negligible. In the ϕ^4 theory the correction Π to the self-energy in the effective potential is given by

$$\begin{aligned}
\Pi^{(1)} &= 12\lambda T \sum_n \int \frac{\mathrm{d}^3 k}{(2\pi)^3} \frac{1}{\omega_n^2 + \omega_k^2} \\
&= 12\lambda T \int \frac{\mathrm{d}^3 k}{(2\pi)^3} \frac{1}{2\omega_k} \frac{\mathrm{d}}{\mathrm{d}\omega_k} \sum_n \log(\omega_n^2 + \omega_k^2) \\
&= 12\lambda \left[\int \frac{\mathrm{d}^3 k}{(2\pi)^3} \frac{1}{2\omega_k} + \int \frac{\mathrm{d}^3 k}{(2\pi)^3} \frac{1}{\omega_k \left(\exp(\beta\omega_k) - 1 \right)} \right]
\end{aligned} \tag{4.32}$$

with $\omega_k^2 = m^2 + \vec{k}^2$. Applying the HTL with $m/T \ll 1$ yields

$$\Pi^{(1)} = \lambda T^2 . \tag{4.33}$$

4.3. Effective Potential at Finite Temperature for General Models

For the models introduced in Chapter 2 it is necessary to expand this formalism. For this, the general framework of [165] is used and the Lagrangian needs to be decomposed into

$$-\mathcal{L}_S = L^i \Phi_i + \frac{1}{2} L^{ij} \Phi_i \Phi_j + \frac{1}{3!} L^{ijk} \Phi_i \Phi_j \Phi_k + \frac{1}{4!} L^{ijkl} \Phi_i \Phi_j \Phi_k \Phi_l , \tag{4.34}$$

$$-\mathcal{L}_F = \frac{1}{2} Y^{IJk} \Psi_I \Psi_J \Phi_k + c.c. , \tag{4.35}$$

$$\mathcal{L}_G = \frac{1}{4} G^{abij} A_{a\mu} A_b^\mu \Phi_i \Phi_j , \tag{4.36}$$

where Φ_i are the n_{Higgs} real scalar fields which make up the scalar multiplets (e.g. eight real scalar fields in the 2HDM) with $i = 1, \ldots, n_{\text{Higgs}}$. The fermion mulitplets are expressed through the Weyl spinors Ψ_I with $I = 1, \ldots, n_{\text{fermion}}$. The gauge bosons are given by the four-vectors A_μ^a where the group index a runs from 1 to n_{gauge}. L^i, L^{ij}, L^{ijk} and L^{ijkl} are the parameters of the Higgs potential, Y^{IJk} the interactions between two fermions and one scalar particle and G^{abij} the interactions between two gauge bosons and two scalar particles. After symmetry breaking the scalar fields can be expanded around their VEVs as

$$\Phi_i = \omega_i + \phi_i \,. \tag{4.37}$$

This yields

$$-\mathcal{L}_S = \Lambda + \Lambda_{(S)}^i \phi_i + \frac{1}{2}\Lambda_{(S)}^{ij}\phi_i\phi_j + \frac{1}{3!}\Lambda_{(S)}^{ijk}\phi_i\phi_j\phi_k + \frac{1}{4!}\Lambda_{(S)}^{ijkl}\phi_i\phi_j\phi_k\phi_l \,, \tag{4.38}$$

$$-\mathcal{L}_F = \frac{1}{2}M^{IJ}\Psi_I\Psi_J + \frac{1}{2}Y^{IJk}\Psi_I\Psi_J\phi_k \,, \tag{4.39}$$

$$\mathcal{L}_G = \frac{1}{2}\Lambda_{(G)}^{ab}A_{a\mu}A_b^\mu + \frac{1}{2}\Lambda_{(G)}^{abi}A_{a\mu}A_b^\mu\phi_i + \frac{1}{4}\Lambda_{(G)}^{abij}A_{a\mu}A_b^\mu\phi_i\phi_j \,. \tag{4.40}$$

The tensors are given by

$$\Lambda = V^{(0)} = L^i\omega_i + \frac{1}{2}L^{ij}\omega_i\omega_j + \frac{1}{3!}L^{ijk}\omega_i\omega_j\omega_k + \frac{1}{4!}L^{ijkl}\omega_i\omega_j\omega_k\omega_l \,, \tag{4.41a}$$

$$\Lambda_{(S)}^i = L^i + L^{ij}\omega_j + \frac{1}{2}L^{ijk}\omega_j\omega_k + \frac{1}{6}L^{ijkl}\omega_j\omega_k\omega_l \,, \tag{4.41b}$$

$$\Lambda_{(S)}^{ij} = L^{ij} + L^{ijk}\omega_k + \frac{1}{2}L^{ijkl}\omega_k\omega_l \,, \tag{4.41c}$$

$$\Lambda_{(S)}^{ijk} = L^{ijk} + L^{ijkl}\omega_l \,, \tag{4.41d}$$

$$\Lambda_{(S)}^{ijkl} = L^{ijkl} \,, \tag{4.41e}$$

$$\Lambda_{(G)}^{ab} = \frac{1}{2}G^{abij}\omega_i\omega_j \,, \tag{4.41f}$$

$$\Lambda_{(G)}^{abi} = G^{abij}\omega_j \,, \tag{4.41g}$$

$$\Lambda_{(G)}^{abij} = G^{abij} \,, \tag{4.41h}$$

$$\Lambda_{(F)}^{IJ} = M^{*IL}M_L^J = Y^{*ILk}Y_L^{\,Jm}\omega_k\omega_m \,, \tag{4.41i}$$

$$M^{IJ} = Y^{IJk}\omega_k \,. \tag{4.41j}$$

The Coleman-Weinberg potential is then given by

$$V^{\text{CW}} = \frac{1}{64\pi^2}\sum_{X=S,G,F}(-1)^{2s_X}(1+2s_X)\text{Tr}\left[\left(\Lambda_{(X)}^{xy}\right)^2\left(\log\left(\frac{1}{\mu^2}\Lambda_{(X)}^{xy}\right) - k_X\right)\right] \,, \tag{4.42}$$

where

$$s_X = \begin{cases} 0 & \text{scalars} \\ \dfrac{1}{2} & \text{fermion} \\ 1 & \text{gauge boson} \end{cases} \tag{4.43}$$

describes the spin of the field X. The indices xy relate to the corresponding indices ij, ab or IJ for $X = S, G$ or F. The $\overline{\text{MS}}$ scheme sets the value of k_X as

$$k_X = \begin{cases} \dfrac{5}{6} & \text{gauge boson} \\ \dfrac{3}{2} & \text{scalar and fermions} \end{cases} \,. \tag{4.44}$$

Following the recipe of Sec. 4.1 the thermal corrections were calculated and published in [4] for a theory described by Eqs. (4.34) to (4.36). The temperature-dependent part of the potential is then given by

$$V^{\mathrm{T}} = \sum_{X=S,G,F} (-1)^{2s_X}(1+2s_X)\frac{T^4}{2\pi^2}J_{\pm}\left(\Lambda^{xy}_{(X)}/T^2\right) \tag{4.45}$$

with

$$J_{\pm}\left(\Lambda^{xy}_{(X)}/T^2\right) = \mathrm{Tr}\left[\int\limits_0^{\infty}\mathrm{d}k k^2\log\left[1\pm\exp\left(-\sqrt{k^2+\Lambda^{xy}_{(X)}/T^2}\right)\right]\right], \tag{4.46}$$

where J_- is for bosons and J_+ for fermions.

As in the previous section for the ϕ^4 theory, the Debye corrections have to be included to cancel the divergences through the Matsubara zero modes of the bosons. In the notation of Eqs. (4.34) to (4.36) they read as

$$\Pi^{ij}_{(S)} = \frac{T^2}{24}\left[(-1)^{2s_S}(1+2s_S)\sum_{k=1}^{n_{\mathrm{Higgs}}} L^{ijkk} + (-1)^{2s_G}(1+2s_G)\sum_{a=1}^{n_{\mathrm{gauge}}} G^{aaij}\right.$$
$$\left. -(-1)^{2s_F}(1+2s_F)\frac{1}{2}\sum_{I,J=1}^{n_{\mathrm{fermion}}}\left(Y^{*IJj}Y_{IJ}{}^i + Y^{*IJi}Y_{IJ}{}^j\right)\right], \tag{4.47}$$

$$\Pi^{ab}_{(G)} = T^2\frac{2}{3}\left(\frac{\tilde{n}_H}{8}+5\right)\frac{1}{\tilde{n}_H}\sum_{m=1}^{n_{\mathrm{Higgs}}} G^{aamm}\delta_{ab}, \tag{4.48}$$

where only the longitudinal modes of the gauge bosons receive the Debye corrections and $\tilde{n}_H$ is the number of scalar fields with a non-vanishing coupling to gauge bosons. It is important to note that Eq. (4.48) applies only for theories with no additional fermions or gauge bosons compared to the SM. As this is the case for the 2HDM and N2HDM this poses no problem for this work.

To include the Debye corrections in the effective potential the Arnold-Espinosa method [166] yields the replacement

$$V^{\mathrm{T}}(\omega,T) \to V^{\mathrm{T}}(\omega,T) + V_{\mathrm{Debye}}(\omega,T), \tag{4.49}$$

$$V_{\mathrm{Debye}}(\omega,T) = -\frac{T}{12\pi}\left[\sum_{i=1}^{n_{\mathrm{Higgs}}}\left((\overline{m}_i^2)^{3/2} - (m_i^2)^{3/2}\right) + \sum_{a=1}^{n_{\mathrm{gauge}}}\left((\overline{m}_a^2)^{3/2} - (m_a^2)^{3/2}\right)\right]. \tag{4.50}$$

Here m_i^2 and m_a^2 are the eigenvalues of $\Lambda^{ij}_{(S)}$ and $\Lambda^{ab}_{(G)}$, while $\overline{m}_i^2$ and $\overline{m}_a^2$ are the eigenvalues of the temperature corrected mass matrices $\Lambda^{ij}_{(S)} + \Pi^{ij}_{(S)}$ and $\Lambda^{ab}_{(G)} + \Pi^{ab}_{(G)}$.

Another possible approach to include the Debye corrections is given by the Parwani method [167] where the replacements

$$\Lambda^{ij}_{(S)} \to \Lambda^{ij}_{(S)} + \Pi^{ij}_{(S)}, \tag{4.51}$$

$$\Lambda^{ab}_{(G)} \to \Lambda^{ab}_{(G)} + \Pi^{ab}_{(G)} \tag{4.52}$$

are inserted in Eq. (4.42) and Eq. (4.45). As this partially includes two-loop corrections to the potential through $\overline{m}^4$ terms, the calculations later in this work are done in the Arnold-Espinosa method.

4.4. Numerical Treatment of $J_\pm$

During the evaluation of the thermal potential, cf. Eq. (4.45), the integrals

$$J_\pm(x^2) = \int\limits_0^\infty dk k^2 \log\left[1 \pm \exp\left(-\sqrt{k^2 + x^2}\right)\right] \tag{4.53}$$

need to be calculated numerically. As this is very time consuming it is not suitable for a numerical evaluation over a large amount of parameter points in a phenomenological study. In [163] the function was therefore expanded in regions of small and large $x^2 = m^2/T^2$. For small x^2 the expansion is given by

$$
\begin{aligned}
J_{+,s}(x^2, n) = {}&- \frac{7\pi^4}{360} + \frac{\pi^2}{24}x^2 + \frac{1}{32}x^4\left(\log x^2 - c_+\right) \\
&- \pi^2 x^2 \sum_{l=2}^n \left(-\frac{x^2}{4\pi^2}\right)^l \frac{(2l-3)!!\zeta(2l-1)}{(2l)!!(l+1)}\left(2^{2l-1} - 1\right),
\end{aligned} \tag{4.54}
$$

$$
\begin{aligned}
J_{-,s}(x^2, n) = {}&- \frac{\pi^4}{45} + \frac{\pi^2}{12}x^2 - \frac{\pi}{6}\left(x^2\right)^{3/2} - \frac{1}{32}x^4\left(\log x^2 - c_-\right) \\
&+ \pi^2 x^2 \sum_{l=2}^n \left(-\frac{x^2}{4\pi^2}\right)^l \frac{(2l-3)!!\zeta(2l-1)}{(2l)!!(l+1)}
\end{aligned} \tag{4.55}
$$

with

$$c_+ = \frac{3}{2} + 2\log\pi - 2\gamma_E, \qquad c_- = c_+ + 2\log 4. \tag{4.56}$$

Here γ_E denotes the Euler-Mascheroni constant, $(x)!!$ the double factorial and $\zeta(x)$ the Riemann ζ−function. For large x^2 the expansion is given by

$$J_{\pm,l}(x^2, n) = -\exp\left(-(x^2)^{1/2}\right)\left(\frac{\pi}{2}\left(x^2\right)^{3/2}\right)^{1/2} \sum_{l=0}^n \frac{1}{2^l l!}\frac{\Gamma(5/2 + l)}{\Gamma(5/2 - l)}(x^2)^{-l/2}. \tag{4.57}$$

To ensure a smooth transition from the expansion of small values of x^2 to the large ones, the expansions and their derivatives are enforced to be continuous. For this, a small shift in the absolute values of the functions is introduced. The integrals can then be approximated by

$$J_+(x^2) = \begin{cases} -J_{\pm,l}(x^2, 3) & x^2 \geq x_+^2 \\ -(J_{+,s}(x^2, 4) + \delta_+) & x^2 < x_+^2 \end{cases}, \tag{4.58}$$

$$J_-(x^2) = \begin{cases} J_{\pm,l}(x^2, 3) & x^2 \geq x_-^2 \\ J_{-,s}(x^2, 3) + \delta_- & x^2 < x_-^2 \end{cases}, \tag{4.59}$$

with

$$x_+^2 = 2.2161, \qquad \delta_+ = -0.015603, \tag{4.60}$$

$$x_-^2 = 9.4692, \qquad \delta_- = 0.0063109. \tag{4.61}$$

To check for the impact of the introduced finite shift $\delta_\pm$ the function $J_\pm$, cf. Eq. (4.53), has been evaluated at several values of x^2 and compared to the corresponding series expansion, cf. Eqs. (4.58) and (4.59). For J_- the relative difference between the expansion and the numerical evaluation does not exceed 1% while J_+ has a maximal deviation of $\sim 1.3\%$ around the transition point.

4.5. Renormalisation

The radiative corrections included in the Coleman-Weinberg potential in the $\overline{\text{MS}}$ scheme change the masses and mixing angles of the theory compared to their tree-level values. For phenomenological studies, it would be more convenient to work in an on-shell renormalisation scheme, where corrections to the masses are absorbed into additional contributions. In this case the relations between the tree-level masses are the same as the input masses and the tree-level relations between the masses and the parameters of the potential can be used to calculated the parameters of the tree-level potential. In the effective potential approach, such a scheme can be realised by adding finite counterterm contributions on top of the $\overline{\text{MS}}$ renormalised Coleman-Weinberg potential. This is achieved by replacing every parameter $p^{(0)}$ of the tree-level potential $V^{(0)}$ with the renormalised parameter p and its counterterm δp. The counterterm potential is then given by

$$V^{\text{CT}} = \sum_{i=1}^{n_p} \frac{\partial V^{(0)}}{\partial p_i} \delta p_i + \sum_{k=1}^{n_v} \delta T_k \left(\phi_k + \omega_k \right) . \tag{4.62}$$

Here n_p is the number of potential parameters and δT_k denote the counterterms of the tadpoles T_k obtained from the minimum conditions of the potential, cf. Eq. (2.31) for the 2HDM and Eq. (2.80) for the N2HDM, and vanish at tree-level. As the tadpoles that are calculated w.r.t. fields without a VEV do not contribute later on for the minimisation they can be dropped and only the $n_v \leq n_{\text{Higgs}}$ field directions with a VEV remain.

Imposing the masses and mixing angles being the same at LO and NLO yields the following renormalisation conditions

$$0 = \partial_{\phi_i} \left(V^{\text{CW}} + V^{\text{CT}} \right) \big|_{\phi_k = \langle \phi_k \rangle (T=0)} , \tag{4.63}$$

$$0 = \partial_{\phi_i} \partial_{\phi_j} \left(V^{\text{CW}} + V^{\text{CT}} \right) \big|_{\phi_k = \langle \phi_k \rangle (T=0)} , \tag{4.64}$$

where $\phi_k = \langle \phi_k \rangle (T = 0)$ is the electroweak minimum of the tree-level potential with $i, j, k = 1 \ldots n_{\text{Higgs}}$. To solve Eqs. (4.63) and (4.64) the derivatives of the Coleman-Weinberg potential are necessary which have been derived in [165]. While the renormalisation conditions guarantee that the tree-level minimum still is a local minimum at NLO, it has to be checked numerically if the tree-level minimum is the global minimum at NLO.

The counterterms for the 2HDM and N2HDM are given in Eq. (B.5) respectively Eq. (B.7).

4.6. Calculation of ξ_c

To decide if a concrete parameter point provides an SFOEWPT it is necessary to calculate the quantity $\xi_c = v_c / T_c$ and therefore both the critical temperature T_c and the critical VEV v_c. Therefore it is necessary to minimise the potential

$$V(\omega, T) = V^{(0)}(\omega) + V^{\text{CW}}(\omega) + V^{\text{CT}}(\omega) + V^{\text{T}}(\omega, T) , \tag{4.65}$$

with the tree-level potential $V^{(0)}$, cf. Eq. (4.41a), Coleman-Weinberg potential V^{CW}, cf. Eq. (4.42), counterterm potential, cf. Eq. (4.62) and the thermal corrections V^{T}, cf. Eq. (4.49). During the numerical minimisation of Eq. (4.65) VEV configurations resulting in negative mass squares appear, yielding a complex potential. As the masses, namely the eigenvalues of the Hessian matrix of the potential, are positive in the global minimum, it suffices to minimise the real part of the potential [168]. For this purpose the models were implemented in the `C++`

code BSMPT [4]. BSMPT minimises the effective potential at a fixed temperature and calculates the electroweak VEV

$$\overline{\omega}(T) = \sqrt{\sum_i \overline{\omega}_i(T)^2 \delta_i} \,. \tag{4.66}$$

Here $\overline{\omega}_i(T)$ is the VEV of the Higgs field i at fixed temperature T and δ_i is 1 if the corresponding field couples to $SU(2)$ gauge bosons and 0 otherwise. To calculate the critical temperature the following procedure is then applied:

- Calculate $\omega(T = 0\,\text{GeV})$ and check if the found minimum is the same as the tree-level minimum[13].

- Calculate $\omega(T = 300\,\text{GeV})$ and check if it vanishes. As shown in Fig. 4.1 the VEV can only decrease with rising temperature. Therefore, the VEV is limited by the upper bound $\overline{\omega}(T) \leq v \approx 246\,\text{GeV}$. For temperatures above v the EWPT cannot be of strong first-oder, as $\overline{\omega}/T \leq v/T < 1$. To allow for numerical errors the upper limit is chosen to be $300\,\text{GeV}$.

- Apply a bisection procedure with the end points $T_s = 0\,\text{GeV}$ and $T_e = 300\,\text{GeV}$. If $\omega\left(\dfrac{T_s + T_e}{2}\right)$ vanishes set $T_e = \dfrac{T_s + T_e}{2}$ otherwise $T_s = \dfrac{T_s + T_e}{2}$. This is repeated until a precision of $T_e - T_s \leq 10^{-2}\,\text{GeV}$ is achieved. The critical temperature is then set to $T_c = T_s$ and the critical VEV as $v_c = \overline{\omega}(T_c)$.

4.7. Additional Applications of BSMPT

The name giving purpose of BSMPT [4], `Beyond the SM Phase Transition`, is the calculation of the strength of the EWPT, cf. Sec. 4.6. The program can be downloaded from https://github.com/phbasler/BSMPT. BSMPT provides the implementation of the R2HDM, C2HDM and N2HDM. The input file is given through a tabulator separated text file which has the type, cf. Tab. 2.1, and the tree-level parameters of the potential, eg. Eq. (2.33) for the C2HDM. Exemplary input files for all models are provided with the program for all implemented models. Different aspects of the calculation are provided over multiple executables. The output file generated by each executable contains the values of the input file, the numerical values of the parameter of the counterterm potential, cf. Sec. 4.5, as well as the result of the executable. The program provides the following executables

- BSMPT calculates the strength of the EWPT. For this, the critical temperature T_c, all components of the VEV at the EWPT, the electroweak VEV and the strength of the EWPT are attached as new columns.

- VEVEVO calculates the electroweak minimum at fixed temperatures between a given temperature range for given step size. This can be used to investigate the evolution of the electroweak VEV of a fixed parameter point with temperature.

- TripleHiggsCouplingsNLO calculates the coupling between all possible combinations between three Higgs bosons, cf. Eq. (2.70), at vanishing temperature. The resulting output file contains the contribution to the trilinear Higgs couplings from the tree-level, counterterm and Coleman-Weinberg potential.

- NLOVEV calculates the electroweak minimum at NLO today and attaches all components of the NLO electroweak VEV as columns. This can be used to check if the electroweak minimum is stable at NLO.

---

[13]Through the counterterm potential defined in Sec. 4.5 the tree-level minimum is a local minimum at NLO, but it has still to be ensured that it is the global minimum.

- `Test` checks if the implementation of a new model was successful. For this, all particle masses are calculated and the fermion and gauge boson masses are compared to their implemented values and the Higgs boson masses are compared to their NLO values.

- `CalcCT` calculates only the parameters of the counterterm potential.

Additional models can be implemented with the general framework for the theory given in Eqs. (4.34) to (4.36). A detailed explanation of how to implement them is given in the manual [4].

Impact of the Electroweak Phase Transition on Phenomenology

In this chapter, the impact of constraining the phenomenology of the C2HDM and N2HDM through EWPT is investigated. At first, the criteria applied to the parameter space are described. Afterwards, a direct comparison between the models is used to show the influence of the EWPT and to discuss possible discovery signals. These investigations in the C2HDM have been published in [3], while [5] provides an update on the C2HDM together with the investigation in the N2HDM. As [5] is not finalised yet, the figures in [5] may differ from those shown in this chapter.

5.1. The Allowed Parameter Space

To scan the parameter space of the C2HDM and N2HDM both models have been implemented in `ScannerS` [68, 78], with their theoretical constraints, cf. Secs. 2.2.5 and 2.3.4. The results from LHC Run2, LEP and Tevatron Higgs searches were checked with `Higgs-Bounds` v5.5.0 [79–84]. `ScannerS` generates the masses and mixing matrix elements with a randomised uniform distribution. The decay widths and branching ratios were calculated with `C2HDM_HDECAY` [85, 87, 169] for the C2HDM and `N2HDECAY` [75, 85, 87] for the N2HDM respectively and checked against the experimental limits through `HiggsSignals` v.2.3.0 [170–172]. Additionally, the $B \rightarrow s\gamma$ measurements [90–94] were taken into account. For the C2HDM the EDM of the electron was taken into account with the upper limits provided by the `ACME` collaboration [98]. As the main contribution from the fermions to the EWPT is given by the top coupling, the difference between type I and type II in the calculation of the EWPT has a subleading effect. As the two types greatly differ in the allowed parameter space, the allowed region for successful SFOEWPT differs accordingly [1, 3]. As the EDM and $B \rightarrow s\gamma$ constraints are more stringent in type II than in type I the latter has been chosen for the comparison between the N2HDM and C2HDM. The used ranges for the parameter scans are given in Tab. 5.1. Instead of denoting the 3 neutral mass eigenstates with m_{h_1}, m_{h_2} and m_{h_3}, cf. Secs. 2.2.4 and 2.3.3, they were relabeld $m_h, m_{H_\downarrow}$ and $m_{H_\uparrow}$ where m_h is the SM-like Higgs boson and $H_\downarrow$ and $H_\uparrow$ are ordered such that $m_{H_\downarrow} \leq m_{H_\uparrow}$. The SM parameters are given in Appendix A.

The reduction in the number of parameter points applying these constrains is shown in Tab. 5.2. While the samples are generated with a randomised uniform distribution and

	C2HDM	N2HDM
$m_h \, [\text{GeV}]$	125.09	125.09
$m_{H_\downarrow} \, [\text{GeV}]$	$30 \ldots 1500$	$30 \ldots 1500$
$m_{H_\uparrow} \, [\text{GeV}]$	$30 \ldots 1500$	$30 \ldots 1500$
$m_{H^\pm} \, [\text{GeV}]$	$150 \ldots 1500$	$150 \ldots 1500$
$m_A \, [\text{GeV}]$	-	$30 \ldots 1500$
$\tan \beta$	$0.8 \ldots 20$	$0.8 \ldots 20$
$\Re m_{12}^2 \, [\text{GeV}^2]$	$10^{-3} \ldots 5 \times 10^5$	$10^{-3} \ldots 5 \times 10^5$
$v_s \, [\text{GeV}]$	-	$1 \ldots 3000$

Table 5.1.: Input parameter for both scans described in Sec. 5.1. In the N2HDM m_{12}^2 is real and, therefore, $m_{12}^2 = \Re m_{12}^2$.

Applied constraint	C2HDM	N2HDM
Total number of parameter points	233163	271743
NLO vacuum stability	97.32%	83.64%
NLO vacuum stability + NLO perturbative unitarity	91.03%	80.32%
SFOEWPT + NLO vacuum stability + NLO perturbative unitarity	0.013%	0.353%

Table 5.2.: Reduction of the number of parameter points before and after applying NLO vacuum stability, NLO pertubative unitarity and SFOEWPT.

roughly the same number of parameter points, more points are not longer valid once NLO vacuum stability is considered in the N2HDM than in the C2HDM. This is due to the additional pseudoscalar Higgs boson providing an additional term proportional to $m_A^4 \log m_A^2$ in the Coleman-Weinberg potential, cf. Eq. (4.21), yielding possible large corrections to the NLO potential. These large corrections also explains the parameter points which are no longer valid after applying the approximated NLO unitariy constraints. While the N2HDM has a higher loss than the C2HDM at vanishing temperature through the additional Higgs boson, it increases the viable parameter space for EWPT as the pseudoscalar Higgs boson does not contribute to the electroweak VEV but influences the effective potential.

5.2. Effects on the masses of the non-SM-like Higgs Bosons

Figure 5.1 shows the charged Higgs mass $m_{H^\pm}$ as a function of $\tan \beta$, C2HDM on the left and N2HDM on the right. For Fig. 5.1 and all following figures the parameter points surviving all constraints in Sec. 5.1 are shown in black. Additionally, for all points it has been checked if

their NLO VEVs are the same as at LO, calculated with `BSMPT` [4]. To have a first check of the perturbative unitarity at NLO the constraints Eqs. (2.54) and (2.91) have been tested after replacing the quartic tree-level couplings λ_i with their NLO shifted values, defined through $\lambda_i \rightarrow \lambda_i + \delta\lambda_i$. Here $\delta\lambda_i$ are the parameters of the counterterm potential defined through the renormalisation scheme described in Sec. 4.5 and calculated through the formulae in Appendix B. The λ_i on the right-hand side are obtained through the tree-level relations from the masses and mixing angles, cf. Eqs. (2.45) and (2.90). Parameter points providing additionally a stable NLO vacuum and successful perturbative unitarity at NLO compared to the black points are shown in grey. All parameter points shown with the given colour scale provide an SFOEWPT. While it seems like the N2HDM is more restricted for higher values of $\tan\beta$ this is an artefact of the scan procedure. The scan is set up in such a way that a fixed number of valid parameter points are generated. As the N2HDM spectrum has an additional Higgs boson as compared to the C2HDM there are more valid parameter points in the N2HDM for each pixel in the $m_{H^\pm} - \tan\beta$ plane. The few points for $\tan\beta \gtrsim 12$ show that points in this area are still possible, just not as likely as parameter points with $\tan\beta \lesssim 12$. While most of the points in the C2HDM providing an SFOEWPT have a charged Higgs mass of at least $m_{H^\pm} \sim 450\,\text{GeV}$ three points with $m_{H^\pm} \leq 175\,\text{GeV}$ were found. These are also the ones with an inverted hierarchy, meaning that the SM-like Higgs boson m_h is not the lightest one but the heaviest. For those points the masses are closely together, the biggest difference is $m_h - m_{H_\downarrow} \approx 30\,\text{GeV}$, and, therefore, no decays into lighter Higgs bosons are possible. For the other points, a large charged Higgs mass of 450 to 650 GeV comes along with neutral masses above the SM-like Higgs boson mass. In the N2HDM the allowed region for parameter points providing an SFOEWPT is much larger than in the C2HDM, which results from the extra degree of freedom in the Higgs particle spectrum. This is highlighted in Fig. 5.2. The black parameter points fulfil the constraints described in Sec. 5.1, while the grey points additionally provide a NLO stable vacuum and approximated NLO perturbative unitarity. The coloured point show all parameter points providing an SFOEWPT. On the left side, the difference $m_{H_\uparrow} - m_{H^\pm}$ is shown as a function of $m_{H_\downarrow} - m_{H^\pm}$ in the C2HDM which can be divided into three regions. The left and upper areas are defined by $m_{H_\downarrow} < m_{H_\uparrow} \approx m_{H^\pm}$ and $m_{H_\downarrow} \approx m_{H^\pm} < m_{H_\uparrow}$, respectively, which provided a possible parameter region for SFOEWPT, cf. Figure 5 in [3]. Through updates of the exclusion limits in `HiggsBounds` and `HiggsSignals` the outer regions of these areas are largely excluded and, therefore, the possible parameter region for SFOEWPT is reduced. The third region is the diagonal in the lower right where $m_{H_\downarrow} \approx m_{H_\uparrow}$ with both possibilities for the charged Higgs mass below and above the other masses. For the bulk of the parameter points providing an SFOEWPT the charged Higgs mass is above the others. Combining this with the mass scale of the charged Higgs mass in Fig. 5.1 yields a medium spectrum which would be mostly excluded through $B \rightarrow s\gamma$ constraints in the type II scenario. In the N2HDM the situation is more relaxed. Because of the enlarged Higgs spectrum the mass distribution is not as restricted in the N2HDM in the C2HDM. In order to describe the mass distribution the relative difference between the masses of two Higgs bosons X and Y is introduced as

$$\Delta_{m_X, m_Y} = \frac{m_X - m_Y}{m_X + m_Y}\,. \tag{5.1}$$

This is shown in the right side of Fig. 5.2. Here the coloured points are the ones providing an SFOEWPT while the colour code indicates the difference between the additional pseudoscalar Higgs boson A and the charged Higgs boson. Contrary to the C2HDM there are parameter points with a large spread between $m_{H_\downarrow}, m_{H_\uparrow}$ and $m_{H^\pm}$ while the charged Higgs is approximately degenerate with the pseudoscalar Higgs boson, shown by the purple (dark) points. For most of the parameter points with low masses of the charged Higgs boson with $m_{H^\pm} \lesssim 300\,\text{GeV}$, the neutral CP-even Higgs bosons are also low while the pseudoscalar Higgs boson is heavy, which strengthens the EWPT while not contributing to the electroweak VEV.
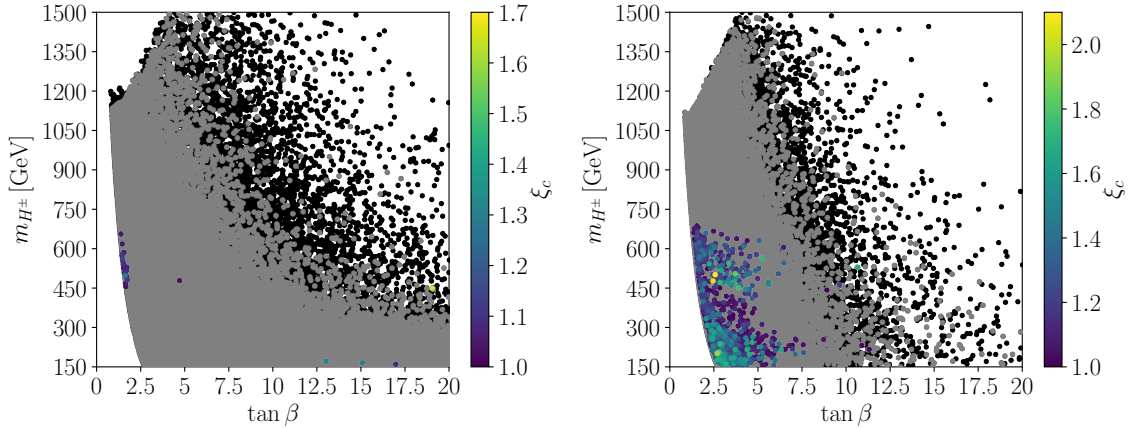
Figure 5.1.: The charged Higgs boson mass as a function of $\tan\beta$, on the left for the type I C2HDM and on the right the type I N2HDM with the colour indicating the strength of the EWPT. The black show the parameter points surviving the constraints described in Sec. 5.1, while the grey points additionally provide a NLO stable vacuum and approximated NLO perturbative unitarity.

For the other parameter points with a low mass of the charged Higgs boson $m_{H^\pm} \lesssim 400\,\text{GeV}$, the charged Higgs boson is degenerate with the pseudoscalar Higgs boson either $H_\downarrow$ or $H_\uparrow$ has a large singlet contribution and, therefore, does not contribute to the electroweak VEV but to the strength of the EWPT.

5.3. Impact on the SM-like Higgs Boson Trilinear Self-Coupling

While the couplings between the SM-like Higgs boson with two fermions or two gauge bosons are measured to be close to the SM values, the trilinear self-coupling between three SM-like Higgs bosons is only loosely constraint [173–175]. To get a comparison with the SM value Fig. 5.3 shows the NLO trilinear self-coupling of the SM-like Higgs boson $\lambda_{hhh}^{\text{NLO}}$ as a function of the LO value, both calculated with BSMPT [4] and normalised to the SM value. The used reference SM values at LO and NLO are given by [176]

$$\lambda_{hhh}^{\text{LO,SM}} = -\frac{3m_h^2}{v}\,, \tag{5.2}$$

$$\lambda_{hhh}^{\text{NLO,SM}} = -\frac{3\pi^2}{v}\left[1 - \frac{1}{\pi^2}\frac{m_t^4}{m_h^2 v^2}\right]\,, \tag{5.3}$$

where the NLO value has been calculated with only taking the dominant top quark contributions into account[14]. The N2HDM, on the right of Fig. 5.3, provides a larger band of possible trilinear self-couplings than the C2HDM, on the left of Fig. 5.3. On the other hand, the grey area, showing parameter points additionally yielding a NLO stable vacuum and surviving the approximative NLO perturbative unitarity constraints compared to the black points, yield similar maximal values. The excluded parameter points, shown in black, in the N2HDM with large NLO corrections to their trilinear self-coupling are mostly excluded because the vacuum is not stable at NLO. Due to large masses and missing cancellations between the individual contributions of the terms proportional to $m^4 \log m^2$ in the Coleman-Weinberg potential, cf. Eq. (4.42), these parameter points have large corrections to the trilinear self-coupling but simultaneously leads to too large corrections to the NLO vacuum so that the vacuum is not

---

[14]Compared to [176] Eq. (5.3) has a different sign. This is due to the matching to the convention in Sec. 2.2.6.3. Additionally, $N_c = 3$ has already been used to simplify the relation.
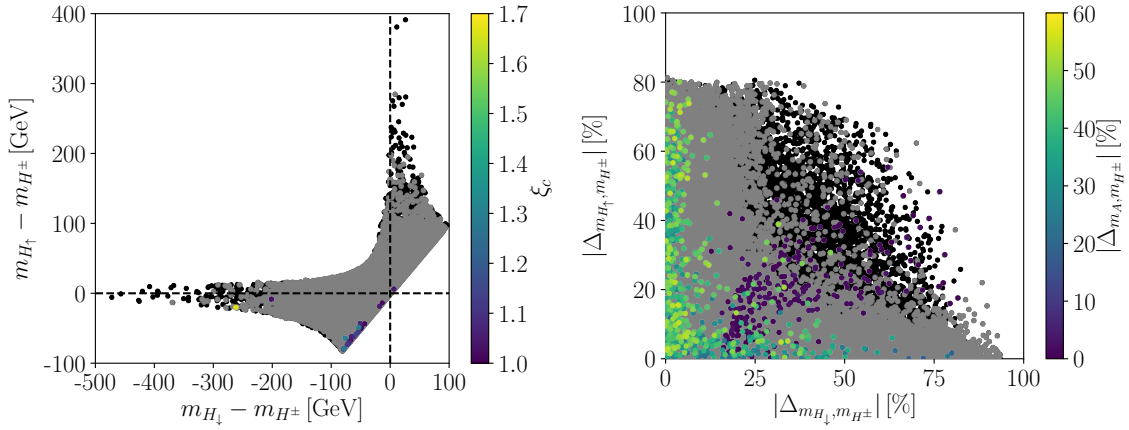
Figure 5.2.: The difference between the additional Higgs bosons for both models. On the left the difference $m_{H_\uparrow} - m_{H^\pm}$ is shown as a function of $m_{H_\downarrow} - m_{H^\pm}$ in the C2HDM with the colour bar showing the strength of the EWPT. The dashed line shows the degeneracy limit with either $m_{H_\downarrow} = m_{H^\pm}$ or $m_{H_\uparrow} = m_{H^\pm}$. On the right the relative difference, cf. Eq. (5.1), in the N2HDM between $m_{H_\uparrow}$ and $m_{H^\pm}$ is shown as a function of the relative difference $m_{H_\downarrow}$ and $m_{H^\pm}$. The colour bar denotes the relative difference m_A and $m_{H^\pm}$ for all points with an SFOEWPT.
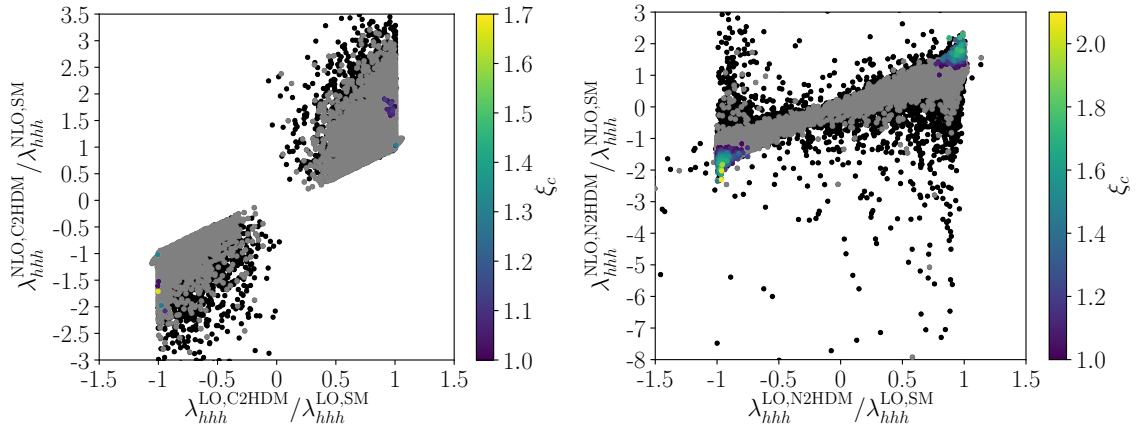
Figure 5.3.: The triple Higgs coupling between three SM-like Higgs bosons at NLO as a function of the LO value, each normalised to the corresponding SM value. On the left shown for the C2HDM while the right shows the result for the N2HDM. The colour code indicates the strength of the EWPT.

stable anymore. Additionally, due to the large corrections through the Coleman-Weinberg potential, the counterterm parameters, cf. Eq. (B.7), are large and therefore the perturbative unitarity constraints, cf. Eq. (2.91), approximated at NLO by replacing $\lambda \to \lambda + \delta\lambda$ are not fulfilled. Due to the singlet-admixture in the N2HDM, it is still possible to have vanishing self-couplings while the limits on the coupling between the SM-like Higgs boson and two gauge bosons disfavour such parameter configurations in the C2HDM. Having one less Higgs boson than the N2HDM, the trilinear self-coupling for parameter points fulfilling all constraints in Sec. 5.1 in the C2HDM is much more constrained around the SM-like value. Only looking at the parameter points providing an SFOEWPT the allowed coupling modifications of the trilinear coupling of the SM-like Higgs boson of the C2HDM and N2HDM, respectively, with respect to the SM trilinear Higgs couplings, both at NLO, reduce to

$$\lambda_{hhh}^{\text{NLO,C2HDM}}/\lambda_{hhh}^{\text{NLO,SM}} \in [-2.08, -1.02] \cup [1.02, 1.90] \,, \tag{5.4}$$

$$\lambda_{hhh}^{\text{NLO,N2HDM}}/\lambda_{hhh}^{\text{NLO,SM}} \in [-2.33, -1.15] \cup [1.00, 2.26] \,. \tag{5.5}$$

Therefore, the absolute value of the trilinear self-coupling has to be at least the SM value but still around this value. Future linear colliders will be able to measure this coupling with enough precision to either confirm or exclude its finite value [177, 178]. Measuring an value for the trilinear coupling at the edge of the allowed range in the N2HDM, cf. Eq. (5.5), could be used to exclude an SFOEWPT for the C2HDM, but still allow it in the N2HDM, therefore providing a possibility to distinguish the two models.

5.4. Impact on Di-Higgs Boson Production

The production of two Higgs bosons yields insight on the trilinear self-coupling between three SM-like Higgs bosons [179, 180]. Due to this, there has been an increased effort to measure this process, cf. [180] for a recent overview. While the di-Higgs production cross section at the LHC with a center of mass energy of $\sqrt{s} = 14\,\text{TeV}$ amounts to approximately $33\,\text{fb}$ at NLO with full top-mass effects [181–183], the cross section can be increased for a Higgs self-coupling that differs from the SM value [184]. This is due to the trilinear self-coupling of the SM Higgs boson only entering in one of the contributions to the SM Higgs pair production which interfere destructively. In models with additional Higgs bosons, the cross section can also be increased due to the on-shell production of a heavier Higgs boson decaying into two SM-like ones. For the lighter Higgs boson $H_\downarrow$ the on-shell production with following decay into two SM-like Higgs bosons is shown in Fig. 5.4 as a function of its mass, on the left for the C2HDM and the N2HDM on the right. For masses $m_{H_\downarrow} \leq 2m_h$ the decay $H_\downarrow \to hh$ is kinematically forbidden and, therefore, no parameter points with $m_{H_\downarrow} \lesssim 250\,\text{GeV}$ are shown. While both models yield a maximal signal strength of a few pb, approximately a factor 100 higher than the SM Higgs pair production cross section, the models lead to different results if only parameter points with an SFOEWPT are considered. In this case the N2HDM can still have parameter points with a cross section value of $1.66\,\text{pb}$ while the C2HDM di-Higgs production cross section is decreased to $0.10\,\text{pb}$, still a factor ~ 3 larger than the SM Higgs pair production cross section value. Therefore, for parameter points with an SFOEWPT the di-Higgs production cross section provides an possibility to distinguish between the C2HDM and N2HDM if a signal above $1\,\text{pb}$ is measured.

5.5. Conclusion

While the allowed parameter regions of the C2HDM and N2HDM differ only marginally for parameter points surviving theoretical and experimental constraints, the difference between the models is significant once an SFOEWPT is required. This is driven, on the one hand,
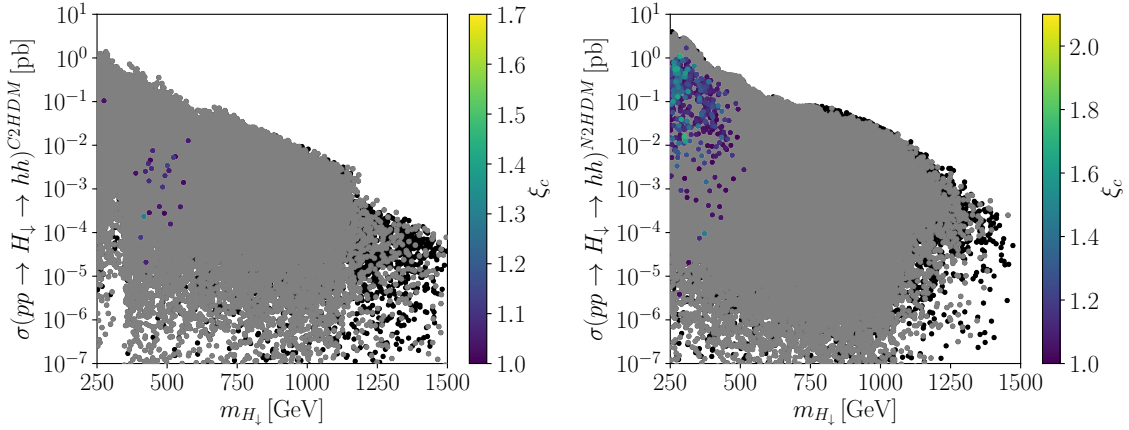
Figure 5.4.: The cross section in pb for the production of the second neutral Higgs boson $H_\downarrow$ decaying into two SM-like Higgs bosons as a function of the mass $m_{H_\downarrow}$. On the left shown for the C2HDM while the right shows the result for the N2HDM with the colour indicating the strength of the EWPT.

by the additional Higgs boson which can strengthen the EWPT and, on the other hand, by the possibility of the N2HDM pseudoscalar Higgs boson in the N2HDM being degenerate with the charged Higgs boson yielding an increased mass range for the $H_\downarrow$ and $H_\uparrow$. This impacts the Higgs self-coupling as its absolute value is $\mathcal{O}(10\%)$ larger in the N2HDM than in the C2HDM. The production of two SM-like Higgs bosons is not only modified through the trilinear self-coupling, but also through the on-shell decay of a heavier Higgs boson into two SM-like ones. This provides interesting signals to distinguish between the N2HDM and C2HDM as both models provide a production cross section value higher than the SM-like Higgs pair production, but the maximum cross section value for parameter points with an SFOEWPT in the N2HDM is one order of magnitude higher than in the C2HDM.

Electroweak Baryogenesis in the C2HDM

The Sakharov conditions [21] provide the necessary requirements to achieve EWBG [23, 45, 120–155]. The first two are given by baryon number violation, which can be achieved through sphaleron processes [185–187], and C and CP-violation. The third condition requires the particles to be out of thermal equilibrium, which can be translated into the *baryon washout condition* [28, 156]

$$\xi_c = \frac{v_c}{T_c} \geq 1 \,, \tag{6.1}$$

where T_c denotes the *critical temperature* and v_c the VEV of the broken minimum at the critical temperature. It was shown in [25–27, 188–191] that the washout condition is not fulfilled in the SM if the mass of the SM Higgs boson is above $70\,\mathrm{GeV}$. On the other hand, a simple extension of the SM with one additional singlet field [192, 193] can fulfil the washout condition.

While providing an SFOEWPT is a necessary condition for EWBG, it is not guaranteed to achieve the measured BAU. This asymmetry is given by the baryon to photon ratio [20]

$$\eta = \frac{n_b - n_{\bar{b}}}{s} = (6.2 \pm 0.4) \cdot 10^{-10} \,, \tag{6.2}$$

where n_b is the number of baryons, $n_{\bar{b}}$ the number of antibaryons and s the entropy density of the Universe.

In this chapter, the basics of the calculation of the EWBG are given as well as numerical results of some parameter points described in Chapter 5. The necessary calculations in this chapter follow [140, 142]. A different and detailed approach can be found in [139][15].

6.1. Basic Description of the EWBG

Triggered through the EWPT bubbles, containing the broken phase $\langle \phi \rangle \neq 0$, expand in the plasma, surrounded by the symmetric phase with $\langle \phi \rangle = 0$. Through the different couplings of left- and right-handed fermions to the Higgs fields, induced by CP-violation, a semiclassical

---

[15]A new approach where the CP-violation is in the dark sector is given in [152]
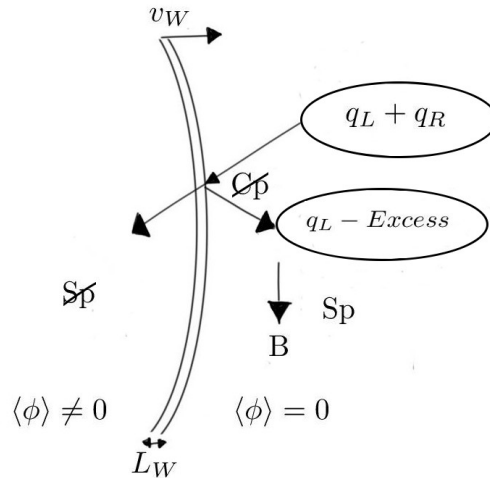
Figure 6.1.: Schematic overview of the necessary steps for EWBG. The CP-violation $\cancel{CP}$ generates a different semiclassical force for the left- and right-handed fermions, q_L and q_R respectively. Through this, an excess of left-handed fermions is generated in front of the bubble wall with thickness L_W and velocity v_W in the symmetric phase with the vanishing VEV $\langle \phi \rangle = 0$. The excess is converted into baryons B through sphalerons, shown as Sp in the schematic. After diffusing into the bubble the conversion of the baryons into left-handed quarks is suppressed as the vacuum is in a broken state, with $\langle \phi \rangle \neq 0$ and, therefore, the sphaleron rate is suppressed, shown with $\cancel{Sp}$.

force is induced which acts differently on left-handed and right-handed fermions. This is sketched in Fig. 6.1 where the left-handed fermions are reflected in front of the bubble wall while the right-handed ones pass through the bubble wall. This induces a non-equilibrium and a left-handed quark excess in front of the bubble. The necessary B-violation [126, 127, 140] is given through sphalerons processes which convert the left-handed quarks to baryons and back. As the bubble expands the baryons diffuse through the bubble wall. Inside the bubble, in the broken phase, the conversion between baryons and left-handed quarks does not continue as the sphaleron decay rate is strongly suppressed.

6.2. Numerical Input

In the following, several approximations will be introduced. To test the numerical uncertainties introduced by these approximations in the C2HDM the parameter point given in Tab. 6.1 is used. A detailed scan of the parameter space of the C2HDM has shown only quantitative changes of those points, not qualitative ones. Therefore, the parameter point in Tab. 6.1 has been chosen as its η value, the BAU, yields the closest result to Eq. (6.2) from all parameter points given in the scan, even though it would be ruled out by current collider constraints. The parameter points shown in Chapter 5 yield a value for η three orders of magnitude below the observed value.

6.3. The Transport Equations

The BAU is given by [122, 147]

$$\eta_{\mathrm{B}} = \frac{405\Gamma_{ws}}{4\pi^2 v_W g_* T} \int\limits_0^\infty \mathrm{d}z\, \mu_{B_L}(z) \exp\left(-\frac{45\Gamma_{ws}}{4v_W}z\right), \tag{6.3}$$

	BM			BM
Type	2	λ_3		-4.019509
m_{H_1} [GeV]	125.09	λ_4		4.255520
m_{H_2} [GeV]	543.45	λ_5		$-4.647570 - \mathrm{i}\,0.638572$
m_{H_3} [GeV]	545.96	$\Re m_{12}^2$ [GeV^2]		6868.28
$m_{H^\pm}$ [GeV]	160.35	$\arg(m_{12}^2)/\pi$		-0.302553
$\tan\beta$	0.89	$\overline{\omega}_c/T_c$		4.377520
λ_1	4.353002	$\overline{\omega}_c$ [GeV]		246.436000
λ_2	5.684883	T_c [GeV]		56.295800

Table 6.1.: Benchmark point used to check the numerical effects of different approximations throughout this chapter. Additionally to the masses and the input parameters, cf. Eq. (2.33), the critical temperature T_c, the electroweak VEV $\overline{\omega}_c$ and the strength of the EWPT $\overline{\omega}_c/T_c$ is given.

where $g_* = 106.75$ is the effective number of degrees of freedom in the plasma [122, 147], v_W the velocity of the wall and Γ_{ws} is the weak sphaleron rate, given by [131, 194, 195]

$$\Gamma_{ws} = 10^{-6}T\,. \tag{6.4}$$

The calculation of the chemical potential of the left-handed quark-excess μ_{B_L} requires the knowledge of the chemical potentials of all contributing particles in front of the bubble wall. For this, the transport equations derived in this section are used to calculate the chemical potential of the contributing particles. To derive the transport equations, fluctuations around the chemical and kinetic equilibrium are allowed in the distribution functions and inserted into the Boltzmann equations. For the collision terms in the Boltzmann equations, it is necessary to investigative the interaction of the particles with the bubble wall. In the Wentzel-Kramers-Brillouin (WKB) method [145] it is possible to describe the diffusion from particles in the symmetric phase through the wall. This method is only valid if the wall thickness is larger then the mean free path of the particles passing through the wall, given by the inverse temperature. The WKB method describes the interactions in a first-order gradient description of the bubble wall. Through the CP-violating couplings between the fermions and the Higgs field different forces on the left- and right-handed quarks are induced. This generates a left-handed quark excess in front of the bubble wall which is then translated into a baryon asymmetry through the sphaleron decay. The WKB method was applied for different models in [121–125, 146, 196]. As shown in [126–129, 140] the more general Kadanoff-Baym equations yield the same result as the WKB expansion if the proper treatment of the canonical momentum is applied and subleading terms are dropped.

Once the bubble has grown large enough the wall can be approximated by a planar profile, otherwise additional effects due to the curvature of the bubble wall have to been taken into account. The wall is assumed to expand with a constant velocity v_W. As the wall is assumed to be flat the calculation is performed in the rest frame of the wall in which the problem can be reduced to an effective 1+1 dimensional problem. The perpendicular distance z to the wall is defined such that the symmetric phase is at $z = +\infty$ and the broken phase at $z = -\infty$.
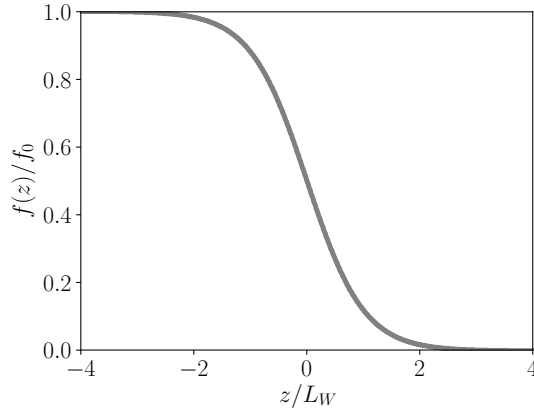
Figure 6.2.: profile of a kink-shaped function defined through Eq. (6.5).

The profile of the VEVs as a function of the distance z and the wall thickness L_W can be approximated through a kink-shaped function

$$f(z) = \frac{f_0}{2} \left(1 - \tanh \frac{z}{L_W} \right) , \tag{6.5}$$

shown in Fig. 6.2. As the VEVs change with the kink-profile depending on the coordinate z so do the particle masses as functions of the VEVs. The CP-violation in the Yukawa coupling induces a complex mass of the top quark. The mass $\mathcal{M}$ of the top quark can then be expressed as

$$\mathcal{M} = m(z) \exp\left(\mathrm{i}\theta(z) \right) , \tag{6.6}$$

where $m(z)$ is the absolute value of the mass and $\theta(z)$ is the CP-violating phase, both depending on the distance to the wall z. In the C2HDM $\mathcal{M}$ is given by (with the unphysical VEV $\omega_{\mathrm{CB}} = 0$)

$$\mathcal{M}_{\mathrm{C2HDM}} = \frac{y_t}{\sqrt{2}} \left(\omega_2 - \mathrm{i}\omega_{\mathrm{CP}} \right) , \tag{6.7}$$

$$= \frac{y_t}{\sqrt{2}} \sqrt{\omega_2^2 + \omega_{\mathrm{CP}}^2} \exp\left(\mathrm{i} \arg\left(\omega_2 - \mathrm{i}\omega_{\mathrm{CP}} \right) \right) , \tag{6.8}$$

where y_t is the Yukawa coupling between two top quarks and the second Higgs doublet, cf. Eq. (2.60), and ω_i are the VEVs of the $SU(2)$ doublets, cf Eq. (2.17). This defines the CP-violating phase in the broken phase as

$$\theta_{\mathrm{brk}} = - \arg(\overline{\omega}_2 + \mathrm{i}\overline{\omega}_{\mathrm{CP}}) , \tag{6.9}$$

where $\overline{\omega}_i$ are the VEVs in the broken phase at the EWPT with the critical VEV $\overline{\omega}_c$ and the critical temperature T_c. The profile of the VEVs ω_i and the phase θ are then parameterised through a kink profile, cf. Fig. 6.2, in terms of the wall thickness L_W as [142]

$$\omega_i(z) = \frac{\overline{\omega}_i}{2} \left(1 - \tanh \frac{z}{L_W} \right) , \tag{6.10}$$

$$\theta(z) = \frac{1}{1 + \tan^2 \beta_{\mathrm{T}}} \left[\theta_{\mathrm{brk}} - \frac{\theta_{\mathrm{brk}} - \theta_{\mathrm{sym}}}{2} \left(1 + \tanh \frac{z}{L_W} \right) \right] , \tag{6.11}$$

with

$$1 + \tan^2 \beta_{\mathrm{T}} = 1 + \frac{\overline{\omega}_2^2 + \overline{\omega}_{\mathrm{CP}}^2}{\overline{\omega}_1^2} = \frac{\overline{\omega}_c^2}{\overline{\omega}_1^2} . \tag{6.12}$$

Here the relation between the electroweak VEV $\overline{\omega}_c$ and its components

$$\overline{\omega}_c^2 = \overline{\omega}_1^2 + \overline{\omega}_2^2 + \overline{\omega}_{\mathrm{CP}}^2 \tag{6.13}$$

is used.

Due to the large coupling between the top quark and the Higgs particle, it is common practice [142, 153] to ignore the masses of the other fermions and consider the top quark as the only massive Dirac fermion[16]. Without flavour mixing of the fermions, the dispersion relation to first order in the gradient expansion for a fermion with complex mass $m\exp(i\theta)$ and momentum p in a varying background Higgs field is given by [128, 129, 140]

$$E = E_0 \mp s\frac{(\partial_z\theta(z))\,m(z)^2}{2E_0(z)E_{0z}(z)}\,, \tag{6.14}$$

where

$$E_0(z) = \sqrt{p_x^2 + p_y^2 + p_z^2 + m(z)^2}\,, \tag{6.15}$$

$$E_{0z}(z) = \sqrt{p_z^2 + m(z)^2} \tag{6.16}$$

describe the energies of the quasi-particles states in front of the bubble wall. s describes the spin of the top quark and the upper (lower) sign is for particles (antiparticles). The group velocity of the WKB wave-packet is then given by

$$v_{\mathrm{g}} = \frac{p_z}{E_0(z)}\left(1 \pm \frac{s}{2}\,(\partial_z\theta(z))\,\frac{m^2(z)}{E_0(z)^2 E_{0z}(z)}\right)\,. \tag{6.17}$$

Applying the WKB Ansatz to the canocial equations of motions yields the semiclassical force

$$F_z = -\frac{\partial_z m^2(z)}{2E_0(z)} \pm s\frac{\partial_z\left(m^2(z)\partial_z\theta(z)\right)}{2E_0(z)E_{0z}(z)} \mp s\frac{(\partial_z\theta(z))\,m^2(z)\partial_z\left(m^2(z)\right)}{4E_0(z)^3 E_{0z}(z)}\,. \tag{6.18}$$

While the first part of Eq. (6.18) is defined by the change of the mass, as expected in a classical force, the second and third part are proportional to the spin and the change in the phase and therefore semiclassical and generates the difference in the force on particles and antiparticles.

In the rest frame of the wall, the particle distributions f_i are described through a set of Boltzmann equations. These depend only on the distance to the wall z, the momentum perpendicular to the Wall p_z and the absolute momentum $p = \sqrt{p_x^2 + p_y^2 + p_z^2}$. The distributions obey the Boltzmann equations

$$\left(v_{\mathrm{g}}\partial_z + F_z\partial_{p_z}\right)f_i = \mathbf{C}_i[f]\,, \tag{6.19}$$

where $\mathbf{C}_i[f]$ describe the collision terms. Allowing for small fluctuations around the chemical and kinetic equilibrium the distribution functions are given by

$$f_i = \left[\exp\left(\beta\left(\gamma_w\left(E_i + v_W p_z\right) - \mu_i\right)\right) \pm 1\right]^{-1} + \delta f_i(z, p, p_z)\,, \tag{6.20}$$

where i denotes the particle species, $\beta = 1/T$ describes the inverse temperature and $\gamma_w = 1/\sqrt{1 - v_W^2}$ the Lorentz boost factor of the wall. The $+(-)$ refers to fermions (bosons) given by the particle species, $\mu_i(z)$ describes the chemical potential as a departure from chemical equilibrium and δf_i the perturbation around the kinetic equilibrium in response to the force

---

[16]If additional fermions are considered massive possible mixing terms have to been taken into account [149].

on the particle. The deviation of the kinetic equilibrium does not contribute to the particle density. It is necessary to expand the perturbations around the chemical equilibrium to the second-order as the CP-even and CP-odd components are equal at first order [197]. The perturbations are therefore expanded in

$$\mu_i = \mu_{i,1e} + \mu_{i,2o} + \mu_{i,2e} , \qquad \delta f_i = \delta f_{i,1e} + \delta f_{i,2o} + \delta f_{i,2e} , \qquad (6.21)$$

where i denotes the particle species, 1 or 2 the order of the expansion and $e(o)$ is for the CP-even (CP-odd) component. In order to calculate the baryon asymmetry, the excess in left-handed quarks and leptons is necessary. Therefore, the expansion is inserted into Eq. (6.20). Calculating the difference in the force between particles and antiparticles, cf. Eq. (6.18), only the difference between the CP-odd part remains in the Boltzmann equations, cf.Eq. (6.19), given as

$$\mu_{i,2} = \mu_{i,2o} - \overline{\mu}_{i,2o} . \qquad (6.22)$$

Here μ denotes the chemical potential of the particle species i and $\overline{\mu}$ of the corresponding antiparticle.

To decide which interactions have to be considered and which can be neglected a short discussion on the timescales of the process is useful [155]. To contribute to the generation of the BAU the corresponding particle density to a given process must diffuse before the wall catches up. Assuming an effective diffusion constant D the diffusion length d_{diff} for a given time t is given by $d_{\text{diff}} = \sqrt{Dt}$. During the same time interval, the wall passes the distance $d_W = v_W t$. Requiring that the diffusion happens before the wall catches up yields the requirement that the time scale of the diffusion is below $\tau_{\text{diff}} = \dfrac{D}{v_W^2}$. Therefore, all processes with a timescale below τ_{diff} must be included while processes with a higher time scale effectively decouple from the systems. Typical diffusion constants of the order of $D \approx 50/T$ and wall velocities of $v_W \approx 0.1$ yield a diffusion time scale of the order of $\tau_{\text{diff}} \in \mathcal{O}\left(10^4 T^{-1}\right)$. Therefore, all processes with a decay width $\Gamma \gtrsim 10^{-4} T$ have to be included. For the C2HDMl the interaction rates corresponding to the W boson scattering Γ_W, the top Yukawa interaction Γ_y, the strong sphalerons Γ_{ss}, the top helicity flips Γ_m and the Higgs boson interactions Γ_h are taken into account. After the q_L-excess is in thermal equilibrium in the first part of the two-step approach chosen for this calculation [153], the weak sphalerons convert it to baryons with the decay rate Γ_{ws} in the second step.

Truncating the Boltzmann equations in zeroth and first-order of p_z/E_0 [140] introduces the plasma velocities

$$u_i \equiv \left\langle \frac{p_z}{E_0} \delta f_i \right\rangle , \qquad (6.23)$$

where $\langle X \rangle$ describes the thermal average of X. Inserting Eqs. (6.17), (6.18), (6.20) and (6.21) into the Boltzmann equations, cf. Eq. (6.19), yields [142] eight coupled ordinary differential equations (ODEs) in the chemical potentials of the left-handed $SU(2)$ doublet top $\mu_{t,2}$, left-handed $SU(2)$ doublet bottom $\mu_{b,2}$, left-handed $SU(2)$ singlet top $\mu_{t^c,2}$, as well as the potential of the Higgs boson $\mu_{h,2}$ and their corresponding plasma velocities. Analogous to the chemical potential, cf. Eq. (6.22), the transport equations only depend on the difference of the CP-odd components of the plasma velocity between the particles $u_{i,2o}$ and their antiparticles $\overline{u}_{i,2o}$, namely

$$u_{i,2} = u_{i,2o} - \overline{u}_{i,2o} . \qquad (6.24)$$

The collsion terms weighted with p_z/E_0 can be expressed through the total interaction rates [140] of the top quark Γ_t^{tot}, bottom quark Γ_b^{tot} and the Higgs boson Γ_h^{tot}. The transport equations are then given by [142]

$$
\begin{aligned}
0 = {}& 3v_W K_{1,t} \left(\partial_z \mu_{t,2}\right) + 3v_W K_{2,t} \left(\partial_z m_t^2\right) \mu_{t,2} + 3\left(\partial_z u_{t,2}\right) \\
& - 3\Gamma_y \left(\mu_{t,2} + \mu_{t^c,2} + \mu_{h,2}\right) - 6\Gamma_m \left(\mu_{t,2} + \mu_{t^c,2}\right) - 3\Gamma_W \left(\mu_{t,2} - \mu_{b,2}\right) \\
& - 3\Gamma_{ss} \left[(1 + 9K_{1,t})\mu_{t,2} + (1 + 9K_{1,b})\mu_{b,2} + (1 - 9K_{1,t})\mu_{t^c,2}\right], & (6.25\text{a})
\end{aligned}
$$

$$
\begin{aligned}
0 = {}& 3v_W K_{1,b} \left(\partial_z \mu_{b,2}\right) + 3\left(\partial_z u_{b,2}\right) - 3\Gamma_y \left(\mu_{b,2} + \mu_{t^c,2} + \mu_{h,2}\right) - 3\Gamma_W \left(\mu_{b,2} - \mu_{t,2}\right) \\
& - 3\Gamma_{ss} \left[(1 + 9K_{1,t})\mu_{t,2} + (1 + 9K_{1,b})\mu_{b,2} + (1 - 9K_{1,t})\mu_{t^c,2}\right], & (6.25\text{b})
\end{aligned}
$$

$$
\begin{aligned}
0 = {}& 3v_W K_{1,t} \left(\partial_z \mu_{t^c,2}\right) + 3v_W K_{2,t} \left(\partial_z m_t^2\right) \mu_{t^c,2} + 3\left(\partial_z u_{t^c,2}\right) \\
& - 3\Gamma_y \left(\mu_{t,2} + \mu_{b,2} + 2\mu_{t^c,2} + 2\mu_{h,2}\right) - 6\Gamma_m \left(\mu_{t,2} + \mu_{t^c,2}\right) \\
& - 3\Gamma_{ss} \left[(1 + 9K_{1,t})\mu_{t,2} + (1 + 9K_{1,b})\mu_{b,2} + (1 - 9K_{1,t})\mu_{t^c,2}\right], & (6.25\text{c})
\end{aligned}
$$

$$
0 = 4v_W K_{1,h} \left(\partial_z \mu_{h,2}\right) + 4\left(\partial_z u_{h,2}\right) - 3\Gamma_y \left(\mu_{t,2} + \mu_{b,2} + 2\mu_{t^c,2} + 2\mu_{h,2}\right) - 4\Gamma_h \mu_{h,2}, \quad (6.25\text{d})
$$

$$
S_t = -3K_{4,t} \left(\partial_z \mu_{t,2}\right) + 3v_W \tilde{K}_{5,t} \left(\partial_z u_{t,2}\right) + 3v_W \tilde{K}_{6,t} \left(\partial_z m_t^2\right) u_{t,2} + 3\Gamma_t^{\text{tot}} u_{t,2}, \quad (6.25\text{e})
$$

$$
0 = -3K_{4,b} \left(\partial_z \mu_{b,2}\right) + 3v_W \tilde{K}_{5,b} \left(\partial_z u_{b,2}\right) + 3\Gamma_b^{\text{tot}} u_{b,2}, \quad (6.25\text{f})
$$

$$
S_t = -3K_{4,t} \left(\partial_z \mu_{t^c,2}\right) + 3v_W \tilde{K}_{5,t} \left(\partial u_{t^c,2}\right) + 3v_W \tilde{K}_{6,t} \left(\partial_z m_t^2\right) u_{t^c,2} + 3\Gamma_t^{\text{tot}} u_{t^c,2}, \quad (6.25\text{g})
$$

$$
0 = -4K_{4,h} \left(\partial_z \mu_{h,2}\right) + 4v_W \tilde{K}_{5,h} \left(\partial_z u_{h,2}\right) + 4\Gamma_h^{\text{tot}} u_{h,2}, \quad (6.25\text{h})
$$

with the source term of the top quark[17] [142]

$$
S_t = -v_W K_{8,t} \partial_z \left(m_t^2 \partial_z \theta\right) + v_W K_{9,t} \left(\partial_z \theta\right) m_t^2 \left(\partial_z m_t^2\right). \quad (6.26)
$$

The K_i denote thermal averages and are defined as [140, 196]

$$
K_{1,i} = -\left\langle \frac{p_z^2}{E_0} \partial_E^2 f_{i,0} \right\rangle, \quad (6.27\text{a})
$$

$$
K_{2,i} = \left\langle \frac{\partial_E^2 f_{i,0}}{2E_0} \right\rangle, \quad (6.27\text{b})
$$

$$
K_{4,i} = \left\langle \frac{p_z^2}{E_0^2} \partial_E f_{i,0} \right\rangle, \quad (6.27\text{c})
$$

$$
\tilde{K}_{5,i} = \left[\frac{p_z^2}{E_0} \partial_E f_{i,0} \right], \quad (6.27\text{d})
$$

$$
\tilde{K}_{6,i} = \left[\frac{E_0^2 - p_z^2}{2E_0^3} \partial_E f_{i,0} \right], \quad (6.27\text{e})
$$

$$
K_{8,i} = \left\langle \frac{|p_z| \partial_E f_{i,0}}{2E_0^2 E_{0z}} \right\rangle, \quad (6.27\text{f})
$$

$$
K_{9,i} = \left\langle \frac{|p_z|}{4E_0^3 E_{0z}} \left(\frac{\partial_E f_{i,0}}{E_0} - \partial_E^2 f_{i,0} \right) \right\rangle, \quad (6.27\text{g})
$$

where the brackets define the normalisation

$$
\langle X \rangle = \frac{\int \mathrm{d}^3 p X(p)}{\int \mathrm{d}^3 p \partial_E f_{0+}(m = 0)}, \quad (6.28)
$$

$$
[X] = \frac{\int \mathrm{d}^3 p X(p)}{\int \mathrm{d}^3 p f_{i,0,v_W}} = \frac{\int \mathrm{d}^3 p X(p)}{\int \mathrm{d}^3 p f_{i,0}|_{v_W=0}} \quad (6.29)
$$

---

[17] Due to the smallness of the bottom mass with $m_b^2/m_t^2 \approx 10^{-3}$ the source term of the bottom quark can be neglected [142].

and the different expansions of the distribution function f_i, cf. Eq. (6.20)

$$f_{i,0} = f_i|_{\mu_i=0,\delta f_i=0,v_W=0} \, , \tag{6.30}$$

$$f_{0+} = f_i|_{i=\text{fermion},\mu_i=0,\delta f_i=0,v_W=0} \, , \tag{6.31}$$

$$f_{i,0,v_w} = f_{i,0} + v_W p_z \partial_{E_0} f_{i,0} \, . \tag{6.32}$$

Here the first two expansions describe the distribution function in chemical equilibrium and the third is the Taylor serios of the distribution in chemical equilibrium for small wall velocities.

To solve Eq. (6.25) it is necessary to know the boundary conditions for the chemical potentials and the plasma velocities. A different approach is to rewrite Eq. (6.25) into four second order differential equations. For this the derivatives of Eqs. (6.25e) to (6.25h) w.r.t. z are solved for the first derivative of the plasma velocities. As the WKB ansatz is only a first-order expansion consistency requires to drop terms which would also appear at higher orders. For this terms of the kind $\partial_z K_i$, $\partial_z^3 \theta$ and $\partial_z^n m_t^2$ with $n \geq 2$ must be dropped. This yields

$$\partial_z u_{t,2} = \frac{\partial_z S_t + 3K_{4,t}\partial_z^2 \mu_{t,2}}{3\left(\Gamma_t^{\text{tot}} + K_{6,t}v_W \partial_z m_t^2\right)} \, , \tag{6.33a}$$

$$\partial_z u_{t^c,2} = \frac{\partial_z S_t + 3K_{4,t}\partial_z^2 \mu_{t^c,2}}{3\left(\Gamma_t^{\text{tot}} + K_{6,t}v_W \partial_z m_t^2\right)} \, , \tag{6.33b}$$

$$\partial_z u_{b,2} = \frac{K_{4,b}}{\Gamma_b^{\text{tot}}}\partial_z^2 \mu_{b,2} \, , \tag{6.33c}$$

$$\partial_z u_{h,2} = \frac{K_{4,h}}{\Gamma_h^{\text{tot}}}\partial_z^2 \mu_{h,2} \, , \tag{6.33d}$$

with

$$\partial_z S_t = v_W K_{9,t}\left(m_t^2 \partial_z^2 \theta + \partial_z \theta \partial_z m_t^2\right)\partial_z m_t^2 - 2v_W K_{8,t}\partial_z m_t^2 \partial_z^2 \theta \, . \tag{6.34}$$

Inserting this into Eqs. (6.25a) to (6.25d) yields four second order differential equations in the chemical potentials. The boundary conditions in the symmetric phase force the chemical potentials and all its derivatives to vanish.

Another merit of the second-order differential equations is the possibility to relate the total interaction rates $\Gamma_{t,b,h}^{\text{tot}}$ with the diffusion constants of the corresponding particles. They are given as [122]

$$D_t = \frac{K_{4,t}}{K_{1,t}\Gamma_t^{\text{tot}}} \, , \tag{6.35}$$

$$D_b = \frac{K_{4,b}}{K_{1,b}\Gamma_b^{\text{tot}}} \, , \tag{6.36}$$

$$D_h = \frac{K_{4,h}}{K_{1,t}\Gamma_h^{\text{tot}}} \, . \tag{6.37}$$

Solving the transport equations, cf. Eq. (6.25), yields the chemical potentials μ_i of each particle species. Assuming local baryon number conservation the chemical potential of the left-handed quarks is then given by

$$\mu_{B_L} = \frac{1}{2}\left(1 + 4K_{1,t}\right)\mu_{t,2} + \frac{1}{2}\left(1 + 4K_{1,b}\right)\mu_{b,2} - 2K_{1,t}\mu_{t^c,2} \, . \tag{6.38}$$

6.4. The Calculation of the Wall Width

The semiclassical force, cf. Eq. (6.18), depends on the change of the mass, and therefore of the change of the VEVs, and the phase w.r.t. the distance to the wall. These are given by the kink profiles in Eqs. (6.10) and (6.11). In addition to the values in the symmetric and broken phase, the kink profile is also dependent on the wall thickness L_W, which is defined as [142]

$$L_W \equiv \sqrt{\frac{\overline{\omega}_c^2}{8V_b}}\,, \tag{6.39}$$

where $\overline{\omega}_c$ is the electroweak VEV of the broken minimum $\vec{\omega}_b$ and V_b is the height of the potential barrier. To calculate the barrier it is necessary to calculate the path through the potential from the broken minimum to the symmetric minimum $\vec{\omega}_s$. As this is rather time-consuming the following approximation is used

- Define the direct line

$$\vec{\omega}(t) = \vec{\omega}_s + t\vec{n}\,, \tag{6.40}$$
$$\vec{n} = \vec{\omega}_b - \vec{\omega}_s\,, \tag{6.41}$$

  with $t \in [0,1]$.

- Define $N+1$ equidistant steps $t_i = \dfrac{i}{N}$ with $i = 0, \ldots, N$.

- For a given t_i calculate the point $\vec{\omega}_l(t_i)$. In the plane spanned by the point vector $\vec{\omega}_l(t_i)$ and the normal vector $\vec{n}$ *minimise* the potential on the given plane with the minimum at $\vec{\omega}_p(t_i)$ and the value of the potential $V_i = V(\vec{\omega}_p(t_i), T_c)$.

- Once all V_i are calculated the function $V_m(t)$ is interpolated through the grid points $(t_i | V_i)$. Since the broken and the symmetric minimum are degenerate at T_c the potential values are equal and therefore $V_m(0) = V_m(1) = V(\vec{\omega}_s, T_c) = V(\vec{\omega}_b, T_c)$.

- Calculate the maximimum $V_{\max}$ of $V_m(t)$ for $t \in [0,1]$.

- The potential barrier is then defined as

$$V_b = V_{\max} - V(\vec{\omega}_b, T_c)\,. \tag{6.42}$$

Fig. 6.3 shows the squared distance between the components of $\vec{\omega}_p(t_i)$ and the base point $\vec{\omega}_l(t_i)$ normalised to the squared maximum value of all $\vec{\omega}_l(t_i)$ and $\vec{\omega}_p(t_i)$ in the corresponding component for the parameter point given in Tab. 6.1, defined by

$$\Delta\omega_j^2 = |\omega_{p,j} - \omega_{l,j}|^2 / n_j^2\,, \tag{6.43}$$
$$n_j^2 = \max_{t\in[0,1]} \left(\omega_{p,j}^2, \omega_{l,j}^2\right) \tag{6.44}$$

for $j = 1, 2, \mathrm{CP}, \mathrm{CB}$. The charge breaking component is not shown as it is always zero and all deviations in the distance are numerical fluctuations. While the CP-even VEVs ω_1 and ω_2 do not deviate from the straight line in the tunnel path the CP-odd VEV ω_{CP} deviates notably from the path. To compare both tunnel paths the wall thickness, cf. Eq. (6.39), is calculated for both paths for the parameter point given in Tab. 6.1. For a straight line the potential barrier yields

$$V_b^{\mathrm{line}} = 2.626 \cdot 10^7 \, \mathrm{GeV}^4 \tag{6.45}$$
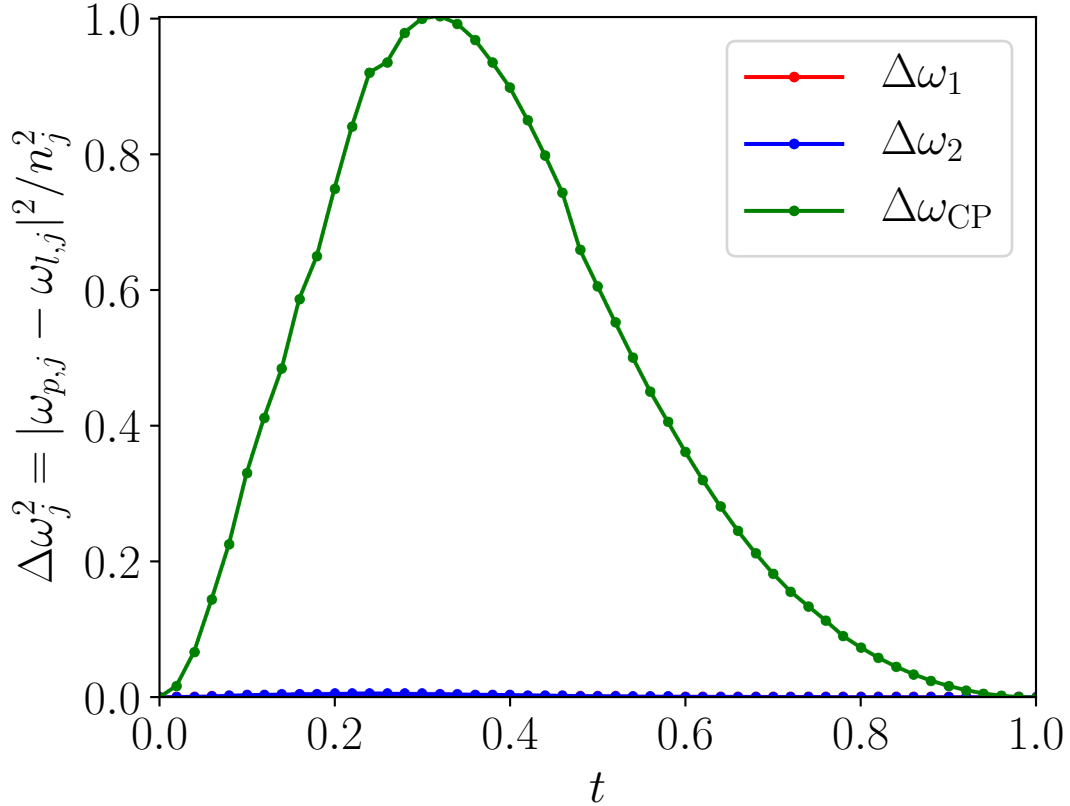
Figure 6.3.: The deviation from the straight line path where $\vec{\omega}_l$ are the points along the direct line from $\vec{\omega}_s$ to $\vec{\omega}_b$ while $\vec{\omega}_p$ are the minima in the planes as described in Sec. 6.4. The normalisation n_j^2 is defined as the maximum value of all points $\vec{\omega}_{l,j}^2$ and $\vec{\omega}_{p,j}^2$ for the corresponding component, cf. Eqs. (6.43) and (6.44).

while the bent path calculated with the approach listed above yields

$$V_b = 2.106 \cdot 10^7 \, \text{GeV}^4 \,. \tag{6.46}$$

This correpsonds to the wall thickness, cf. Eq. (6.39)

$$L_W^{\text{line}} = 0.01700 \, \text{GeV}^{-1} \,, \tag{6.47}$$

for the straight line and

$$L_W = 0.01898 \, \text{GeV}^{-1} \tag{6.48}$$

for the benth path. The relative difference of L_W^{line} to the wall width calculated with the bent path is given by approximately 10%. Changing the number of steps $N + 1$ in the above-described method to calculate the wall thickness from $N = 10$ to $N = 50$, on the other hand, does not change the wall thickness beyond numerical fluctuations.

6.5. The CP-violating phase of the symmetric phase

For a non-vanishing result of the transport equations it is necessary for the source term Eq. (6.26) to be finite. For this, it is necessary for the derivative of the CP-violating phase θ, defined in Eq. (6.11), to be uniquely defined. While the phase in the broken phase is uniquely defined through the finite VEVs it is not defined in the symmetric phase as the VEVs

vanish there. It is still possible to define it shortly *before* before the symmetric minimum as this recaptures the path from the broken phase to the symmetric phase. Analogous to the calculation of the wall thickness the effective potential will be minimised in the plane with the point vector[18] $\vec{p} = \vec{\omega}_s + 10^{-2}\,(\vec{\omega}_b - \vec{\omega}_s)$ and the normal vector $\vec{\omega}_b - \vec{\omega}_s$. The CP-violating phase of this minimum will be taken as the phase of the symmetric minimum. The minimum in front of the bubble wall for the chosen numerical input, cf. Tab. 6.1, is

$$\omega_{\mathrm{CB}} = 0\,\mathrm{GeV}\,, \qquad \omega_1 = 2.7667\,\mathrm{GeV}\,, \qquad \omega_2 = 6.0127\,\mathrm{GeV}\,, \qquad \omega_{\mathrm{CP}} = 1.1392\,\mathrm{GeV}\,. \quad (6.49)$$

The phase between ω_{CP} and ω_2 is

$$\theta_{\mathrm{sym}} = -0.345\pi\,. \tag{6.50}$$

6.6. Numerical Evaluation of the functions K_1 to K_9

While solving the transport equations Eq. (6.25) the functions K_1 to K_9, cf. Eq. (6.27) have to be evaluated at different distances z from the wall. As the integrals in the functions K_i do not have an analytical solution, they need to be integrated numerically. As this can be rather time consuming, an equidistant two dimensional grid in the (m^2, T) plane with $m^2 \in [0, (200)^2]\,\mathrm{GeV}^2$ and $T \in [10, 250]\,\mathrm{GeV}$ has been generated for all numerators of K_1 to K_9. The grid is then interpolated using the bicubic interpolation method implemented in GSL [198] The normalisation given in Eq. (6.28) can be calculated analytically. It is given by

$$\int \mathrm{d}^3 p\, \partial_E f_{0+}(m = 0)\,. \tag{6.51}$$

Using

$$E|_{m=0} = \sqrt{p^2 + m^2}|_{m=0} = p \tag{6.52}$$

the norm can be simplified to

$$\int \mathrm{d}^3 p\, \partial_E f_{0+}(m = 0) = \int \mathrm{d}^3 p\, \partial_E \frac{1}{\exp\left(\frac{E}{T}\right) + 1}$$

$$= 4\pi \int\limits_0^\infty \mathrm{d}E\, E^2 \partial_E \frac{1}{\exp\left(\frac{E}{T}\right) + 1}$$

$$= -4\pi \int\limits_0^\infty \mathrm{d}E\, \frac{1}{T} \frac{E^2 \exp\left(\frac{E}{T}\right)}{\left(1 + \exp\left(\frac{E}{T}\right)\right)^2}$$

$$= -\frac{2}{3}\pi^3 T^2\,. \tag{6.53}$$

For the normalisation of $[X]$, cf. Eq. (6.29), it is possible to reduce it to a function of one parameter

$$\int \mathrm{d}^3 p\, f_{i,0} = 4\pi \int \mathrm{d}|p|\, \frac{|p|^2}{\exp\left(\sqrt{\frac{m^2}{T^2} + \frac{|p|^2}{T^2}}\right) \pm 1}\,,$$

$$= 4\pi T^3 \int\limits_0^\infty \mathrm{d}x\, \frac{x^2}{\exp\left(\sqrt{\frac{m^2}{T^2} + x^2}\right) \pm 1}$$

$$= T^3 N_2\left(\frac{m^2}{T^2}\right)\,, \tag{6.54}$$

---

[18]Choosing a smaller number then 10^{-2} yields an absolute value of the VEVs which vanishes except for numerical fluctuations. Due to this, the phase cannot be defined uniquely in that case.

with

$$N_2(y) = 4\pi \int_0^\infty dx \frac{x^2}{\exp\left(\sqrt{y + x^2}\right) \pm 1} \,. \tag{6.55}$$

Using the same range for m^2 and T as in the numerators of K_i, the function $N_2(y)$ has been evaluated at $N_2(i), i = 0, 1, 2, \ldots, 400$ and interpolated with the `cubic_b_spline` algorithm of `Boost` [96].

6.7. Calculating the Baryon Asymmetry

With the diffusion constants [122, 130]

$$D_t = D_b = \frac{6}{T} \,, \tag{6.56}$$

$$D_h = \frac{20}{T} \,. \tag{6.57}$$

and the widths [131, 194, 195]

$$\Gamma_{ss} = 4.9 \cdot 10^{-4} T \,, \tag{6.58a}$$

$$\Gamma_y = 4.2 \cdot 10^{-3} T \,, \tag{6.58b}$$

$$\Gamma_m = \frac{m_t^2(z, T)}{63T} \,, \tag{6.58c}$$

$$\Gamma_h = \frac{m_W^2(z, T)}{50T} \,, \tag{6.58d}$$

$$\Gamma_W = \Gamma_h^{\text{tot}} \,, \tag{6.58e}$$

the Runge-Kutta algorithm, implemented in `Boost`, can be used to solve the transport equations, cf. Eq. (6.25), numerically at a fixed distance z from the wall. With the chemical potential known, the BAU η_B is given by [122, 147]

$$\eta_B = \frac{405\Gamma_{ws}}{4\pi^2 v_W g_* T} \int_0^\infty dz \mu_{B_L}(z) \exp\left(-\frac{45\Gamma_{ws}}{4v_W} z\right) \,, \tag{6.59}$$

where $g_* = 106.75$ is the effective number of degrees of freedom in the plasma [122, 147], and Γ_{ws} is the weak sphaleron rate, given by [131, 194, 195]

$$\Gamma_{ws} = 10^{-6} T \,. \tag{6.60}$$

As the integral in Eq. (6.59) is evaluated numerically, it has to be estimated which numerical upper limit can be used to estimate infinity. For this, the impact of the damping factor on the integrand has to be checked. For this, the damping factor can be rewritten as

$$\exp\left(-\frac{45\Gamma_{ws}}{4v_W} z\right) = \exp\left(-\frac{45 \times 10^{-6}}{4} \frac{L_W T}{v_W} \frac{z}{L_W}\right) \,. \tag{6.61}$$

Using the thick wall approach, namely $L_W T > 1$, and assuming typical, non-relativistic, wall velocities of $\mathcal{O}(0.1)$ the damping factor is above 0.99 for distances $z/L_W \lesssim 90$. Therefore, in the region close to the wall Eq. (6.59) is determined by the chemical potential μ_{B_L}. To estimate where the cutoff for the chemical potential μ_{B_L} can be set it is useful to investigate the source term, cf. Eq. (6.26), as the system reaches equilibrium if the source term vanishes, which vanishes if the top mass and its derivative vanishes. This is achieved if the VEVs vanish.
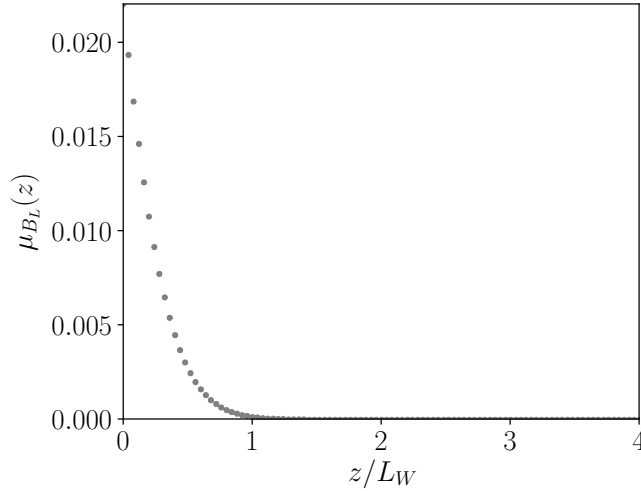
Figure 6.4.: The chemical potential μ_{B_L} shown as a function of the distance z to the wall for the numerical input given in Tab. 6.1 for $v_W = 0.1$.

As the VEVs away from the wall are described through the kink profile, cf. Eq. (6.10), for distances $z \geq 4L_W$ the VEVs are below $\omega_i(z \geq 4L_W) \lesssim 10^{-4}\overline{\omega}_i$, $i = 1, 2, \mathrm{CP}, \mathrm{CB}$ and $\overline{\omega}_i$ is the VEV in the broken minimum. This is in the area of numerical fluctuations and, therefore, the source term can be assumed to vanish for distances of $z \geq 4L_W$. Therefore, the boundary condition $\mu_{B_L}(z = 4L_W) = 0$ has be used to solve the transport equations, cf. Eq. (6.25). It has been tested with different limits that the choice of $4L_W$ does not change the final result beyond numerical fluctuations compared to choosing $3L_W$ or $5L_W$.

To speed up the integration over the chemical potential μ_{B_L} it is evaluated at 101 equidistant points between $z = 0$ and $z = 4L_W$. The given data points were multiplied with $\exp\left(-\dfrac{45\Gamma_{ws}}{4v_W}z\right)$ to achieve a grid for the integrand in Eq. (6.59). This grid was interpolated with the `cubic_b_spline` algorithm of `Boost`. This spline is then integrated with the `QAGS` algorithm implemented in `GSL`. For the parameter point given in Tab. 6.1 the interpolation points for μ_{B_L} are shown in Fig. 6.4. For the figure $v_W = 0.1$ is assumed. As inserted as a boundary condition the chemical potential vanishes for $z = 4L_W$, but there are no contributions for the area under the shown curve for $z \geq 2L_W$ which confirms the findings that the choice of $4L_W$ or $5L_W$ for the boundary condition does not influence the final result.

While the shown result is positive, negative values of μ_{B_L} can appear. In this case, the definition of matter and antimatter can be swapped such that the correct sign is restored.

While almost all parameters in Eq. (6.59) are derived quantities, the wall velocity v_W is still a free input[19]. To investigate the effect of the wall velocity v_W on η_B, cf. Eq. (6.59), η_B is shown as a function of v_W in Fig. 6.5. Using the redefinition of matter and antimatter Fig. 6.5 shows the absolute value of the BAU in the top panel. The lower panel shows the relative difference of $|\eta_B|$ to its mean value $\overline{|\eta_B|}$ of those parameter points in the upper figure of Fig. 6.5. It is given by

$$\overline{|\eta_B|} = 1.024552 \times 10^{-10}\,. \tag{6.62}$$

It shows that varying the wall velocity can change the BAU by roughly 4%. As mentioned in Sec. 6.3 there are two methods to solve the transport equations, cf. Eq. (6.25). The first

---

[19]While there are first attempts to derive the wall velocity at the EWPT through other quantities [199], the given approach does not work for models with several scalar fields. Therefore, the wall velocity is treated as a free input for this analysis.
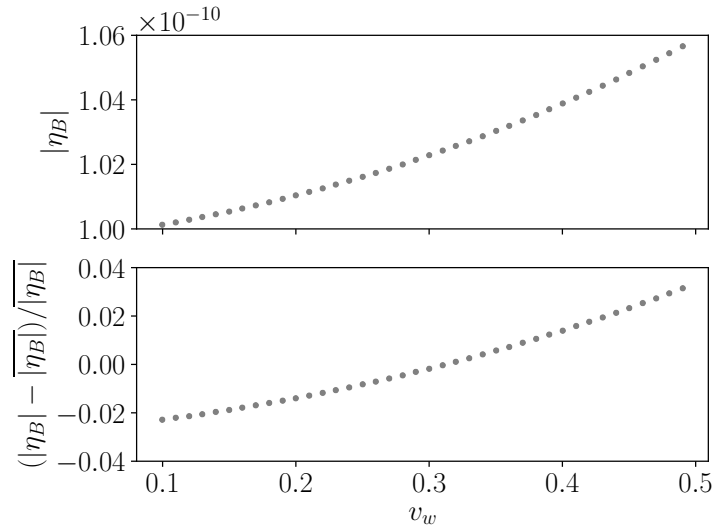
Figure 6.5.: The absolute value $|\eta_B|$ of the BAU shown as a function of the bubble wall velocity v_W in the top panel. The lower panel shows the normalised difference between the absolute value $|\eta_B|$ and the mean value of $|\eta_B|$ as a function of the wall velocity.

method is the replacement of the plasma velocities with Eq. (6.33) while the second one is to assume they vanish far away from the wall [148]. For the parameter point in Tab. 6.1 both methods are shown in Fig. 6.6. As can also be seen in Fig. 6.5 the first method, called the differential method in Fig. 6.6, depends only weakly on the wall velocity v_W. On the other hand, solving the transport equations with $u(z = \infty) = 0$ yields a stronger dependence on the wall velocity. For small wall velocities both methods yield the same order of magnitude but for velocities $v_W \geq 0.3$ the latter method starts to grow exponentially. This exponential growth indicates a numerical instability in the scheme, caused by the breakdown of some approximations which only hold for small wall velocities. The difference in both methods is due to the dropped terms in the derivation of Eq. (6.33). As some of these terms are dependent on the wall velocity, the difference between the two methods also depends on the wall velocity. For a wall velocity of $v_W = 0.1$ the parameter point in Tab. 6.1 yields similar BAUs calculated with the differential approach, η_B^{d}, and setting $u(z = \infty) = 0$, η_B^u, namely

$$\eta_B^{\mathrm{d}} = 1.001500 \times 10^{-10} \, , \tag{6.63}$$

$$\eta_B^u = 1.256120 \times 10^{-10} \tag{6.64}$$

which is of the same order of magnitude as the experimental constraint, cf. Eq. (6.2).

Applying the calculation to the parameter points used in Chapter 5 yields no point providing a BAU explaining the measured value of Eq. (6.2). While the parameter space of the C2HDM is constrained by many experimental signatures, the strongest constraint is given through the ACME experiment with their limits on the EDM [98], limiting the amount of allowed CP-violation in the Yukawa couplings. Additionally, previously known parameter regions with a successful EWBG, cf. [141, 142], either have a light spectrum for all Higgs masses, including the charged Higgs boson, which is excluded by now through several constraints, or are ruled out by the recent EDM constraints.

6.8. Conclusion

This chapter has given a basic introduction into the calculation of the BAU and all its necessary components in the C2HDM. For all necessary components, the given method was
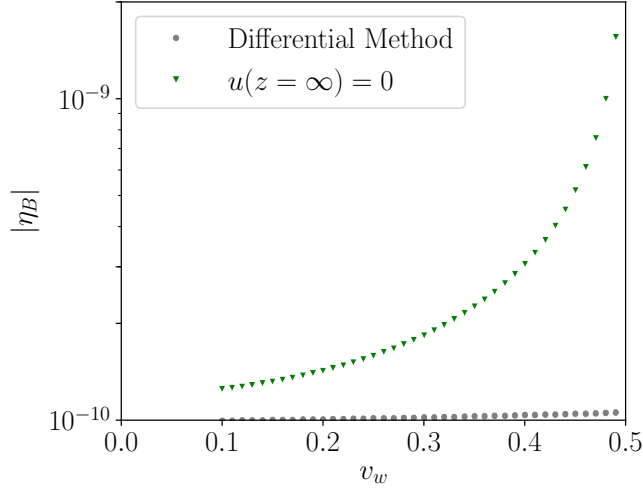
Figure 6.6.: The absolute value $|\eta_B|$ of the BAU shown as a function of the bubble wall velocity v_W. The grey points (dots) show the result if Eq. (6.33) is applied while the green points (triangle) show the result for solving Eq. (6.25) with the assumption $u(z = \infty) = 0$.

applied to the parameter point given in Tab. 6.1 and the influence of different approaches for the calculation of the wall thickness was discussed. The discussion on the tunnel path, cf. Sec. 6.4, has shown the necessity to include the CP-odd VEV ω_{CP} as a free parameter for determining the tunnel path as the CP-even VEVs do not differ from the straight line contrary to the CP-odd one. This results in a non-negligible difference in the wall thickness. To solve the transport equations, cf. Sec. 6.3, a numerical method for the fast calculation of the $K-$functions was given in Sec. 6.6. While no parameter point fulfilling all constraints set in Chapter 5 provides a strong enough BAU to satisfy Eq. (6.2), the parameter point in Tab. 6.1 shows that the model is capable of successful EWBG.

Final Conclusion and Outlook

In this thesis, the behaviour of the vacuum structure of several extensions of the SM either at high scale or at high temperatures has been investigated. For this a short introduction in the SM and the chosen extensions, the R2HDM, C2HDM and N2HDM have been given in Chapter 2. As the vacuum of the SM becomes metastable at high scales, Chapter 3 describes how the R2HDM and C2HDM provide possibilities to provide a stable vacuum and investigates the possible regions of parameter space. The result is that the SM-like Higgs boson in these models behaves more and more SM-like the higher the cut-off scale is set, while other features of the models, e.g. the CP-mixing between the other two Higgs bosons in the C2HDM, is barely limited for high cut-off scales.

To investigate the behaviour of the vacuum structure of the C2HDM and the N2HDM in the early universe, Chapter 4 provides the theoretical basis to include finite temperature effects at one-loop order in the effective potential. The general formalism described therein was also used to develop the `C++` Code `BSMPT` which allows for studies of finite temperature effects in a specific extension of the SM by only providing the tree-level potential of the extension. With the formalism described therein the strength of the EWPT, for given parameter points, can be calculated. This is a crucial component in the calculation of the BAU through EWBG and the peak frequency of gravitational waves produced through bubble collision at the EWPT.

In Chapter 5 these calculations were confronted with up-to-date theoretical and experimental constraints in the C2HDM and N2HDM. While the neutral Higgs boson with a CP-even admixture provide a similar spectrum, the result differs if an SFOEWPT is required. Though both models provide parameter points compatible with up-to-date collider constraints and an SFOEWPT, the viable parameter space is much more constrained in the C2HDM than in the N2HDM. The determination of the coupling between three SM-like Higgs boson will provide critical insight for the viable parameter space of EWPT in both models. While the N2HDM still allows parameter points with a vanishing trilinear Higgs coupling, requiring an SFOEWPT requires the trilinear couplings to be at least as large as the SM value in both models. Yet the SFOEWPT also constrains the coupling from above, as the models allow larger couplings without it. In total the SFOEWPT requires the absolute value of the trilinear coupling to be at least as big as the SM expectation value but not larger than a factor of ~ 2.3 compared to it. Therefore, once there are experimental constraints from future colliders, this coupling can be used as an indicator whether or not SFOEWPT is possible in the given

model. Not only the coupling between three SM-like Higgs bosons is of interest, but also the resonant production of two SM-like Higgs boson yields the possibility to distinguish between the models, once SFOEWPT is required as the N2HDM provides signals about a 100 times larger than the SM while the C2HDM yields similar results to the SM.

Providing an SFOEWPT is only one of the necessary condition to generate the BAU. For this, Chapter 6 provides the necessary ingredients for EWBG in the C2HDM. While the used transport equations to calculate the chemical potential of the left-handed quark excess in front of the bubble wall were already known in literature, this thesis looked into two different possibilities to solve them, both yielding similar results. The calculation of the tunnel path of the particles through the bubble wall is usually assumed to be a straight line. In this thesis it was shown that the inclusion of a CP-odd VEV leads to a deviation of the tunnel path from the straight line, yielding a difference in the wall width of about to 10% compared to the approximation of the tunnel path through a straight line. A numerically efficient way to calculate the tunnel path was given in this thesis. To evaluate the numerical effects the necessary calculations have been implemented in an in-house version of `BSMPT`, which will be released shortly. Through the modular setup in `BSMPT`, it is possible to implement different approaches to calculate the EWBG. This could be used to compare the different approaches in specific beyond the Standard Model realisations which, so far, has not been done in literature. The numerical evaluation has shown that the C2HDM can provide parameter points with a successful EWBG but due to the improved experimental constrains in flavour physics, the exclusion limits on charged Higgs decays and the updated limits on the EDM of the electron the calculated EWBG is not compatible anymore with up-to-date experimental constraints.

As shown in Chapter 5 the EWPT can be stronger in the N2HDM than in the C2HDM which benefits the EWBG. The next step for a model combining EWBG with up-to-date constrains would be therefore a combination of the C2HDM and the N2HDM by allowing the softly $\mathbb{Z}_2$-breaking parameter m_{12}^2 and λ_5 in the N2HDM to be become complex. The formalism provided in this thesis, along with the `C++` code `BSMPT`, can be used to investigate the EWPT of such models, while small adjustments to the transport equations have to be done by hand. The hope is therefore that the setup provided by this thesis enables the combination of EWBG with up-to-date collider constraints with minimal effort for future studies.

RGEs for the 2HDM

In this appendix the one-loop RGEs used in [2] and Chapter 3 for the 2HDM, cf. Eq. (2.16), are given. The one-loop RGEs for the gauge, quartic and Yukawa couplings are taken from [48] while the one-loop RGEs for the quadratic terms m_{ij}^2 are taken from [200]. Everything has been cross-checked with SARAH [101–105]. For an easier notation the change of the parameter x w.r.t. the renormalisation scale μ is defined as

$$\beta_x = 16\pi^2 \frac{\partial x}{\partial \ln \mu} \ . \tag{A.1}$$

The RGEs for the $U(1)_Y$, $SU(2)_L$ and $SU(3)$ gauge couplings (g_1, g_2 and g_s) are given as

$$\beta_{g_1} = 7g_1^3 \,, \tag{A.2}$$

$$\beta_{g_2} = -3g_2^3 \,, \tag{A.3}$$

$$\beta_{g_s} = -7g_s^3 \,. \tag{A.4}$$

To avoid FCNCs Chapter 3 investigated the type I and II scenario of the 2HDM, cf. Tab. 2.1. For type I the RGEs for the Yukawa couplings are given by

$$\beta_{Y_u} = a_u Y_u + T_{22} Y_u - \frac{3}{2} \left(Y_d Y_d^\dagger - Y_u Y_u^\dagger \right) Y_u \,, \tag{A.5a}$$

$$\beta_{Y_d} = a_d Y_d + T_{22} Y_d + \frac{3}{2} \left(Y_d Y_d^\dagger - Y_u Y_u^\dagger \right) Y_d \,, \tag{A.5b}$$

$$\beta_{Y_e} = a_e Y_e + T_{22} Y_e + \frac{3}{2} Y_e Y_e^\dagger Y_e \,. \tag{A.5c}$$

For type II the RGEs for the Yukawa couplings change to

$$\beta_{Y_u} = a_u Y_u + T_{22} Y_u + \frac{1}{2} \left(Y_d Y_d^\dagger + 3 Y_u Y_u^\dagger \right) Y_u \,, \tag{A.6a}$$

$$\beta_{Y_d} = a_d Y_d + T_{11} Y_d + \frac{1}{2} \left(Y_u Y_u^\dagger + 3 Y_d Y_d^\dagger \right) Y_d \,, \tag{A.6b}$$

$$\beta_{Y_e} = a_e Y_e + T_{11} Y_e + \frac{3}{2} Y_e Y_e^\dagger Y_e \,, \tag{A.6c}$$

where the parameters in these two cases are defined as

$$T_{11} = \begin{cases} 0 & \text{type I} \\ 3Y_d^\dagger Y_d + Y_e^\dagger Y_e & \text{type II} \end{cases}, \tag{A.7a}$$

$$T_{22} = \begin{cases} 3Y_u^\dagger Y_u + 3_d^\dagger Y_d + Y_e^\dagger Y_e & \text{type I} \\ 3Y_u^\dagger Y_u & \text{type II} \end{cases}, \tag{A.7b}$$

and

$$a_d = -8g_s^2 - \frac{9}{4}g_2^2 - \frac{5}{12}g_1^2 \,, \tag{A.8a}$$

$$a_u = -8g_s^2 - \frac{9}{4}g_2^2 - \frac{17}{12}g_1^2 \,, \tag{A.8b}$$

$$a_e = -\frac{9}{4}g_2^2 - \frac{15}{4}g_1^2 \,. \tag{A.8c}$$

For the RGEs of the quartic and quadratic parameters of the potential, cf. Eq. (2.16), it is useful to define the anomalous dimensions as

$$\gamma_1 = \frac{9}{4}g_2^2 + \frac{3}{4}g_1^2 - T_{11} \,, \tag{A.9a}$$

$$\gamma_2 = \frac{9}{4}g_2^2 + \frac{3}{4}g_1^2 - T_{22} \,. \tag{A.9b}$$

With this, in type I the RGEs for the quartic parameters are

$$\beta_{\lambda_1} = 12\lambda_1^2 + 4\lambda_3^2 + 4\lambda_3\lambda_4 + 2\lambda_4^2 + 2|\lambda_5|^2 + \frac{9}{4}g_2^4 + \frac{3}{2}g_2^2 g_1^2 + \frac{3}{4}g_1^4 - 4\gamma_1\lambda_1 \,, \tag{A.10a}$$

$$\beta_{\lambda_2} = 12\lambda_2^2 + 4\lambda_3^2 + 4\lambda_3\lambda_4 + 2\lambda_4^2 + 2|\lambda_5|^2 + \frac{9}{4}g_2^4 + \frac{3}{2}g_2^2 g_1^2 + \frac{3}{4}g_1^4 - 4\gamma_2\lambda_2$$
$$- 12\text{Tr}\left[Y_d^\dagger Y_d Y_d^\dagger Y_d + Y_u^\dagger Y_u Y_u^\dagger Y_u\right] - 4\text{Tr}\left[Y_e^\dagger Y_e Y_e^\dagger Y_e\right] \,, \tag{A.10b}$$

$$\beta_{\lambda_3} = (\lambda_1 + \lambda_2)(6\lambda_3 + 2\lambda_4) + 4\lambda_3^2 + 2\lambda_4^2 + 2|\lambda_5|^2$$
$$+ \frac{9}{4}g_2^4 - \frac{3}{2}g_2^2 g_1^2 + \frac{3}{4}g_1^4 - 2(\gamma_1 + \gamma_2)\lambda_3 \,, \tag{A.10c}$$

$$\beta_{\lambda_4} = 2(\lambda_1 + \lambda_2)\lambda_4 + 8\lambda_3\lambda_4 + 4\lambda_4^2 + 8|\lambda_5|^2 - 2(\gamma_1 + \gamma_2)\lambda_4 + 3g_2^2 g_1^2 \,, \tag{A.10d}$$

$$\beta_{\lambda_5} = 2(\lambda_1 + \lambda_2 + 4\lambda_3 + 6\lambda_4)\lambda_5 - 2(\gamma_1 + \gamma_2)\lambda_5 \,. \tag{A.10e}$$

In type II the RGEs are given by

$$\beta_{\lambda_1} = 12\lambda_1^2 + 4\lambda_3^2 + 4\lambda_3\lambda_4 + 2\lambda_4^2 + 2|\lambda_5|^2 + \frac{9}{4}g_2^4 + \frac{3}{2}g_2^2 g_1^2 + \frac{3}{4}g_1^4 - 4\gamma_1\lambda_1$$
$$- 12\text{Tr}\left[Y_d^\dagger Y_d Y_d^\dagger Y_d\right] - 4\text{Tr}\left[Y_e^\dagger Y_e Y_e^\dagger Y_e\right] \,, \tag{A.11a}$$

$$\beta_{\lambda_2} = 12\lambda_2^2 + 4\lambda_3^2 + 4\lambda_3\lambda_4 + 2\lambda_4^2 + 2|\lambda_5|^2 + \frac{9}{4}g_2^4 + \frac{3}{2}g_2^2 g_1^2 + \frac{3}{4}g_1^4 - 4\gamma_2\lambda_2$$
$$- 12\text{Tr}\left[Y_u^\dagger Y_u Y_u^\dagger Y_u\right] \,, \tag{A.11b}$$

$$\beta_{\lambda_3} = (\lambda_1 + \lambda_2)(6\lambda_3 + 2\lambda_4) + 4\lambda_3^2 + 2\lambda_4^2 + 2|\lambda_5|^2$$
$$+ \frac{9}{4}g_2^4 - \frac{3}{2}g_2^2 g_1^2 + \frac{3}{4}g_1^4 - 2(\gamma_1 + \gamma_2)\lambda_3 - 12\text{Tr}\left[Y_d^\dagger Y_d Y_u^\dagger Y_u\right] \,, \tag{A.11c}$$

$$\beta_{\lambda_4} = 2(\lambda_1 + \lambda_2)\lambda_4 + 8\lambda_3\lambda_4 + 4\lambda_4^2 + 8|\lambda_5|^2 - 2(\gamma_1 + \gamma_2)\lambda_4 + 3g_2^2 g_1^2$$
$$+ 12\text{Tr}\left[Y_d^\dagger Y_d Y_u^\dagger Y_u\right] \,, \tag{A.11d}$$

$$\beta_{\lambda_5} = 2(\lambda_1 + \lambda_2 + 4\lambda_3 + 6\lambda_4)\lambda_5 - 2(\gamma_1 + \gamma_2)\lambda_5 \,. \tag{A.11e}$$

The RGEs of the quadratic parameters are given by

$$\beta_{m_{11}^2} = 6\lambda_1 m_{11}^2 + (4\lambda_3 + 2\lambda_4)\, m_{22}^2 - 2\gamma_1 m_{11}^2 \,, \tag{A.12a}$$

$$\beta_{m_{22}^2} = (4\lambda_3 + 2\lambda_4)\, m_{11}^2 + 6\lambda_2 m_{22}^2 - 2\gamma_2 m_{22}^2 \,, \tag{A.12b}$$

$$\beta_{m_{12}^2} = (2\lambda_3 + 4\lambda_4)\, m_{12}^2 + 6\lambda_5 \left(m_{12}^2\right)^* - (\gamma_1 + \gamma_2)\, m_{12}^2 \,, \tag{A.12c}$$

where $\left(m_{12}^2\right)^*$ denotes the complex conjugate of m_{12}^2.

It is important to note that the RGE for the imaginary part of λ_5, cf. Eqs. (A.10e) and (A.11e), is proportional to $\Im(\lambda_5)$ at the input scale. Therefore, if λ_5 is real at the input scale, it will be real at all scales. Furthermore, the RGE of the imaginary part of m_{12}^2, cf. Eq. (A.12c), can be simplified to

$$\beta_{\Im m_{12}^2} = (2\lambda_3 + 4\lambda_4 - \gamma_1 - \gamma_2)\, \Im m_{12}^2 + 6\left(\Re m_{12}^2 \Im\lambda_5 - \Im m_{12}^2 \Re\lambda_5\right) \,. \tag{A.13}$$

Therefore, if m_{12}^2 and λ_5 are real at the input scale, they both will stay real at all scales.

For the numerical values at the input scale, the following relations were used

$$g_s = \sqrt{4\pi\alpha_s} \,, \tag{A.14a}$$

$$g_2 = \frac{2m_W}{v} \,, \tag{A.14b}$$

$$g_1 = 2\frac{\sqrt{m_Z^2 - m_W^2}}{v} \,, \tag{A.14c}$$

$$Y_u = \frac{\sqrt{2}}{v_2} \begin{pmatrix} m_u & 0 & 0 \\ 0 & m_c & 0 \\ 0 & 0 & m_t \end{pmatrix} \,, \tag{A.14d}$$

$$Y_d = \frac{\sqrt{2}}{v_d} V_{CKM} \begin{pmatrix} m_d & 0 & 0 \\ 0 & m_s & 0 \\ 0 & 0 & m_b \end{pmatrix} V_{CKM}^\dagger \,, \tag{A.14e}$$

$$Y_e = \frac{\sqrt{2}}{v_e} \begin{pmatrix} m_e & 0 & 0 \\ 0 & m_\mu & 0 \\ 0 & 0 & m_\tau \end{pmatrix} \,, \tag{A.14f}$$

$$V_{CKM} = \mathbb{1}_{3\times 3} \,, \tag{A.14g}$$

where $\alpha_s = g_s^2/(4\pi)$ is the strong coupling constant. The VEVs in type I are given by

$$v_e = v_d = v_2 \,, \tag{A.15}$$

and in type II

$$v_e = v_d = v_1 \,. \tag{A.16}$$

The fermion masses are chosen as [201–204]

$$m_u = 0.1\,\text{GeV}\,, \tag{A.17a}$$

$$m_c = 1.51\,\text{GeV}\,, \tag{A.17b}$$

$$m_t = 172.5\,\text{GeV}\,, \tag{A.17c}$$

$$m_d = 0.1\,\text{GeV}\,, \tag{A.17d}$$

$$m_s = 0.1\,\text{GeV}\,, \tag{A.17e}$$

$$m_b = 4.92\,\text{GeV}\,, \tag{A.17f}$$

$$m_e = 0.51099892810^{-3}\,\text{GeV}\,, \tag{A.17g}$$

$$m_\mu = 0.1056583715\,\text{GeV}\,, \tag{A.17h}$$

$$m_\tau = 1.77682\,\text{GeV}\,. \tag{A.17i}$$

The numerical value of the VEV is given by [20]

$$G_F = 1.1663787 \cdot 10^{-5}\,\text{GeV}^{-2}\,, \tag{A.18a}$$

$$v = \frac{1}{\sqrt{\sqrt{2}G_F}} \approx 246.22\,\text{GeV}\,, \tag{A.18b}$$

and the strong coupling is [20]

$$\alpha_s = 0.119\,. \tag{A.19}$$

The W and Z boson masses are given by [201, 202]

$$m_W = 80.385\,\text{GeV}\,, \tag{A.20}$$

$$m_Z = 91.1876\,\text{GeV}\,. \tag{A.21}$$

The input scale was chosen to be the Z-boson mass m_Z.

Counterterm potential for the C2HDM and N2HDM

As described in Chapter 4 the parameters of the counterterm potential are derived by the equations

$$\partial_{\phi_i}\left(V^{\mathrm{CW}}+V^{\mathrm{CT}}\right)\big|_{\phi_k=\langle\phi_k\rangle(T=0)}=0\,, \tag{B.1a}$$

$$\partial_{\phi_i}\partial_{\phi_j}\left(V^{\mathrm{CW}}+V^{\mathrm{CT}}\right)\big|_{\phi_k=\langle\phi_k\rangle(T=0)}=0\,, \tag{B.1b}$$

where $\phi_k=\langle\phi_k\rangle\,(T=0)$ is the electroweak minimum of the tree-level potential with $i,j,k=1\ldots n_{\mathrm{Higgs}}$ at vanishing temperature. These relations enforce that the minimum of the tree-level potential is still a local minimum at NLO with the same masses and mixing angles. The necessary derivatives of the Coleman-Weinberg potential are given in [165]. For the remainder of this chapter, the following abbreviation is used

$$N_{\phi_i}^{\mathrm{CW}}=\partial_{\phi_i}V^{\mathrm{CW}}\,, \tag{B.2}$$

$$H_{\phi_i,\phi_j}^{\mathrm{CW}}=\partial_{\phi_i}\partial_{\phi_j}V^{\mathrm{CW}}\,. \tag{B.3}$$

The solution of Eq. (B.1) is given in Appendix B.1 for the C2HDM and for the N2HDM in Appendix B.2. Evaluating the derivatives of the Coleman-Weinberg potential leads to infrared divergences for the Goldstone bosons in the Landau gauge [143, 163, 165, 205–207]. To cure these divergences Appendix B.3 introduces modifications to the derivatives in [165] resulting in finite results.

B.1. The counterterm potential of the C2HDM

Applying Eq. (4.62) to the C2HDM, cf. Eq. (2.16), the counterterm potential reads

$$\begin{aligned}
V^{\mathrm{CT}}=&\,\delta m_{11}^2\Phi_1^\dagger\Phi_1+\delta m_{22}^2\Phi_2^\dagger\Phi_2-2\delta\Re(m_{12}^2)\Re\left(\Phi_1^\dagger\Phi_2\right)+2\delta\Im\left(m_{12}^2\right)\Im\left(\Phi_1^\dagger\Phi_2\right)\\
&+\frac{\delta\lambda_1}{2}\left(\Phi_1^\dagger\Phi_1\right)^2+\frac{\delta\lambda_2}{2}\left(\Phi_2^\dagger\Phi_2\right)^2+\delta\lambda_3\left(\Phi_1^\dagger\Phi_1\right)\left(\Phi_2^\dagger\Phi_2\right)\\
&+\delta\lambda_4\left(\Phi_1^\dagger\Phi_2\right)\left(\Phi_2^\dagger\Phi_1\right)+\delta\Re\lambda_5\Re\left(\left(\Phi_1^\dagger\Phi_2\right)^2\right)-\delta\Im\lambda_5\Im\left(\left(\Phi_1^\dagger\Phi_2\right)^2\right)\\
&+\delta T_1\left(\zeta_1+\omega_1\right)+\delta T_2\left(\zeta_2+\omega_2\right)+\delta T_{\mathrm{CP}}\left(\psi_2+\omega_{\mathrm{CP}}\right)+\delta T_{\mathrm{CB}}\left(\rho_2+\omega_{\mathrm{CB}}\right)\,.
\end{aligned} \tag{B.4}$$

Here $\omega_i, i = 1, 2, \mathrm{CP}, \mathrm{CB}$ are the VEVs of the real fields $\zeta_1, \zeta_2, \psi_2, \rho_2$ of the doublets, cf. Eq. (2.17). Solving Eq. (B.1) yields the one-dimensional space of solutions for the counterterms of the parameters of V^{CT}, given by

$$\delta m_{11}^2 = \frac{1}{2} \left[H_{\zeta 1, \zeta 1}^{\mathrm{CW}} + 2 H_{\rho_1, \rho_1}^{\mathrm{CW}} + \frac{v_2}{v_1} \left(H_{\zeta_1, \zeta_2}^{\mathrm{CW}} - H_{\eta_1, \eta_2}^{\mathrm{CW}} \right) - 5 H_{\rho_1, \rho_1}^{\mathrm{CW}} \right] + v_2^2 t \,, \tag{B.5a}$$

$$\delta m_{22}^2 = \frac{1}{2} \left[H_{\zeta_2, \zeta_2}^{\mathrm{CW}} - 3 H_{\eta_2, \eta_2}^{\mathrm{CW}} + \frac{v_1}{v_2} \left(H_{\zeta_1, \zeta_2}^{\mathrm{CW}} - H_{\eta_1, \eta_1}^{\mathrm{CW}} \right) \right.$$
$$\left. + \frac{v_1^2}{v_2^2} \left(H_{\psi_1, \psi_1}^{\mathrm{CW}} - H_{\rho_1, \rho_1}^{\mathrm{CW}} \right) \right] + v_1^2 t \,, \tag{B.5b}$$

$$\delta \Re(m_{12}^2) = H_{\eta_1, \eta_2}^{\mathrm{CW}} + \frac{v_1}{v_2} \left(H_{\psi_1, \psi_1}^{\mathrm{CW}} - H_{\rho_1, \rho_1}^{\mathrm{CW}} \right) + v_1 v_2 t \,, \tag{B.5c}$$

$$\delta \lambda_1 = \frac{1}{v_1^2} \left[2 H_{\rho_1, \rho_1}^{\mathrm{CW}} - H_{\psi_1, \psi_1}^{\mathrm{CW}} - H_{\zeta_1, \zeta_1}^{\mathrm{CW}} \right] - \frac{v_2^2}{v_1^2} t \,, \tag{B.5d}$$

$$\delta \lambda_2 = \frac{1}{v_2^2} \left[H_{\eta_2, \eta_2}^{\mathrm{CW}} - H_{\zeta_2, \zeta_2}^{\mathrm{CW}} \right] + \frac{v_1^2}{v_2^4} \left[H_{\rho_1, \rho_1}^{\mathrm{CW}} - H_{\psi_1, \psi_1}^{\mathrm{CW}} \right] - \frac{v_1^2}{v_2^2} t \,, \tag{B.5e}$$

$$\delta \lambda_3 = \frac{1}{v_1 v_2} \left[H_{\eta_1, \eta_2}^{\mathrm{CW}} - H_{\zeta_1, \zeta_2}^{\mathrm{CW}} \right] + \frac{1}{v_2^2} \left[H_{\rho_1, \rho_1}^{\mathrm{CW}} - H_{\psi_1, \psi_1}^{\mathrm{CW}} \right] - t \,, \tag{B.5f}$$

$$\delta \lambda_4 = t \,, \tag{B.5g}$$

$$\delta \Re(\lambda_5) = \frac{2}{v_2^2} \left(H_{\psi_1, \psi_1}^{\mathrm{CW}} - H_{\rho_1, \rho_1}^{\mathrm{CW}} \right) + t \,, \tag{B.5h}$$

$$\delta \Im(\lambda_5) = - \frac{2}{v_2^2} H_{\zeta_1, \psi_1}^{\mathrm{CW}} \,, \tag{B.5i}$$

$$\delta \Im(m_{12}^2) = - H_{\zeta_1, \psi_2}^{\mathrm{CW}} - 2 \frac{v_1}{v_2} H_{\zeta_1, \psi_1}^{\mathrm{CW}} \,, \tag{B.5j}$$

$$\delta T_1 = H_{\eta_1, \eta_2}^{\mathrm{CW}} v_2 + H_{\rho_1, \rho_1}^{\mathrm{CW}} v_1 - N_{\zeta_1}^{\mathrm{CW}} \,, \tag{B.5k}$$

$$\delta T_2 = H_{\eta_1, \eta_2}^{\mathrm{CW}} v_1 + H_{\eta_2, \eta_2}^{\mathrm{CW}} v_2 - N_{\zeta_2}^{\mathrm{CW}} \,, \tag{B.5l}$$

$$\delta T_{\mathrm{CP}} = \frac{v_1^2}{v_2^2} H_{\zeta_1, \psi_1}^{\mathrm{CW}} + H_{\zeta_1, \psi_2}^{\mathrm{CW}} - N_{\psi_2}^{\mathrm{CW}} \,, \tag{B.5m}$$

$$\delta T_{\mathrm{CB}} = - N_{\rho_2}^{\mathrm{CW}} \,, \tag{B.5n}$$

where $t \in \mathbb{R}$ describes the free parameter in the one-dimensional space of solutions.

Inserting the electroweak minimum, cf. Eq. (2.29), yields that Eq. (B.4) is independent of t, therefore, t is set to zero. The counterterms of the tadpole parameter δT do not have a counterpart in the tree-level potential. Therefore, if no symmetry is broken at one-loop, vanishing one-loop Tadpoles as a check of the implementation of the equations. In the limit of CP-conservation, cf. Eq. (2.48), the mixed second-order derivatives of the Coleman-Weinberg potential w.r.t. one CP-even and one CP-odd field vanishes. Therefore, the counterterms $\delta \Im(\lambda_5)$ and $\delta \Im(m_{12}^2)$ vanish and no CP-violation is introduced through one-loop effects if the potential is CP-conserving at tree level.

B.2. The counterterm potential of the N2HDM

Applying Eq. (4.62) to the N2HDM, the counterterm potential reads

$$
\begin{aligned}
V^{\mathrm{CT}} =& \delta m_{11}^2 \Phi_1^\dagger \Phi_1 + \delta m_{22}^2 \Phi_2^\dagger \Phi_2 - \delta m_{12}^2 \left(\Phi_1^\dagger \Phi_2 + \Phi_2^\dagger \Phi_1 \right) + \frac{\delta\lambda_1}{2} \left(\Phi_1^\dagger \Phi_1 \right)^2 + \frac{\delta\lambda_2}{2} \left(\Phi_2^\dagger \Phi_2 \right)^2 \\
&+ \delta\lambda_3 \left(\Phi_1^\dagger \Phi_1 \right) \left(\Phi_2^\dagger \Phi_2 \right) + \delta\lambda_4 \left(\Phi_1^\dagger \Phi_2 \right) \left(\Phi_2^\dagger \Phi_1 \right) + \frac{\delta\lambda_5}{2} \left[\left(\Phi_1^\dagger \Phi_2 \right)^2 + \left(\Phi_2^\dagger \Phi_1 \right)^2 \right] \\
&+ \frac{1}{2} \delta m_S^2 \Phi_S^2 + \frac{\delta\lambda_6}{8} \Phi_S^4 + \frac{\delta\lambda_7}{2} \left(\Phi_1^\dagger \Phi_1 \right) \Phi_S^2 + \frac{\delta\lambda_8}{2} \left(\Phi_2^\dagger \Phi_2 \right) \Phi_S^2 \\
&+ \delta T_1 (\zeta_1 + \omega_1) + \delta T_2 (\zeta_2 + \omega_2) + \delta T_{\mathrm{CP}} (\psi_2 + \omega_{\mathrm{CP}}) \\
&+ \delta T_{\mathrm{CB}} (\rho_2 + \omega_{\mathrm{CB}}) + \delta T_S (\zeta_S + \omega_S) \, .
\end{aligned}
\tag{B.6}
$$

Here $\omega_i, i = 1, 2, \mathrm{CP}, \mathrm{CB}, S$ are the VEVs of the real fields $\zeta_1, \zeta_2, \psi_2, \rho_2, \zeta_S$ of the doublets, cf. Eqs. (2.17) and (2.75).

Solving Eq. (B.1) yields the two-dimensional space of solutions for the counterterms of the parameters of V^{CT}, given by

$$
\delta m_{11}^2 = \frac{1}{2} \left[\frac{v_s}{v_1} H_{\zeta_1,\zeta_S}^{\mathrm{CW}} + \frac{v_2}{v_1} \left(H_{\zeta_1,\zeta_2}^{\mathrm{CW}} - H_{\eta_1,\eta_2}^{\mathrm{CW}} \right) + 2 H_{\psi_1,\psi_1}^{\mathrm{CW}} - 5 H_{\eta_1,\eta_1}^{\mathrm{CW}} + H_{\zeta_1,\zeta_1}^{\mathrm{CW}} \right] + t_H v_2^2
\tag{B.7a}
$$

$$
\begin{aligned}
\delta m_{22}^2 = & \frac{1}{2} \left[\frac{v_s}{v_2} H_{\zeta_2,\zeta_S}^{\mathrm{CW}} + H_{\zeta_2,\zeta_2}^{\mathrm{CW}} - 3 H_{\psi_2,\psi_2}^{\mathrm{CW}} + \frac{v_1}{v_2} \left(H_{\zeta_1,\zeta_2}^{\mathrm{CW}} - H_{\eta_1,\eta_2}^{\mathrm{CW}} \right) \right. \\
& \left. + 5 \frac{v_1^2}{v_2^2} \left(H_{\psi_1,\psi_1}^{\mathrm{CW}} - H_{\eta_1,\eta_1}^{\mathrm{CW}} \right) \right] + t_H v_1^2
\end{aligned}
\tag{B.7b}
$$

$$
\delta m_{12}^2 = H_{\eta_1,\eta_2}^{\mathrm{CW}} + \frac{v_1}{v_2} \left(H_{\psi_1,\psi_1}^{\mathrm{CW}} - H_{\eta_1,\eta_1}^{\mathrm{CW}} \right) + t_H v_1 v_2
\tag{B.7c}
$$

$$
\delta\lambda_1 = \frac{1}{v_1^2} \left(2 H_{\eta_1,\eta_1}^{\mathrm{CW}} - H_{\psi_1,\psi_1}^{\mathrm{CW}} - H_{\zeta_1,\zeta_1}^{\mathrm{CW}} \right) - t_H \frac{v_2^2}{v_1^2}
\tag{B.7d}
$$

$$
\delta\lambda_2 = \frac{1}{v_2^2} \left(H_{\psi_2,\psi_2}^{\mathrm{CW}} - H_{\zeta_2,\zeta_2}^{\mathrm{CW}} \right) + 2 \frac{v_1^2}{v_2^4} \left(H_{\eta_1,\eta_1}^{\mathrm{CW}} - H_{\psi_1,\psi_1}^{\mathrm{CW}} \right) - t_H \frac{v_1^2}{v_2^2}
\tag{B.7e}
$$

$$
\delta\lambda_3 = \frac{1}{v_2^2} \left(H_{\eta_1,\eta_1}^{\mathrm{CW}} - H_{\psi_1,\psi_1}^{\mathrm{CW}} \right) + \frac{1}{v_1 v_2} \left(H_{\eta_1,\eta_2}^{\mathrm{CW}} - H_{\zeta_1,\zeta_2}^{\mathrm{CW}} \right) - t_H
\tag{B.7f}
$$

$$
\delta\lambda_4 = t_H
\tag{B.7g}
$$

$$
\delta\lambda_5 = \frac{2}{v_2^2} \left(H_{\psi_1,\psi_1}^{\mathrm{CW}} - 2 H_{\eta_1,\eta_1}^{\mathrm{CW}} \right) + t_H
\tag{B.7h}
$$

$$
\delta m_S^2 = \frac{1}{2} \left(H_{\zeta_S,\zeta_S}^{\mathrm{CW}} + \frac{v_2}{v_s} H_{\zeta_2,\zeta_S}^{\mathrm{CW}} + \frac{v_1}{v_s} H_{\zeta_1,\zeta_S}^{\mathrm{CW}} - \frac{3}{v_S} N_{\zeta_S}^{\mathrm{CW}} \right) - t_S \frac{3}{2 v_s}
\tag{B.7i}
$$

$$
\delta\lambda_6 = \frac{1}{v_s^3} \left(N_{\zeta_S}^{\mathrm{CW}} - v_s H_{\zeta_S,\zeta_S}^{\mathrm{CW}} \right) - t_S \frac{1}{v_s^3}
\tag{B.7j}
$$

$$
\delta\lambda_7 = - \frac{1}{v_s v_1} H_{\zeta_1,\zeta_S}^{\mathrm{CW}}
\tag{B.7k}
$$

$$
\delta\lambda_8 = - \frac{1}{v_s v_2} H_{\zeta_2,\zeta_S}^{\mathrm{CW}}
\tag{B.7l}
$$

$$
\delta T_1 = H_{\eta_1,\eta_1}^{\mathrm{CW}} v_1 + H_{\eta_1,\eta_2}^{\mathrm{CW}} v_2 - N_{\zeta_1}^{\mathrm{CW}}
\tag{B.7m}
$$

$$
\delta T_2 = \frac{v_1^2}{v_2} \left(H_{\rho_1,\rho_1}^{\mathrm{CW}} - H_{\psi_1,\psi_1}^{\mathrm{CW}} \right) + H_{\eta_1,\eta_2}^{\mathrm{CW}} v_1 + H_{\psi_2,\psi_2}^{\mathrm{CW}} v_2 - N_{\zeta_2}^{\mathrm{CW}}
\tag{B.7n}
$$

$$
\delta T_S = t_S
\tag{B.7o}
$$

$$
\delta T_{\mathrm{CP}} = - N_{\psi_2}^{\mathrm{CW}}
\tag{B.7p}
$$

$$
\delta T_{\mathrm{CB}} = - N_{\rho_2}^{\mathrm{CW}} \, ,
\tag{B.7q}
$$

where $t_H, t_S \in \mathbb{R}$ describe the free parameters in the two-dimensional space of solutions. As t_H equals the free parameter t in the counterterms for the C2HDM, cf. Eq. (B.5), the same argumentation can be used to set $t_H = 0$ as Eq. (B.6) is independent of t_H after inserting the electroweak minimum, cf. Eq. (2.77). The counterterms of the tadpole parameter δT do not have a counterpart in the tree-level potential. Therefore, if no symmetry is broken at one-loop, vanishing one-loop Tadpoles as a check of the implementation of the equations. As δT_S is given by the free parameter t_S it can be set to zero as it is not needed to solve Eq. (B.1).

B.3. Modifications to the Derivatives of the Coleman-Weinberg potential

The calculation of the second and third derivative, used in the calculation of the trilinear self couplings, of the Coleman-Weinberg potential [165] includes the evaluation of the function

$$f_{ab}^{(1)} = \frac{m_a^2 \log\left(\frac{m_a^2}{\mu^2}\right) - m_b^2 \log\left(\frac{m_b^2}{\mu^2}\right)}{m_a^2 - m_b^2}\,, \tag{B.8}$$

$$f_{abc}^{(1)} = \frac{(m_b^2 - m_c^2)m_a^2 \log\left(\frac{m_a^2}{\mu^2}\right) + \left(m_c^2 - m_a^2\right)m_b^2 \log\left(\frac{m_b^2}{\mu^2}\right) + \left(m_a^2 - m_b^2\right)m_c^2 \log\left(\frac{m_c^2}{\mu^2}\right)}{\left(m_a^2 - m_b^2\right)\left(m_a^2 - m_c^2\right)\left(m_b^2 - m_c^2\right)}\,. \tag{B.9}$$

If at least two masses are degenerate and vanish, these functions would diverge. This divergence is known in the literature [165, 206, 207]. However, these divergences can be understood as an artefact of the vanishing momenta approximation in the Coleman-Weinberg potential and do not appear if these calculations are performed including all momentum dependent parts [165, 207, 208]. Taking the limit of vanishing momenta of the diagrammatic approach in [209, 210], the second and third derivatives yield finite result. To recreate those results the limits of degenerate masses of Eqs. (B.8) and (B.9) are taken and the diverging parts are omitted. Evaluating Eq. (B.8) in the limit of two degenerate masses yields

$$f_{aa}^{(1)} = \lim_{m_b^2 \to m_a^2} f_{ab}^{(1)} = 1 + \log\left(\frac{m_a^2}{\mu^2}\right)\,. \tag{B.10}$$

Dropping the divergent part for the limit $m_a^2 \to 0$ then yields

$$\lim_{m_a^2 \to 0} f_{aa}^{(1)} = 1\,. \tag{B.11}$$

Taking the limits of degenerate masses in Eq. (B.9) yields

$$f_{aac}^{(1)} = \lim_{m_b^2 \to m_a^2} f_{abc}^{(1)} = \frac{m_c^2 \log\left(\frac{m_c^2}{\mu^2}\right) - m_c^2}{(m_a^2 - m_c^2)^2} + \frac{m_a^2 - m_c^2 \log\left(\frac{m_a^2}{\mu^2}\right)}{(m_a^2 - m_c^2)^2}\,, \tag{B.12}$$

$$f_{aaa}^{(1)} = \lim_{m_c^2 \to m_a^2} f_{aac}^{(1)} = \frac{1}{2m_a^2}\,. \tag{B.13}$$

Taking the limits of vanishing masses and dropping the divergent parts results in the final parts

$$\lim_{m_a^2 \to 0} f_{aac}^{(1)} = \frac{\log\left(\frac{m_c^2}{\mu^2}\right) - 1}{m_c^2}\,, \tag{B.14}$$

$$\lim_{m_a^2 \to 0} f_{aaa}^{(1)} = 0\,. \tag{B.15}$$

The limits Eqs. (B.11), (B.14) and (B.15) are implemented in `BSMPT` [4] to evaluate the second and third derivatives of the Coleman-Weinberg potential.

Acknowledgements (Danksagungen)

[1]   P. Basler, M. Krause, M. Muhlleitner, J. Wittbrodt, and A. Wlotzka. "Strong First Or-
       der Electroweak Phase Transition in the CP-Conserving 2HDM Revisited". In: *JHEP*
       02 (2016), p. 121. DOI: 10.1007/JHEP02(2017)121. arXiv: 1612.04086 [hep-ph].

[2]   Philipp Basler, Pedro M. Ferreira, Margarete Mühlleitner, and Rui Santos. "High scale
       impact in alignment and decoupling in two-Higgs doublet models". In: *Phys. Rev. D
       97, 095024 (2018)* 97.9 (Oct. 28, 2017). DOI: 10.1103/PhysRevD.97.095024. arXiv:
       1710.10410v2 [hep-ph].

[3]   Philipp Basler, Margarete Mühlleitner, and Jonas Wittbrodt. "The CP-Violating 2HDM
       in Light of a Strong First Order Electroweak Phase Transition and Implications for
       Higgs Pair Production". In: *JHEP* 03 (2018), p. 061. DOI: 10.1007/JHEP03(2018)061.
       arXiv: 1711.04097 [hep-ph].

[4]   Philipp Basler and Margarete Mühlleitner. "BSMPT - Beyond the Standard Model
       Phase Transitions -A Tool for the Electroweak Phase Transition in Extended Higgs
       Sectors". In: *Comput. Phys. Commun.* 237 (2019), pp. 62–85. DOI: 10.1016/j.cpc.
       2018.11.006. arXiv: 1803.02846 [hep-ph].

[5]   Philipp Basler, Margarete Mühlleitner, and Jonas Müller. "Electroweak Phase Transi-
       tion in Non-Minimal Higgs Sectors". to be published.

[6]   Georges Aad et al. "Observation of a new particle in the search for the Standard Model
       Higgs boson with the ATLAS detector at the LHC". In: *Phys. Lett.* B716 (2012), pp. 1–
       29. DOI: 10.1016/j.physletb.2012.08.020. arXiv: 1207.7214 [hep-ex].

[7]   Serguei Chatrchyan et al. "Observation of a new boson at a mass of 125 GeV with the
       CMS experiment at the LHC". In: *Phys.Lett.* B716 (2012), pp. 30–61. DOI: 10.1016/
       j.physletb.2012.08.021. arXiv: 1207.7235 [hep-ex].

[8]   G. Aad et al. "Combined Measurement of the Higgs Boson Mass inppCollisions ats=7and
       8 TeV with the ATLAS and CMS Experiments". In: *Physical Review Letters* 114.19
       (2015). DOI: 10.1103/physrevlett.114.191803.

[9]   Georges Aad et al. "Measurements of the Higgs boson production and decay rates
       and constraints on its couplings from a combined ATLAS and CMS analysis of the
       LHC pp collision data at $\sqrt{s} = 7$ and 8 TeV". In: *JHEP* 08 (2016), p. 045. DOI:
       10.1007/JHEP08(2016)045. arXiv: 1606.02266 [hep-ex].

[10]   Vincenzo Branchina, Emanuele Messina, and Dario Zappalà. "Impact of gravity on
       vacuum stability". In: *EPL (Europhysics Letters)* 116.2 (2016), p. 21001. DOI: 10.
       1209/0295-5075/116/21001.

[11]   Nabarun Chakrabarty, Ujjal Kumar Dey, and Biswarup Mukhopadhyaya. "High-scale
       validity of a two-Higgs doublet scenario: a study including LHC data". In: *JHEP* 12
       (2014), p. 166. DOI: 10.1007/JHEP12(2014)166. arXiv: 1407.2145 [hep-ph].

[12] P. S. Bhupal Dev and Apostolos Pilaftsis. "Erratum to: Maximally symmetric two Higgs doublet model with natural standard model alignment". In: *Journal of High Energy Physics* 2015.11 (2015). DOI: 10.1007/jhep11(2015)147.

[13] Dipankar Das and Ipsita Saha. "Search for a stable alignment limit in two-Higgs-doublet models". In: *Physical Review D* 91.9 (2015). DOI: 10.1103/physrevd.91.095024.

[14] Debtosh Chowdhury and Otto Eberhardt. "Global fits of the two-loop renormalized Two-Higgs-Doublet model with soft Z 2 breaking". In: *Journal of High Energy Physics* 2015.11 (2015). DOI: 10.1007/jhep11(2015)052.

[15] Pedro Ferreira, Howard Haber, and Edward Santos. "Erratum: Preserving the validity of the two-Higgs-doublet model up to the Planck scale [Phys. Rev. D92, 033003 (2015)]". In: *Physical Review D* 94.5 (2016). DOI: 10.1103/physrevd.94.059903.

[16] Nabarun Chakrabarty and Biswarup Mukhopadhyaya. "High-scale validity of a two Higgs doublet scenario: metastability included". In: *Eur. Phys. J.* C77.3 (2017), p. 153. DOI: 10.1140/epjc/s10052-017-4705-0. arXiv: 1603.05883 [hep-ph].

[17] Vincenzo Cacchio, Debtosh Chowdhury, Otto Eberhardt, and Christopher W. Murphy. "Next-to-leading order unitarity fits in Two-Higgs-Doublet models with soft $\mathbb{Z}_2$ breaking". In: *JHEP* 11 (2016), p. 026. DOI: 10.1007/JHEP11(2016)026. arXiv: 1609.01290 [hep-ph].

[18] Nabarun Chakrabarty and Biswarup Mukhopadhyaya. "High-scale validity of a two-Higgs-doublet scenario: Predicting collider signals". In: *Physical Review D* 96.3 (2017). DOI: 10.1103/physrevd.96.035028.

[19] Stefania Gori, Howard E. Haber, and Edward Santos. "High scale flavor alignment in two-Higgs doublet models and its phenomenology". In: *JHEP* 06 (2017), p. 110. DOI: 10.1007/JHEP06(2017)110. arXiv: 1703.05873 [hep-ph].

[20] M. Tanabashi et al. "Review of Particle Physics". In: *Physical Review D* 98.3 (2018). DOI: 10.1103/physrevd.98.030001.

[21] A. D. Sakharov. "Violation of CP Invariance, c Asymmetry, and Baryon Asymmetry of the Universe". In: *Pisma Zh. Eksp. Teor. Fiz.* 5 (1967). [Usp. Fiz. Nauk161,61(1991)], pp. 32–35. DOI: 10.1070/PU1991v034n05ABEH002497.

[22] V.A. Kuzmin, V.A. Rubakov, and M.E. Shaposhnikov. "On anomalous electroweak baryon-number non-conservation in the early universe". In: *Physics Letters B* 155.1-2 (1985), pp. 36–42. DOI: 10.1016/0370-2693(85)91028-7.

[23] Andrew G. Cohen, David B. Kaplan, and Ann E. Nelson. "Baryogenesis at the weak phase transition". In: *Nuclear Physics B* 349.3 (1991), pp. 727–742. DOI: 10.1016/0550-3213(91)90395-e.

[24] M. B. Gavela, P. Hernandez, J. Orloff, and O. Pene. "Standard model CP violation and baryon asymmetry". In: *Mod. Phys. Lett.* A9 (1994), pp. 795–810. DOI: 10.1142/S0217732394000629. arXiv: hep-ph/9312215 [hep-ph].

[25] Z. Fodor, J. Hein, K. Jansen, A. Jaster, and I. Montvay. "Simulating the electroweak phase transition in the SU(2) Higgs model". In: *Nucl. Phys.* B439 (1995), pp. 147–186. DOI: 10.1016/0550-3213(95)00038-T. arXiv: hep-lat/9409017 [hep-lat].

[26] M.E. Shaposhnikov. "Baryon asymmetry of the universe in standard electroweak theory". In: *Nuclear Physics B* 287 (1987), pp. 757–775. DOI: 10.1016/0550-3213(87)90127-1.

[27] K. Kajantie, M. Laine, K. Rummukainen, and M. Shaposhnikov. "The Electroweak Phase Transition: A Non-Perturbative Analysis". In: *Nucl.Phys. B466 (1996) 189-258* (Oct. 12, 1995). DOI: `10.1016/0550-3213(96)00052-1`. arXiv: `hep-lat/9510020v1` `[hep-lat]`.

[28] M. Quiros. "Field theory at finite temperature and phase transitions". In: *Helv. Phys. Acta* 67 (1994), pp. 451–583.

[29] Ilya F. Ginzburg and Maria Krawczyk. "Symmetries of two Higgs doublet model and-CPviolation". In: *Physical Review D* 72.11 (2005). DOI: `10.1103/physrevd.72.115013`.

[30] Abdus Salam. "Weak and Electromagnetic Interactions". In: *Conf. Proc.* C680519 (1968), pp. 367–377.

[31] Steven Weinberg. "A Model of Leptons". In: *Physical Review Letters* 19.21 (1967), pp. 1264–1266. DOI: `10.1103/physrevlett.19.1264`.

[32] Sheldon L. Glashow. "Partial-symmetries of weak interactions". In: *Nuclear Physics* 22.4 (1961), pp. 579–588. DOI: `10.1016/0029-5582(61)90469-2`.

[33] G. Arnison et al. "Experimental observation of isolated large transverse energy electrons with associated missing energy at". In: *Physics Letters B* 122.1 (1983), pp. 103–116. DOI: `10.1016/0370-2693(83)91177-2`.

[34] G. Arnison et al. "Experimental observation of lepton pairs of invariant mass around 95 GeV/c2 at the CERN SPS collider". In: *Physics Letters B* 126.5 (1983), pp. 398–410. DOI: `10.1016/0370-2693(83)90188-0`.

[35] P. Bagnaia et al. "Evidence for Z0→e+e- at the CERN p collider". In: *Physics Letters B* 129.1-2 (1983), pp. 130–140. DOI: `10.1016/0370-2693(83)90744-x`.

[36] Peter W. Higgs. "Broken Symmetries and the Masses of Gauge Bosons". In: *Physical Review Letters* 13.16 (1964), pp. 508–509. DOI: `10.1103/physrevlett.13.508`.

[37] P.W. Higgs. "Broken symmetries, massless particles and gauge fields". In: *Physics Letters* 12.2 (1964), pp. 132–133. DOI: `10.1016/0031-9163(64)91136-9`.

[38] F. Englert and R. Brout. "Broken Symmetry and the Mass of Gauge Vector Mesons". In: *Physical Review Letters* 13.9 (1964), pp. 321–323. DOI: `10.1103/physrevlett.13.321`.

[39] G. S. Guralnik, C. R. Hagen, and T. W. B. Kibble. "Global Conservation Laws and Massless Particles". In: *Physical Review Letters* 13.20 (1964), pp. 585–587. DOI: `10.1103/physrevlett.13.585`.

[40] T. W. B. Kibble. "Symmetry Breaking in Non-Abelian Gauge Theories". In: *Physical Review* 155.5 (1967), pp. 1554–1561. DOI: `10.1103/physrev.155.1554`.

[41] Benjamin W. Lee, C. Quigg, and H. B. Thacker. "Weak interactions at very high energies: The role of the Higgs-boson mass". In: *Physical Review D* 16.5 (1977), pp. 1519–1531. DOI: `10.1103/physrevd.16.1519`.

[42] Nicola Cabibbo. "Unitary Symmetry and Leptonic Decays". In: *Physical Review Letters* 10.12 (1963), pp. 531–533. DOI: `10.1103/physrevlett.10.531`.

[43] Makoto Kobayashi and Toshihide Maskawa. "CP-Violation in the Renormalizable Theory of Weak Interaction". In: *Progress of Theoretical Physics* 49.2 (1973), pp. 652–657. DOI: `10.1143/ptp.49.652`.

[44] M. B. GAVELA, P. HERNÁNDEZ, J. ORLOFF, and O. PÈNE. "STANDARD MODEL CP-VIOLATION AND BARYON ASYMMETRY". In: *Modern Physics Letters A* 09.09 (1994), pp. 795–809. DOI: `10.1142/s0217732394000629`.

[45] Sebastian Bruggisser, Thomas Konstandin, and Geraldine Servant. "CP-violation for Electroweak Baryogenesis from Dynamical CKM Matrix". In: (June 26, 2017). DOI: 10.1088/1475-7516/2017/11/034. arXiv: 1706.08534v3 [hep-ph].

[46] T. D. Lee. "A Theory of Spontaneous T Violation". In: *Phys. Rev.* D8 (1973), pp. 1226–1239. DOI: 10.1103/PhysRevD.8.1226.

[47] John F. Gunion, Howard E. Haber, Gordon L. Kane, and Sally Dawson. "The Higgs Hunter's Guide". In: *Front. Phys.* 80 (2000), pp. 1–404.

[48] G. C. Branco et al. "Theory and phenomenology of two-Higgs-doublet models". In: *Phys. Rept.* 516 (2012), pp. 1–102. DOI: 10.1016/j.physrep.2012.02.002. arXiv: 1106.0034 [hep-ph].

[49] Utpal Sarkar. *Particle and Astroparticle Physics (Series in High Energy Physics, Cosmology and Gravitation)*. CRC Press, 2007. ISBN: 9781584889311.

[50] Igor P. Ivanov. "Minkowski space structure of the Higgs potential in 2HDM. II. Minima, symmetries, and topology". In: *Phys. Rev.* D77 (2008), p. 015017. DOI: 10.1103/PhysRevD.77.015017. arXiv: 0710.3490 [hep-ph].

[51] A. Barroso, P. M. Ferreira, and R. Santos. "Neutral minima in two-Higgs doublet models". In: *Phys. Lett.* B652 (2007), pp. 181–193. DOI: 10.1016/j.physletb.2007.07.010. arXiv: hep-ph/0702098 [HEP-PH].

[52] P. M. Ferreira, R. Santos, and A. Barroso. "Stability of the tree-level vacuum in two Higgs doublet models against charge or CP spontaneous violation". In: *Phys. Lett.* B603 (2004). [Erratum: Phys. Lett. **B629**, 114 (2005)], pp. 219–229. DOI: 10.1016/j.physletb.2004.10.022,10.1016/j.physletb.2005.09.074. arXiv: hep-ph/0406231 [hep-ph].

[53] A. Barroso, P. M. Ferreira, I. Ivanov, and Rui Santos. "Tree-level metastability bounds in two-Higgs doublet models". In: *Proceedings, 1st Toyama International Workshop on Higgs as a Probe of New Physics 2013 (HPNP2013): Toyama, Japan, February 13-16, 2013*. 2013. arXiv: 1305.1235 [hep-ph]. URL: https://inspirehep.net/record/1232098/files/arXiv:1305.1235.pdf.

[54] A. Barroso, P. M. Ferreira, I. Ivanov, R. Santos, and João P. Silva. "Avoiding Death by Vacuum". In: *J. Phys. Conf. Ser.* 447 (2013), p. 012051. DOI: 10.1088/1742-6596/447/1/012051. arXiv: 1305.1906 [hep-ph].

[55] A. Barroso, P. M. Ferreira, I. P. Ivanov, and Rui Santos. "Metastability bounds on the two Higgs doublet model". In: *JHEP* 06 (2013), p. 045. DOI: 10.1007/JHEP06(2013)045. arXiv: 1303.5098 [hep-ph].

[56] A. Barroso, P. M. Ferreira, I. P. Ivanov, Rui Santos, and João P. Silva. "Evading death by vacuum". In: *Eur.Phys.J. C73 (2013) 2537* (Nov. 26, 2012). DOI: 10.1140/epjc/s10052-013-2537-0. arXiv: 1211.6119v2 [hep-ph].

[57] M. Tanabashi et al. "Review of Particle Physics". In: *Phys. Rev.* D98.3 (2018), p. 030001. DOI: 10.1103/PhysRevD.98.030001.

[58] P. M. Ferreira and João P. Silva. "A two-Higgs doublet model with remarkable CP properties". In: *The European Physical Journal C* 69.1-2 (2010), pp. 45–52. DOI: 10.1140/epjc/s10052-010-1384-5.

[59] Duarte Fontes, J. C. Romão, and João P. Silva. "$h \to Z\gamma$ in the complex two Higgs doublet model". In: *JHEP* 12 (2014), p. 043. DOI: 10.1007/JHEP12(2014)043. arXiv: 1408.2534 [hep-ph].

[60] Fedor Bezrukov, Mikhail Yu. Kalmykov, Bernd A. Kniehl, and Mikhail Shaposhnikov. "Higgs Boson Mass and New Physics". In: *JHEP* 10 (2012). [,275(2012)], p. 140. DOI: 10.1007/JHEP10(2012)140. arXiv: 1205.2893 [hep-ph].

[61] Giuseppe Degrassi et al. "Higgs mass and vacuum stability in the Standard Model at NNLO". In: *JHEP* 08 (2012), p. 098. DOI: 10.1007/JHEP08(2012)098. arXiv: 1205.6497 [hep-ph].

[62] Dario Buttazzo et al. "Investigating the near-criticality of the Higgs boson". In: *JHEP* 12 (2013), p. 089. DOI: 10.1007/JHEP12(2013)089. arXiv: 1307.3536 [hep-ph].

[63] Nilendra G. Deshpande and Ernest Ma. "Pattern of Symmetry Breaking with Two Higgs Doublets". In: *Phys. Rev.* D18 (1978), p. 2574. DOI: 10.1103/PhysRevD.18.2574.

[64] K. G. Klimenko. "Conditions for certain Higgs potentials to be bounded below". In: *Theoretical and Mathematical Physics* 62.1 (1985), pp. 58–65. ISSN: 1573-9333. DOI: 10.1007/BF01034825. URL: https://doi.org/10.1007/BF01034825.

[65] I. P. Ivanov. "Minkowski space structure of the Higgs potential in 2HDM". In: *Phys. Rev.* D75 (2007). [Erratum: Phys. Rev. **D76**, 039902 (2007)], p. 035001. DOI: 10.1103/PhysRevD.76.039902,10.1103/PhysRevD.75.035001. arXiv: hep-ph/0609018 [hep-ph].

[66] J. Horejsi and M. Kladiva. "Tree-unitarity bounds for THDM Higgs masses revisited". In: *Eur. Phys. J.* C46 (2006), pp. 81–91. DOI: 10.1140/epjc/s2006-02472-3. arXiv: hep-ph/0510154 [hep-ph].

[67] Shinya Kanemura, Takahiro Kubota, and Eiichi Takasugi. "Lee-Quigg-Thacker bounds for Higgs boson masses in a two doublet model". In: *Phys. Lett.* B313 (1993), pp. 155–160. DOI: 10.1016/0370-2693(93)91205-2. arXiv: hep-ph/9303263 [hep-ph].

[68] Rita Coimbra, Marco O. P. Sampaio, and Rui Santos. "ScannerS: Constraining the phase diagram of a complex scalar singlet at the LHC". In: *Eur. Phys. J.* C73 (2013), p. 2428. DOI: 10.1140/epjc/s10052-013-2428-4. arXiv: 1301.2599 [hep-ph].

[69] Ulrich Nierste and Kurt Riesselmann. "Higgs sector renormalization group in theMS and on-mass-shell scheme: The breakdown of perturbation theory for a heavy Higgs boson". In: *Physical Review D* 53.11 (1996), pp. 6638–6652. DOI: 10.1103/physrevd.53.6638.

[70] ATLAS Collaboration. "Search for flavour-changing neutral currents in processes with one top quark and a photon using 81 fb^{-1} of pp collisions at $\sqrt{s} = 13$ TeV with the ATLAS experiment". In: (Aug. 22, 2019). arXiv: 1908.08461v1 [hep-ex].

[71] Alessio Boletti. "$b \to s\ell\ell$ results from CMS". In: *PoS* LHCP2018 (2018), p. 183. DOI: 10.22323/1.321.0183.

[72] *Couplings of the C2HDM*. URL: http://porthos.tecnico.ulisboa.pt/arXiv/C2HDM/ (visited on 08/22/2019).

[73] Chien-Yi Chen, Michael Freid, and Marc Sher. "Next-to-minimal two Higgs doublet model". In: *Phys. Rev.* D89.7 (2014), p. 075009. DOI: 10.1103/PhysRevD.89.075009. arXiv: 1312.3949 [hep-ph].

[74] Aleksandra Drozd, Bohdan Grzadkowski, John F. Gunion, and Yun Jiang. "Extending two-Higgs-doublet models by a singlet scalar field - the Case for Dark Matter". In: *JHEP* 11 (2014), p. 105. DOI: 10.1007/JHEP11(2014)105. arXiv: 1408.2106 [hep-ph].

[75] Margarete Muhlleitner, Marco O. P. Sampaio, Rui Santos, and Jonas Wittbrodt. "The N2HDM under Theoretical and Experimental Scrutiny". In: *JHEP* 03 (2017), p. 094. DOI: 10.1007/JHEP03(2017)094. arXiv: 1612.01309 [hep-ph].

[76] A. V. Bednyakov, B. A. Kniehl, A. F. Pikelner, and O. L. Veretin. "Stability of the Electroweak Vacuum: Gauge Independence and Advanced Precision". In: *Physical Review Letters* 115.20 (2015). DOI: 10.1103/physrevlett.115.201802.

[77] Michael Edward Peskin and Daniel V. Schroeder. *An introduction to quantum field theory*. 4. print. Reading, Mass. [u.a.]: Addison-Wesley, 1997. ISBN: 0-201-50397-2.

[78] Raul Costa, Renato Guedes, Marco O. P. Sampaio, and Rui Santos. SCANNERS *project*. http://scanners.hepforge.org. 2014.

[79] Philip Bechtle, Sven Heinemeyer, Oscar Stal, Tim Stefaniak, and Georg Weiglein. "Applying Exclusion Likelihoods from LHC Searches to Extended Higgs Sectors". In: (July 24, 2015). DOI: 10.1140/epjc/s10052-015-3650-z. arXiv: 1507.06706v1 [hep-ph].

[80] Philip Bechtle et al. "Recent Developments in HiggsBounds and a Preview of HiggsSignals". In: (Jan. 10, 2013). arXiv: 1301.2345v1 [hep-ph].

[81] Philip Bechtle et al. "HiggsBounds-4: Improved Tests of Extended Higgs Sectors against Exclusion Bounds from LEP, the Tevatron and the LHC". In: *Eur.Phys.J. C74 (2014) 2693* C74.3 (Oct. 31, 2013), p. 2693. DOI: 10.1140/epjc/s10052-013-2693-2. arXiv: 1311.0055v1 [hep-ph].

[82] Philip Bechtle, Oliver Brein, Sven Heinemeyer, Georg Weiglein, and Karina E. Williams. "HiggsBounds 2.0.0: Confronting Neutral and Charged Higgs Sector Predictions with Exclusion Bounds from LEP and the Tevatron". In: *Comput. Phys.Commun.182:2605-2631,2011* 182 (Feb. 9, 2011), pp. 2605–2631. DOI: 10.1016/j.cpc.2011.07.015. arXiv: 1102.1898v1 [hep-ph].

[83] Philip Bechtle, Oliver Brein, Sven Heinemeyer, Georg Weiglein, and Karina E. Williams. "HiggsBounds: Confronting Arbitrary Higgs Sectors with Exclusion Bounds from LEP and the Tevatron". In: *Comput.Phys.Commun.181:138-167,2010* 181 (Nov. 25, 2008), pp. 138–167. DOI: 10.1016/j.cpc.2009.09.003. arXiv: 0811.4169v4 [hep-ph].

[84] Tim STEFANIAK et al. "Recent developments in HiggsBounds and a preview of HiggsSignals". In: *Proceedings of Prospects for Charged Higgs Discovery at Colliders — PoS(CHARGED 2012)*. Sissa Medialab, 2013. DOI: 10.22323/1.156.0024.

[85] A. Djouadi, J. Kalinowski, and M. Spira. "HDECAY: A Program for Higgs boson decays in the standard model and its supersymmetric extension". In: *Comput. Phys. Commun.* 108 (1998), pp. 56–74. DOI: 10.1016/S0010-4655(97)00123-9. arXiv: hep-ph/9704448 [hep-ph].

[86] J. M. Butterworth et al. "THE TOOLS AND MONTE CARLO WORKING GROUP Summary Report from the Les Houches 2009 Workshop on TeV Colliders". In: (Mar. 8, 2010). arXiv: 1003.1643v1 [hep-ph].

[87] Abdelhak Djouadi, Jan Kalinowski, Margarete Muehlleitner, and Michael Spira. "HDECAY: Twenty$_{++}$ years after". In: *Comput. Phys. Commun.* 238 (2019), pp. 214–231. DOI: 10.1016/j.cpc.2018.12.010. arXiv: 1801.09506 [hep-ph].

[88] Robert V. Harlander, Stefan Liebler, and Hendrik Mantler. "SusHi: A program for the calculation of Higgs production in gluon fusion and bottom-quark annihilation in the Standard Model and the MSSM". In: *Comput. Phys. Commun.* 184 (2013), pp. 1605–1617. DOI: 10.1016/j.cpc.2013.02.006. arXiv: 1212.3249 [hep-ph].

[89] Robert V. Harlander, Stefan Liebler, and Hendrik Mantler. "SusHi Bento: Beyond NNLO and the heavy-top limit". In: *Comput. Phys. Commun.* 212 (2017), pp. 239–257. DOI: 10.1016/j.cpc.2016.10.015. arXiv: 1605.03190 [hep-ph].

[90] O. Deschamps et al. "The Two Higgs Doublet of Type II facing flavour physics data". In: *Phys. Rev.* D82 (2010), p. 073012. DOI: 10.1103/PhysRevD.82.073012. arXiv: 0907.5135 [hep-ph].

[91] Farvah Mahmoudi and Oscar Stal. "Flavor constraints on the two-Higgs-doublet model with general Yukawa couplings". In: *Phys. Rev.* D81 (2010), p. 035016. DOI: 10.1103/PhysRevD.81.035016. arXiv: 0907.1791 [hep-ph].

[92] Thomas Hermann, Mikolaj Misiak, and Matthias Steinhauser. "$\bar{B} \to X_s\gamma$ in the Two Higgs Doublet Model up to Next-to-Next-to-Leading Order in QCD". In: *JHEP* 11 (2012), p. 036. DOI: 10.1007/JHEP11(2012)036. arXiv: 1208.2788 [hep-ph].

[93] M. Misiak et al. "Updated NNLO QCD predictions for the weak radiative B-meson decays". In: *Phys. Rev. Lett.* 114.22 (2015), p. 221801. DOI: 10.1103/PhysRevLett.114.221801. arXiv: 1503.01789 [hep-ph].

[94] Mikolaj Misiak and Matthias Steinhauser. "Weak Radiative Decays of the B Meson and Bounds on $M_{H^\pm}$ in the Two-Higgs-Doublet Model". In: *Eur. Phys. J.* C77.3 (2017), p. 201. DOI: 10.1140/epjc/s10052-017-4776-y. arXiv: 1702.04571 [hep-ph].

[95] M. Baak et al. "The global electroweak fit at NNLO and prospects for the LHC and ILC". In: *Eur. Phys. J.* C74 (2014), p. 3046. DOI: 10.1140/epjc/s10052-014-3046-5. arXiv: 1407.3792 [hep-ph].

[96] Boost. *Boost C++ Libraries*. http://www.boost.org/. 2017.

[97] Jacob Baron et al. "Order of Magnitude Smaller Limit on the Electric Dipole Moment of the Electron". In: *Science* 343 (2014), pp. 269–272. DOI: 10.1126/science.1248213. arXiv: 1310.7534 [physics.atom-ph].

[98] V. Andreev et al. "Improved limit on the electric dipole moment of the electron". In: *Nature* 562.7727 (2018), pp. 355–360. DOI: 10.1038/s41586-018-0599-8.

[99] Debtosh Chowdhury and Otto Eberhardt. "Global fits of the two-loop renormalized Two-Higgs-Doublet model with soft Z_2 breaking". In: *JHEP* 11 (2015), p. 052. DOI: 10.1007/JHEP11(2015)052. arXiv: 1503.08216 [hep-ph].

[100] Johannes Braathen, Mark D. Goodsell, Manuel E. Krauss, Toby Opferkuch, and Florian Staub. "N-loop running should be combined with N-loop matching". In: *Phys. Rev. D 97, 015011 (2018)* (Nov. 22, 2017). DOI: 10.1103/PhysRevD.97.015011. arXiv: 1711.08460v2 [hep-ph].

[101] F. Staub. "Sarah". In: (June 3, 2008). arXiv: 0806.0538v6 [hep-ph].

[102] Florian Staub. "SARAH 4 : A tool for (not only SUSY) model builders". In: *Comput. Phys. Commun.* 185 (2014), pp. 1773–1790. DOI: 10.1016/j.cpc.2014.02.018. arXiv: 1309.7223 [hep-ph].

[103] Florian Staub. "SARAH 3.2: Dirac Gauginos, UFO output, and more". In: *Comput. Phys. Commun.* 184 (2013), pp. 1792–1809. DOI: 10.1016/j.cpc.2013.02.019. arXiv: 1207.0906 [hep-ph].

[104] Florian Staub. "Automatic Calculation of supersymmetric Renormalization Group Equations and Self Energies". In: *Comput. Phys. Commun.* 182 (2011), pp. 808–833. DOI: 10.1016/j.cpc.2010.11.030. arXiv: 1002.0840 [hep-ph].

[105] Florian Staub. "From Superpotential to Model Files for FeynArts and CalcHep/CompHep". In: *Comput. Phys. Commun.* 181 (2010), pp. 1077–1086. DOI: 10.1016/j.cpc.2010.01.011. arXiv: 0909.2863 [hep-ph].

[106] Stephen P. Martin. "Pole mass of the W boson at two-loop order in the pure $\overline{\text{MS}}$ scheme". In: *Phys. Rev. D* 91 (11 2015), p. 114003. DOI: 10.1103/PhysRevD.91.114003. URL: https://link.aps.org/doi/10.1103/PhysRevD.91.114003.

[107] Stephen P. Martin. "Z-boson pole mass at two-loop order in the pure $\overline{\text{MS}}$ scheme". In: *Phys. Rev. D* 92 (1 2015), p. 014026. DOI: 10.1103/PhysRevD.92.014026. URL: https://link.aps.org/doi/10.1103/PhysRevD.92.014026.

[108] Stephen P. Martin. "Complete two-loop effective potential approximation to the lightest Higgs scalar boson mass in supersymmetry". In: *Phys. Rev. D* 67 (9 2003), p. 095012. DOI: 10.1103/PhysRevD.67.095012. URL: https://link.aps.org/doi/10.1103/PhysRevD.67.095012.

[109] Benjamín Grinstein, Christopher W. Murphy, and Patipan Uttayarat. "One-Loop Corrections to the Perturbative Unitarity Bounds in the CP-Conserving Two-Higgs Doublet Model with a Softly Broken $\mathbb{Z}_2$ Symmetry". In: *JHEP06(2016)070* (Dec. 14, 2015). DOI: 10.1007/JHEP06(2016)070. arXiv: 1512.04567v2 [hep-ph].

[110] Marcel Krause, Robin Lorenz, Margarete Muhlleitner, Rui Santos, and Hanna Ziesche. "Gauge-independent Renormalization of the 2-Higgs-Doublet Model". In: (May 16, 2016). DOI: 10.1007/JHEP09(2016)143. arXiv: 1605.04853v1 [hep-ph].

[111] Marcel Krause, Margarete Mühlleitner, Rui Santos, and Hanna Ziesche. "Higgs-to-Higgs boson decays in a 2HDM at next-to-leading order". In: *Physical Review D* 95.7 (2017). DOI: 10.1103/physrevd.95.075019.

[112] Christophe Grojean and Geraldine Servant. "Gravitational Waves from Phase Transitions at the Electroweak Scale and Beyond". In: *Phys.Rev.D75:043507,2007* (July 10, 2006). DOI: 10.1103/PhysRevD.75.043507. arXiv: hep-ph/0607107v1 [hep-ph].

[113] Arthur Kosowsky, Michael S. Turner, and Richard Watkins. "Gravitational waves from first-order cosmological phase transitions". In: *Physical Review Letters* 69.14 (1992), pp. 2026–2029. DOI: 10.1103/physrevlett.69.2026.

[114] Arthur Kosowsky, Michael S. Turner, and Richard Watkins. "Gravitational radiation from colliding vacuum bubbles". In: *Physical Review D* 45.12 (1992), pp. 4514–4535. DOI: 10.1103/physrevd.45.4514.

[115] Arthur Kosowsky and Michael S. Turner. "Gravitational radiation from colliding vacuum bubbles: Envelope approximation to many-bubble collisions". In: *Physical Review D* 47.10 (1993), pp. 4372–4391. DOI: 10.1103/physrevd.47.4372.

[116] Marc Kamionkowski, Arthur Kosowsky, and Michael S. Turner. "Gravitational radiation from first-order phase transitions". In: *Physical Review D* 49.6 (1994), pp. 2837–2851. DOI: 10.1103/physrevd.49.2837.

[117] Riccardo Apreda, Michele Maggiore, Alberto Nicolis, and Antonio Riotto. "Gravitational waves from electroweak phase transitions". In: *Nuclear Physics B* 631.1-2 (2002), pp. 342–368. DOI: 10.1016/s0550-3213(02)00264-x.

[118] Chiara Caprini et al. "Science with the space-based interferometer eLISA. II: gravitational waves from cosmological phase transitions". In: *Journal of Cosmology and Astroparticle Physics* 2016.04 (2016), pp. 001–001. DOI: 10.1088/1475-7516/2016/04/001.

[119] Chiara Caprini et al. "Detecting gravitational waves from cosmological phase transitions with LISA: an update". In: (Oct. 29, 2019). arXiv: 1910.13125v1 [astro-ph.CO].

[120] Xiao Wang, Fa Peng Huang, and Xinmin Zhang. "Gravitational wave and collider signals in complex two-Higgs doublet model with dynamical CP-violation at finite temperature". In: (Sept. 6, 2019). arXiv: 1909.02978v1 [hep-ph].

[121] James M. Cline and Kimmo Kainulainen. "New Source for Electroweak Baryogenesis in the Minimal Supersymmetric Standard Model". In: *Physical Review Letters* 85.26 (2000), pp. 5519–5522. DOI: 10.1103/physrevlett.85.5519.

[122]   James M Cline, Michael Joyce, and Kimmo Kainulainen. "Supersymmetric electroweak baryogenesis". In: *Journal of High Energy Physics* 2000.07 (2000), pp. 018–018. DOI: 10.1088/1126-6708/2000/07/018.

[123]   S.J. Huber and M.G. Schmidt. "Electroweak baryogenesis: concrete in a SUSY model with a gauge singlet". In: *Nuclear Physics B* 606.1-2 (2001), pp. 183–230. DOI: 10.1016/s0550-3213(01)00250-4.

[124]   S. J. Huber, P. John, and M. G. Schmidt. "Bubble Walls, CP Violation and Electroweak Baryogenesis in the MSSM". In: *Eur.Phys.J.C20:695-711,2001* (Jan. 22, 2001). arXiv: hep-ph/0101249v2 [hep-ph].

[125]   Lars Fromme. "Electroweak Baryogenesis with dimension-6 Higgs interactions". In: *Surveys High Energ.Phys. 19 (2004) 193-201* (Apr. 25, 2005). DOI: 10.1080/0142241 0500160212. arXiv: hep-ph/0504222v1 [hep-ph].

[126]   Kimmo Kainulainen, Tomislav Prokopec, Michael G. Schmidt, and Steffen Weinstock. "First principle derivation of semiclassical force for electroweak baryogenesis". In: *JHEP 0106:031,2001* (May 28, 2001). DOI: 10.1088/1126-6708/2001/06/031. arXiv: hep-ph/0105295v2 [hep-ph].

[127]   Kimmo Kainulainen, Tomislav Prokopec, Michael G. Schmidt, and Steffen Weinstock. "Semiclassical force for electroweak baryogenesis: three-dimensional derivation". In: *Phys.Rev.D66:043502,2002* (Feb. 19, 2002). DOI: 10.1103/PhysRevD.66.043502. arXiv: hep-ph/0202177v1 [hep-ph].

[128]   T. Prokopec, M. G. Schmidt, and S. Weinstock. "Transport equations for chiral fermions to order $\hbar$ and electroweak baryogenesis: Part I". In: *Ann.Phys.314:208-265,2004* (Dec. 9, 2003). DOI: 10.1016/j.aop.2004.06.002. arXiv: hep-ph/0312110v2 [hep-ph].

[129]   Tomislav Prokopec, Michael G. Schmidt, and Steffen Weinstock. "Transport equations for chiral fermions to order h-bar and electroweak baryogenesis. Part II". In: *Annals Phys.* 314 (2004), pp. 267–320. DOI: 10.1016/j.aop.2004.06.001. arXiv: hep-ph/0406140 [hep-ph].

[130]   Michael Joyce, Tomislav Prokopec, and Neil Turok. "Non-local Electroweak Baryogenesis Part II : The Classical Regime". In: *Phys.Rev.D53:2958-2980,1996* (Oct. 13, 1994). DOI: 10.1103/PhysRevD.53.2958. arXiv: hep-ph/9410282v4 [hep-ph].

[131]   Patrick Huet and Ann E. Nelson. "Electroweak Baryogenesis in Supersymmetric Models". In: *Phys.Rev. D53 (1996) 4578-4597* (July 2, 1995). DOI: 10.1103/PhysRevD.53.4578. arXiv: hep-ph/9506477v3 [hep-ph].

[132]   Andrew G. Cohen, D. B. Kaplan, and A. E. Nelson. "Progress in electroweak baryogenesis". In: *Ann. Rev. Nucl. Part. Sci.* 43 (1993), pp. 27–70. DOI: 10.1146/annurev.ns.43.120193.000331. arXiv: hep-ph/9302210 [hep-ph].

[133]   G. C. Dorsch, S. J. Huber, T. Konstandin, and J. M. No. "A Second Higgs Doublet in the Early Universe: Baryogenesis and Gravitational Waves". In: *JCAP* 1705.05 (2017), p. 052. DOI: 10.1088/1475-7516/2017/05/052. arXiv: 1611.05874 [hep-ph].

[134]   Marcela Carena, Germano Nardini, Mariano Quiros, and Carlos E. M. Wagner. "MSSM Electroweak Baryogenesis and LHC Data". In: *JHEP* 02 (2013), p. 001. DOI: 10.1007/JHEP02(2013)001. arXiv: 1207.6330 [hep-ph].

[135]   M. Carena, Germano Nardini, M. Quiros, and C. E. M. Wagner. "The Baryogenesis Window in the MSSM". In: *Nucl. Phys.* B812 (2009), pp. 243–263. DOI: 10.1016/j.nuclphysb.2008.12.014. arXiv: 0809.3760 [hep-ph].

[136]   S. J. Huber and Michael G. Schmidt. "Baryogenesis at the electroweak phase transition for a SUSY model with a gauge singlet". In: *Strong and electroweak matter. Proceedings, Meeting, SEWM 2000, Marseille, France, June 13-17, 2000*. 2000, pp. 272–278. DOI: `10.1142/9789812799913_0034`. arXiv: `hep-ph/0011059 [hep-ph]`.

[137]   Stephan J. Huber, Thomas Konstandin, Tomislav Prokopec, and Michael G. Schmidt. "Electroweak Phase Transition and Baryogenesis in the nMSSM". In: *Nucl. Phys.* B757 (2006), pp. 172–196. DOI: `10.1016/j.nuclphysb.2006.09.003`. arXiv: `hep-ph/0606298 [hep-ph]`.

[138]   Stephan J. Huber, Thomas Konstandin, Tomislav Prokopec, and Michael G. Schmidt. "Baryogenesis in the MSSM, nMSSM and NMSSM". In: *Nucl. Phys.* A785 (2007), pp. 206–209. DOI: `10.1016/j.nuclphysa.2006.11.154`. arXiv: `hep-ph/0608017 [hep-ph]`.

[139]   Thomas Konstandin. "Quantum Transport and Electroweak Baryogenesis". In: *Phys. Usp. 56 (8) (2013)* (Feb. 27, 2013). DOI: `10.3367/UFNe.0183.201308a.0785`. arXiv: `1302.6713v2 [hep-ph]`.

[140]   Lars Fromme and Stephan J. Huber. "Top transport in electroweak baryogenesis". In: *JHEP* 03 (2007), p. 049. DOI: `10.1088/1126-6708/2007/03/049`. arXiv: `hep-ph/0604159 [hep-ph]`.

[141]   Tommi Alanne, Kimmo Kainulainen, Kimmo Tuominen, and Ville Vaskonen. "Baryogenesis in the two doublet and inert singlet extension of the Standard Model". In: *JCAP* 1608.08 (2016), p. 057. DOI: `10.1088/1475-7516/2016/08/057`. arXiv: `1607.03303 [hep-ph]`.

[142]   Lars Fromme, Stephan J. Huber, and Michael Seniuch. "Baryogenesis in the two-Higgs doublet model". In: *JHEP* 11 (2006), p. 038. DOI: `10.1088/1126-6708/2006/11/038`. arXiv: `hep-ph/0605242 [hep-ph]`.

[143]   James M. Cline, Kimmo Kainulainen, and Michael Trott. "Electroweak Baryogenesis in Two Higgs Doublet Models and B meson anomalies". In: *JHEP* 11 (2011), p. 089. DOI: `10.1007/JHEP11(2011)089`. arXiv: `1107.3559 [hep-ph]`.

[144]   A. Menon, D. E. Morrissey, and C. E. M. Wagner. "Electroweak Baryogenesis and Dark Matter in the nMSSM". In: *Phys.Rev.D70:035005,2004* (Apr. 21, 2004). DOI: `10.1103/PhysRevD.70.035005`. arXiv: `hep-ph/0404184v1 [hep-ph]`.

[145]   Michael Joyce, Tomislav Prokopec, and Neil Turok. "Nonlocal electroweak baryogenesis. II. The classical regime". In: *Physical Review D* 53.6 (1996), pp. 2958–2980. DOI: `10.1103/physrevd.53.2958`.

[146]   James M. Cline, Michael Joyce, and Kimmo Kainulainen. "Supersymmetric electroweak baryogenesis in the WKB approximation". In: *Physics Letters B* 417.1-2 (1998), pp. 79–86. DOI: `10.1016/s0370-2693(97)01361-0`.

[147]   James M. Cline and Kimmo Kainulainen. "A New Source for Electroweak Baryogenesis in the MSSM". In: *Phys.Rev.Lett.85:5519-5522,2000* (Feb. 25, 2000). DOI: `10.1103/PhysRevLett.85.5519`. arXiv: `hep-ph/0002272v2 [hep-ph]`.

[148]   Lars Fromme. "Electroweak baryogenesis in extensions of the Standard Model". PhD thesis. Universität Bielefeld, 2006. URL: `https://pub.uni-bielefeld.de/record/2306033`.

[149]   Thomas Konstandin, Tomislav Prokopec, Michael G. Schmidt, and Marcos Seco. "MSSM electroweak baryogenesis and flavor mixing in transport equations". In: *Nucl. Phys.* B738 (2006), pp. 1–22. DOI: `10.1016/j.nuclphysb.2005.11.028`. arXiv: `hep-ph/0505103 [hep-ph]`.

[150] Fa Peng Huang, Zhuoni Qian, and Mengchao Zhang. "Exploring dynamical CP violation induced baryogenesis by gravitational waves and colliders". In: (Apr. 18, 2018). arXiv: 1804.06813v1 [hep-ph].

[151] H. Abedi, M. Ahmadvand, and S. S. Gousheh. "Electroweak baryogenesis via chiral gravitational waves". In: *Phys. Lett.* B786 (2018), pp. 35–38. DOI: 10.1016/j.physletb.2018.07.065. arXiv: 1805.10645 [hep-ph].

[152] Marcela Carena, Mariano Quirós, and Yue Zhang. "Dark CP Violation and Gauged Lepton/Baryon Number for Electroweak Baryogenesis". In: (Aug. 13, 2019). arXiv: 1908.04818v1 [hep-ph].

[153] Jordy de Vries, Marieke Postma, and Jorinde van de Vis. "The role of leptons in electroweak baryogenesis". In: (Nov. 27, 2018). DOI: 10.1007/JHEP04(2019)024. arXiv: 1811.11104v1 [hep-ph].

[154] Mark Trodden. "Electroweak Baryogenesis". In: *Rev.Mod.Phys.71:1463-1500,1999* (Mar. 27, 1998). DOI: 10.1103/RevModPhys.71.1463. arXiv: hep-ph/9803479v2 [hep-ph].

[155] David E. Morrissey and Michael J. Ramsey-Musolf. "Electroweak baryogenesis". In: (June 13, 2012). DOI: 10.1088/1367-2630/14/12/125003. arXiv: 1206.2942v1 [hep-ph].

[156] Guy D. Moore. "Measuring the broken phase sphaleron rate nonperturbatively". In: *Physical Review D* 59.1 (1998). DOI: 10.1103/physrevd.59.014503.

[157] Ashok Das. *Finite Temperature Field Theory.* 2004. ISBN: 9810228562.

[158] Ashok K. Das. "Topics in finite temperature field theory". In: (2000). arXiv: hep-ph/0004125 [hep-ph].

[159] Joseph I. Kapusta. *Finite-Temperature Field Theory (Cambridge Monographs on Mathematical Physics).* Cambridge University Press, July 1989. ISBN: 9780521351553.

[160] Ryogo Kubo. "Statistical-Mechanical Theory of Irreversible Processes. I. General Theory and Simple Applications to Magnetic and Conduction Problems". In: *Journal of the Physical Society of Japan* 12.6 (1957), pp. 570–586. DOI: 10.1143/jpsj.12.570.

[161] Paul C. Martin and Julian Schwinger. "Theory of Many-Particle Systems. I". In: *Physical Review* 115.6 (1959), pp. 1342–1373. DOI: 10.1103/physrev.115.1342.

[162] Sidney R. Coleman and Erick J. Weinberg. "Radiative Corrections as the Origin of Spontaneous Symmetry Breaking". In: *Phys. Rev.* D7 (1973), pp. 1888–1910. DOI: 10.1103/PhysRevD.7.1888.

[163] James M. Cline and Pierre-Anthony Lemieux. "Electroweak phase transition in two Higgs doublet models". In: *Physical Review D* 55.6 (1997), pp. 3873–3881. DOI: 10.1103/physrevd.55.3873.

[164] M. E. Carrington. "Effective potential at finite temperature in the standard model". In: *Physical Review D* 45.8 (1992), pp. 2933–2944. DOI: 10.1103/physrevd.45.2933.

[165] José Eliel Camargo-Molina, António P. Morais, Roman Pasechnik, Marco O. P. Sampaio, and Jonas Wessén. "All one-loop scalar vertices in the effective potential approach". In: *JHEP* 08 (2016), p. 073. DOI: 10.1007/JHEP08(2016)073. arXiv: 1606.07069 [hep-ph].

[166] Peter Brockway Arnold and Olivier Espinosa. "The Effective potential and first order phase transitions: Beyond leading-order". In: *Phys. Rev.* D47 (1993). [Erratum: Phys. Rev.D50,6662(1994)], p. 3546. DOI: 10.1103/PhysRevD.50.6662,10.1103/PhysRevD.47.3546. arXiv: hep-ph/9212235 [hep-ph].

[167] Rajesh R. Parwani. "Resummation in a hot scalar field theory". In: *Phys. Rev.* D45 (1992). [Erratum: Phys. Rev.D48,5965(1993)], p. 4695. DOI: `10.1103/PhysRevD.45.4695,10.1103/PhysRevD.48.5965.2`. arXiv: `hep-ph/9204216 [hep-ph]`.

[168] Erick J. Weinberg and Aiqun Wu. "Understanding complex perturbative effective potentials". In: *Physical Review D* 36.8 (1987), pp. 2474–2480. DOI: `10.1103/physrevd.36.2474`.

[169] Duarte Fontes et al. "The C2HDM revisited". In: *Journal of High Energy Physics* 2018.2 (2018). DOI: `10.1007/jhep02(2018)073`.

[170] Philip Bechtle, Sven Heinemeyer, Oscar Stål, Tim Stefaniak, and Georg Weiglein. "Probing the Standard Model with Higgs signal rates from the Tevatron, the LHC and a future ILC". In: *JHEP 1411 (2014) 039* (Mar. 6, 2014). DOI: `10.1007/JHEP11(2014)039`. arXiv: `1403.1582v2 [hep-ph]`.

[171] Philip Bechtle, Sven Heinemeyer, Oscar Stål, Tim Stefaniak, and Georg Weiglein. "HiggsSignals: Confronting arbitrary Higgs sectors with measurements at the Tevatron and the LHC". In: *Eur.Phys.J. C74 (2014) 2711* (May 8, 2013). DOI: `10.1140/epjc/s10052-013-2711-4`. arXiv: `1305.1933v2 [hep-ph]`.

[172] Oscar Stål and Tim Stefaniak. "Constraining extended Higgs sectors with HiggsSignals". In: (Oct. 15, 2013). arXiv: `1310.4039v1 [hep-ph]`.

[173] G. Degrassi, M. Fedele, and P.P. Giardino. "Constraints on the trilinear Higgs self coupling from precision observables". In: *Journal of High Energy Physics* 2017.4 (2017). DOI: `10.1007/jhep04(2017)155`.

[174] A.M. Sirunyan et al. "Search for a massive resonance decaying to a pair of Higgs bosons in the four b quark final state in proton–proton collisions ats=13TeV". In: *Physics Letters B* 781 (2018), pp. 244–269. DOI: `10.1016/j.physletb.2018.03.084`.

[175] ATLAS Collaboration. "Combination of searches for Higgs boson pairs in *pp* collisions at $\sqrt{s}$ =13 TeV with the ATLAS detector". In: (June 5, 2019). arXiv: `1906.02025v1 [hep-ex]`.

[176] Shinya Kanemura, Shingo Kiyoura, Yasuhiro Okada, Eibun Senaha, and C. P. Yuan. "New physics effect on the Higgs selfcoupling". In: *Phys. Lett.* B558 (2003), pp. 157–164. DOI: `10.1016/S0370-2693(03)00268-5`. arXiv: `hep-ph/0211308 [hep-ph]`.

[177] Keisuke Fujii et al. "Physics Case for the International Linear Collider". In: (June 19, 2015). arXiv: `1506.05992v2 [hep-ex]`.

[178] Keisuke Fujii et al. "Tests of the Standard Model at the International Linear Collider". In: (Aug. 29, 2019). arXiv: `1908.11299v4 [hep-ex]`.

[179] A. Djouadi, W. Kilian, M. Muhlleitner, and P. M. Zerwas. "Testing Higgs selfcouplings at e+ e- linear colliders". In: *Eur. Phys. J.* C10 (1999), pp. 27–43. DOI: `10.1007/s100529900082`. arXiv: `hep-ph/9903229 [hep-ph]`.

[180] B. Di Micco et al. "Higgs boson pair production at colliders: status and perspectives". In: (Sept. 30, 2019). arXiv: `1910.00012v1 [hep-ph]`.

[181] S. Borowka et al. "Higgs Boson Pair Production in Gluon Fusion at Next-to-Leading Order with Full Top-Quark Mass Dependence". In: *Phys. Rev. Lett.* 117.1 (2016). [Erratum: Phys. Rev. Lett. **117**, no.7, 079901 (2016)], p. 012001. DOI: `10.1103/PhysRevLett.117.079901,10.1103/PhysRevLett.117.012001`. arXiv: `1604.06447 [hep-ph]`.

[182] G. Heinrich, S.P. Jones, M. Kerner, G. Luisoni, and E. Vryonidou. "NLO predictions for Higgs boson pair production with full top quark mass dependence matched to parton showers". In: *Journal of High Energy Physics* 2017.8 (2017). DOI: `10.1007/jhep08(2017)088`.

[183] J. Baglio et al. "Gluon fusion into Higgs pairs at NLO QCD and the top mass scheme". In: *The European Physical Journal C* 79.6 (2019). DOI: `10.1140/epjc/s10052-019-6973-3`.

[184] J. Baglio et al. "The measurement of the Higgs self-coupling at the LHC: theoretical status". In: *JHEP* 04 (2013), p. 151. DOI: `10.1007/JHEP04(2013)151`. arXiv: `1212.5581 [hep-ph]`.

[185] F. R. Klinkhamer and N. S. Manton. "A saddle-point solution in the Weinberg-Salam theory". In: *Physical Review D* 30.10 (1984), pp. 2212–2220. DOI: `10.1103/physrevd.30.2212`.

[186] N. S. Manton. "Topology in the Weinberg-Salam theory". In: *Physical Review D* 28.8 (1983), pp. 2019–2026. DOI: `10.1103/physrevd.28.2019`.

[187] G. 't Hooft. "Computation of the quantum effects due to a four-dimensional pseudoparticle". In: *Physical Review D* 14.12 (1976), pp. 3432–3450. DOI: `10.1103/physrevd.14.3432`.

[188] K. Kajantie, K. Rummukainen, and M. Shaposhnikov. "A lattice Monte Carlo study of the hot electroweak phase transition". In: *Nuclear Physics B* 407.2 (1993), pp. 356–372. DOI: `10.1016/0550-3213(93)90062-t`.

[189] K. Jansen. "Status of the finite temperature electroweak phase transition on the lattice". In: *Nucl. Phys. Proc. Suppl.* 47 (1996), pp. 196–211. DOI: `10.1016/0920-5632(96)00045-X`. arXiv: `hep-lat/9509018 [hep-lat]`.

[190] K. Kajantie, M. Laine, K. Rummukainen, and M. Shaposhnikov. "Is there a hot electroweak phase transition at m(H) larger or equal to m(W)?" In: *Phys.Rev.Lett.77:2887-2890,1996* (May 12, 1996). DOI: `10.1103/PhysRevLett.77.2887`. arXiv: `hep-ph/9605288v1 [hep-ph]`.

[191] F. Csikor, Z. Fodor, and J. Heitger. "Endpoint of the hot electroweak phase transition". In: *Phys.Rev.Lett. 82 (1999) 21-24* (Sept. 7, 1998). DOI: `10.1103/PhysRevLett.82.21`. arXiv: `hep-ph/9809291v1 [hep-ph]`.

[192] Stefano Profumo, Michael J. Ramsey-Musolf, and Gabe Shaughnessy. "Singlet Higgs phenomenology and the electroweak phase transition". In: *JHEP* 08 (2007), p. 010. DOI: `10.1088/1126-6708/2007/08/010`. arXiv: `0705.2425 [hep-ph]`.

[193] Jose R. Espinosa, Thomas Konstandin, and Francesco Riva. "Strong Electroweak Phase Transitions in the Standard Model with a Singlet". In: *Nucl. Phys.* B854 (2012), pp. 592–630. DOI: `10.1016/j.nuclphysb.2011.09.010`. arXiv: `1107.5441 [hep-ph]`.

[194] Guy D. Moore. "Do We Understand the Sphaleron Rate?" In: (Sept. 14, 2000). DOI: `10.1142/9789812799913_0007`. arXiv: `hep-ph/0009161v1 [hep-ph]`.

[195] Guy D. Moore. "Computing the Strong Sphaleron Rate". In: *Phys.Lett. B412 (1997) 359-370* (May 6, 1997). DOI: `10.1016/S0370-2693(97)01046-0`. arXiv: `hep-ph/9705248v2 [hep-ph]`.

[196] Dietrich Bodeker, Lars Fromme, Stephan J. Huber, and Michael Seniuch. "The Baryon asymmetry in the Standard Model with a low cut-off". In: *JHEP0502:026,2005* (Dec. 23, 2004). DOI: `10.1088/1126-6708/2005/02/026`. arXiv: `hep-ph/0412366v1 [hep-ph]`.

[197]   A.D. Dolgov and K. Kainulainen. "Fermi-Dirac corrections to the relic abundances". In: *Nuclear Physics B* 402.1-2 (1993), pp. 349–359. DOI: `10.1016/0550-3213(93)90646-7`.

[198]   M. Galassi et al. "GNU Scientific Library Reference Manual". In: (2016). URL: `http://www.gnu.org/software/gsl/`.

[199]   G.C. Dorsch, S.J. Huber, and T. Konstandin. "Bubble wall velocities in the Standard Model and beyond". In: *Journal of Cosmology and Astroparticle Physics* 2018.12 (2018), pp. 034–034. DOI: `10.1088/1475-7516/2018/12/034`.

[200]   Howard E. Haber and Ralf Hempfling. "The Renormalization group improved Higgs sector of the minimal supersymmetric model". In: *Phys. Rev.* D48 (1993), pp. 4280–4309. DOI: `10.1103/PhysRevD.48.4280`. arXiv: `hep-ph/9307201 [hep-ph]`.

[201]   K. A. Olive et al. "Review of Particle Physics". In: *Chin. Phys.* C38 (2014), p. 090001. DOI: `10.1088/1674-1137/38/9/090001`.

[202]   A. Denner et al. *LHCHXSWG-INT-2015-006.* https://cds.cern.ch/record/2047636.

[203]   LHC Higgs Cross SectionWorking Group. URL: `https://twiki.cern.ch/twiki/bin/view/LHCPhysics/LHCHXSWG`.

[204]   S. Dittmaier et al. "Handbook of LHC Higgs Cross Sections: 1. Inclusive Observables". In: (2011). DOI: `10.5170/CERN-2011-002`. arXiv: `1101.0593 [hep-ph]`.

[205]   G. C. Dorsch, S. J. Huber, and J. M. No. "A strong electroweak phase transition in the 2HDM after LHC8". In: *JHEP* 10 (2013), p. 029. DOI: `10.1007/JHEP10(2013)029`. arXiv: `1305.6610 [hep-ph]`.

[206]   Stephen P. Martin. "Taming the Goldstone contributions to the effective potential". In: *Physical Review D* 90.1 (2014). DOI: `10.1103/physrevd.90.016013`.

[207]   J. Elias-Miró, J. R. Espinosa, and T. Konstandin. "Taming infrared divergences in the effective potential". In: *Journal of High Energy Physics* 2014.8 (2014). DOI: `10.1007/jhep08(2014)034`.

[208]   J.A. Casas, J.R. Espinosa, M. Quirós, and A. Riotto. "The lightest Higgs boson mass in the Minimal Supersymmetric Standard Model". In: *Nuclear Physics B* 436.1-2 (1995), pp. 3–29. DOI: `10.1016/0550-3213(94)00508-c`.

[209]   Marcel Krause, Robin Lorenz, Margarete Mühlleitner, Rui Santos, and Hanna Ziesche. "Gauge-independent renormalization of the 2-Higgs-doublet model". In: *Journal of High Energy Physics* 2016.9 (2016). DOI: `10.1007/jhep09(2016)143`.

[210]   Marcel Krause, Margarete Muhlleitner, Rui Santos, and Hanna Ziesche. "2HDM Higgs-to-Higgs Decays at Next-to-Leading Order". In: *Phys. Rev.* D95.7 (2017), p. 075019. DOI: `10.1103/PhysRevD.95.075019`. arXiv: `1609.04185 [hep-ph]`.